Interactive Electrocardiograph Display

A Major Qualifying Project Report
submitted to the faculty of
WORCESTER POLYTECHNIC INSTITUTE
in partial fulfillment of the requirements for the
Degree of Bachelor of Science

Submitted by:
Jody Carregal
William Crafa
Morgan Shubert

Submitted on: December 13, 2019

Project Advisor:
Edward A. Clancy

Abstract

The target of our Major Qualifying Project was to produce an educational demonstration meant to aid Worcester Polytechnic Institute's (WPI) Department of Electrical and Computer Engineering (ECE) in exhibiting the opportunities available to those interested in pursuing a career in ECE. To accomplish this goal we created an interactive project for WPI's annual "Touch Tomorrow" event in the Spring of 2020 and into the future. The interactive project we created utilized Elenco Electronics Snap-Circuit pieces to produce a two-electrode electrocardiography (ECG) circuit allowing users to visualize the electrical activity of their heart after building portions of the ECG circuit themselves.

Acknowledgements

The success of this project was made possible by Professor Edward Clancy, Professor Stephen Bitar, Professor Reinhold Ludwig, Professor Donald Brown, Professor Alexander Wyglinski, William Appleyard, and Ian Costanzo. We would also like to thank the New England Center for Analog and Mixed Signal Design at WPI for sponsoring our work. Professor Clancy was an invaluable asset to the completion of our project by providing support and advice throughout the semester. Professor Bitar, Professor Ludwig, Professor Brown, and Professor Wyglinski aided in the brainstorming process of our project. William Appleyard helped in obtaining the necessary resources for the assembly of our final product. Ian Costanzo provided valuable advice and aided us through the progression of our project. Finally, we would like to thank the entire Electrical and Computer Engineering Department for helping us grow as independent and innovative thinkers throughout our years at WPI.

Table of Contents

Table of Figures

Table of Equations

Table of Tables

1. Introduction

Our team produced an educational demonstration which depicted the biomedical instrumentation concentration of Electrical and Computer Engineering (ECE) at Worcester Polytechnic Institute (WPI). Simultaneously, we constructed a proposal for an additional interactive display for the lobby of Atwater Kent, the location of WPI's ECE department.

As a team, we wanted to assist in promoting how versatile ECE is as a major to students interested in the STEM (Science, Technology, Engineering, and Mathematics) fields. As of recently, the ECE department at WPI has come to the realization that fewer students are turning to ECE as a career path and more are pursuing Computer Science (CS), Mechanical Engineering (ME), Biomedical Engineering (BME) or Robotics Engineering (RBE). The top five majors pursued at WPI are ME, CS, BME, and RBE leaving ECE as the fifth most pursued major. Referring to Figure 1, as of 2018, 18.8% of WPI's student body pursued ME as a career path, 15.3% pursued CS, 9.6% pursued BME, 7.9% pursued RBE and only 7.6% pursued ECE (WPI Institutional Research).

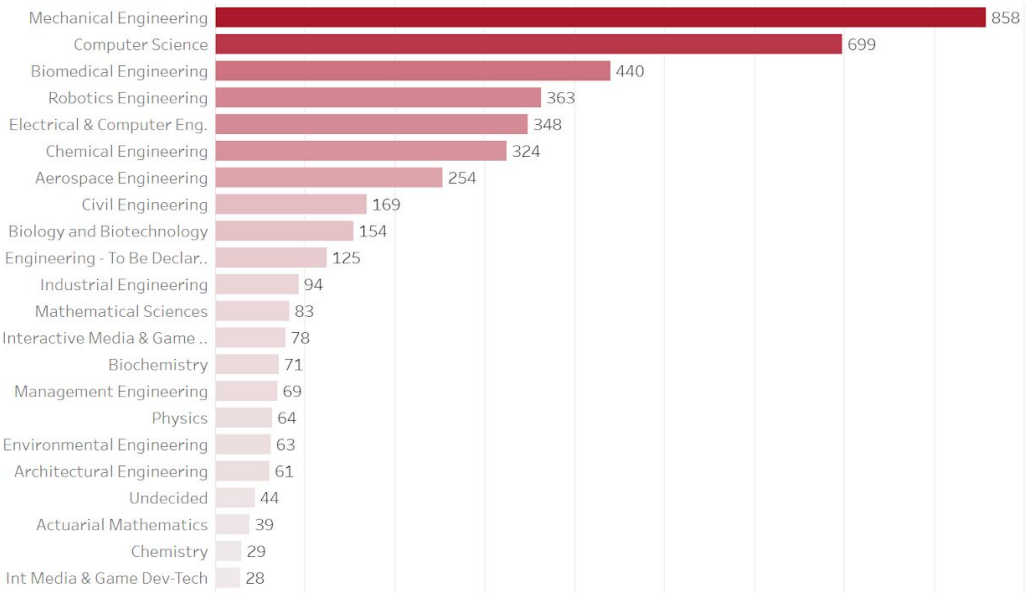

Figure 1 Major Enrollment of Undergraduate Students in Fall of 2018 (WPI Institutional Research)

In 2017, WPI matriculated 1,124 students. Of these students, 67 declared ECE as their major while 124 declared BME and 181 declared CS. In 2018, WPI matriculated an additional 152 students making this class a colossal size of 1,276. Of these students, 81 declared ECE while 150 declared BME and 184 declared CS as their major. In terms of percentages, only 6% of the first-year students that entered in 2018 pursued ECE while 12% pursued BME and 14% pursued CS (WPI Institutional Research).

We believe that by actively promoting ECE as a major to the public, by producing displays and relaying information to interested students, the ECE field can grow. It is possible that ECE is declining as a popular major simply because students are not aware of the opportunities available within our major. To assist in relaying the opportunities available to the public our team created custom parts from Elenco Electronics Snap-Circuit components to produce a simple electrocardiogram (ECG) circuit. At WPI's annual "Touch Tomorrow" event, students will be provided with instructions on how to build an ECG circuit and asked to create the featured circuit. They will then be able to see their own ECG displayed on an oscilloscope.

2. Background

2.1 Electrocardiogram (ECG) Signal

The human heart is a specialized muscle that contracts regularly and continuously, pumping blood to the body and the lungs (Anderson et al., 2015). The pumping of the heart is caused by electricity that repeatedly flows through the heart in a cycle. The sinoatrial (SA) node is the heart's pacemaker which initially sends out electrical signals from the atria, or upper chambers, causing the atria to contract and pump blood into the ventricles, or lower chambers. Then, the atrioventricular (AV) node, commonly referred to as the "junction box," conducts the electrical impulse from the atria to the ventricles which causes the muscle to contract and pump the blood out. The blood from the right ventricle travels to the lungs and the blood from the left ventricle travels throughout the rest of the body. Figure 2 portrays the flow of electricity in the human heart.

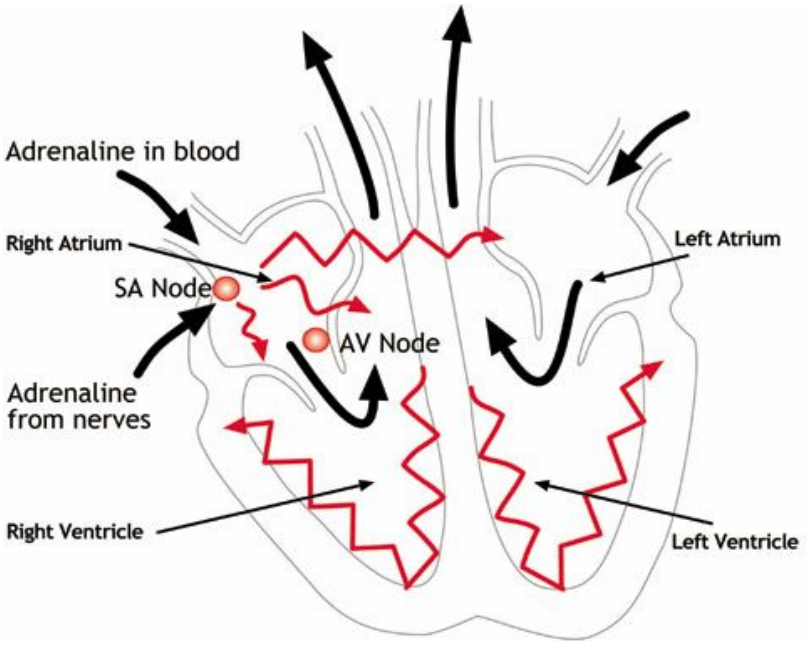

Figure 2 How the Heart Functions Electrically (Issa et al., 2019)

The electrical activity of the heart can be recorded through an ECG (Hirsch et al., 2002). An ECG measures how electrical impulses move through the heart as the muscle contracts and relaxes (Bag et al., 2019). These electrical impulses are measured through electrodes that are placed on the limbs and chest of the human body. There are two common types of electrodes utilized to measure an ECG signal. There are adhesive electrodes that stick to the patient's skin and there are metal electrodes which are pressed against the patient's skin. The standard clinical ECG utilizes ten electrodes and twelve leads. One lead is comprised of two electrodes to "represent the electrical heart activity in a differential electrical activity" (Salinet & Silva, 2019). A bipolar limb lead measures the potential difference between two electrodes. A unipolar chest lead measures the potential difference between one electrode and a reference point on the body. An augmented unipolar limb lead measures the potential difference between one limb and a combination of other limbs (Salinet & Silva, 2019). The twelve lead ECG includes three bipolar limb leads (I, II, and III), six unipolar chest leads (V1, V2, V3, V4, V5, and V6), and three augmented unipolar limb leads (aVR, aVL, and aVF). While the ten-electrode ECG is the most common for clinical evaluation, there are other methods to measure an ECG signal which will be discussed in Section 2.2. See Figure 3 for a diagram depicting a ten-electrode ECG.

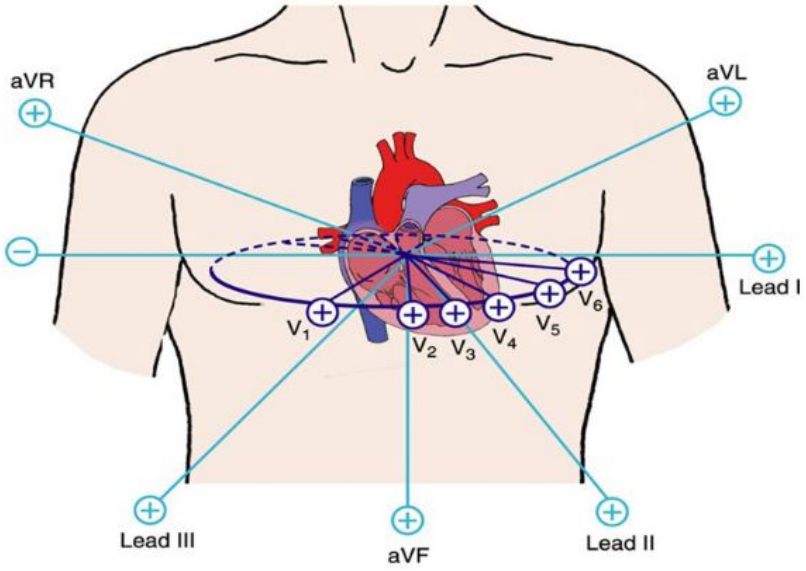

Figure 3 Placement of Twelve Leads in Ten-Electrode ECG (Goldberger et al., 2018)

The six unipolar chest leads view the heart in the horizontal plane, while the three bipolar limb leads and three augmented unipolar limb leads view the heart in the vertical plane. Leads II, III, and aVF view the interior surface of the heart; leads V1, V2, V3, and V4 view the anterior surface; leads I, aVL, V5, and V6 view the lateral surface; and leads V1 and aVR look through the right atrium into the cavity of the left ventricle (Meek & Morris, 2002). The ECG must be able to detect extremely weak signals ranging from 0.5 mV to 5 mV with a maximum $\pm$ 300 mV DC offset which is caused by the electrode-skin contact. The appropriate bandwidth of an ECG signal ranges from 0.05 Hz to 100 Hz, with the majority of the power occupying a bandwidth of 0.05 Hz to 10 Hz (Bag et al., 2019). The power spectral density of an ECG signal is portrayed in Figure 4.

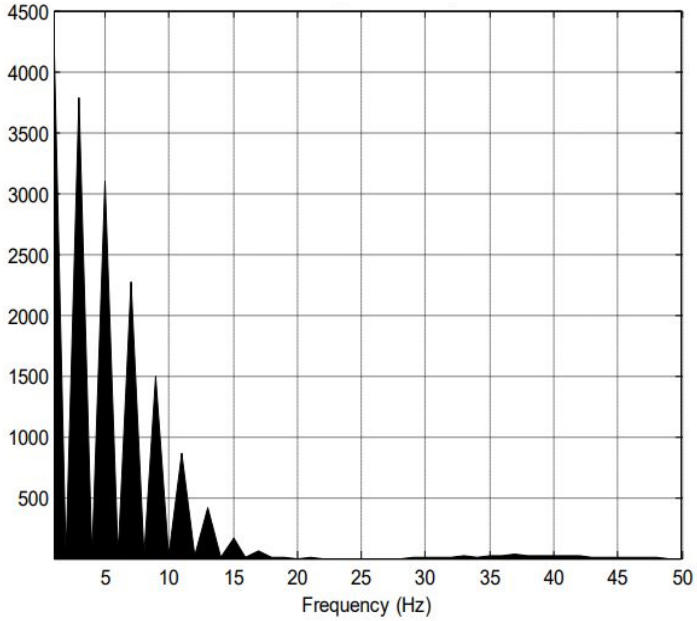

Figure 4 Power Spectral Density of an ECG (Brayner et al., 2019)

ECGs are used to assess the condition of the heart by analyzing the heart beat signal in search of irregularities. An ECG can also detect areas of muscle that are deprived of oxygen as well as dead tissue in the heart. There are seven main components of an ECG signal: P wave, QRS complex, PR interval, PR segment, ST segment, T wave, and the QT interval (Goldberger et al., 2018). Figure 5 portrays a single cycle of a typical ECG signal with each of the seven sections labeled.

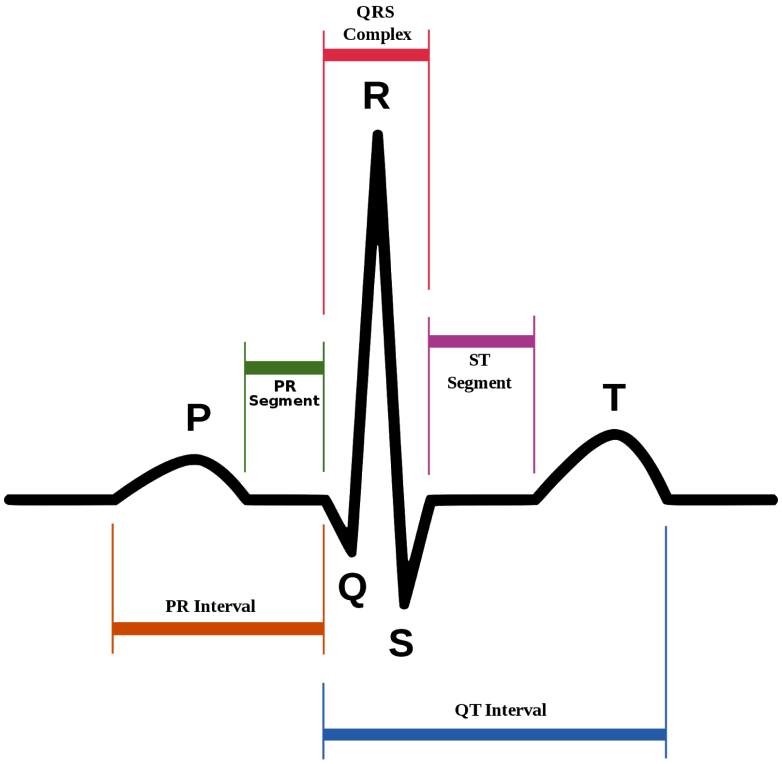

Figure 5 Typical Single Cycle of ECG Signal (Goldberger et al., 2018)

Each element of the ECG wave translates different information about the heart. The P wave represents the depolarization (activation) of the atria of the heart. The atria contracts shortly after the P wave begins. Generally, the P wave will be rounded and smooth, no more than 0.25 mV in amplitude, and no more than 0.11 seconds in duration. The P wave will be positive in leads I, II, aVF, V1, V2, V3, V4, V5, and V6 (Goldberger et al., 2018). The P wave can be analyzed to diagnose certain health issues including atrial fibrillation and atrial flutter. Of these two rhythms, if the P wave is absent from the ECG signal, then the diagnosis is atrial fibrillation, an irregular heartbeat that could lead to blood clots, stroke, heart failure, and other heart-related complications. If the P wave is not rounded, but a sawtooth formation, then the diagnosis is atrial flutter, which, if not treated, could also lead to blood clots, stroke, and heart failure (American Heart Association, 2016).

The QRS complex consists of the Q wave, R wave, and the S wave which occur. The Q wave is represented as the initial negative deflection of the QRS complex. The first positive

deflection in the complex is the R wave and the negative deflection following the R wave is called the S wave. The ventricles contract shortly after the QRS complex begins, similar to the P wave. In general, the duration of the QRS complex will be between 0.06 and 0.10 seconds with an amplitude of roughly 1 mV. The QRS complex will be positive in leads I, II, III, aVL, aVF, V5, and V6 (Goldberger et al., 2018). If the QRS amplitude is abnormally large it could indicate left ventricular hypertrophy. Left ventricular hypertrophy is the enlargement and thickening of the walls of the heart's main pumping chamber (left ventricle) and could lead to stroke, sudden cardiac arrest, or heart failure (American Heart Association, 2016).

The PR interval is the time between the beginning of the P wave and the beginning of the QRS complex (Goldberger et al., 2018). The duration of the PR interval is between 0.14 and 0.21 seconds. A short PR interval may suggest an accessory pathway, which allows early ventricular depolarization, or pre-excitation. A long PR interval represents slow conduction through the AV node, which can indicate bradycardia, or slow heart rate (American Heart Association, 2016).

The PR segment is the time between the end of the P wave and the beginning of the QRS complex and it represents the slow impulse conduction through the AV node. The PR segment, also referred to as the reference line or isoelectric line, serves as the baseline of the ECG curve. The amplitude of any deflection or wave is measured in reference to the PR segment (Goldberger et al., 2018).

The ST segment is typically a straight, level line between the end of the QRS complex and the beginning of the T wave. The ST segment portrays when the ventricle is contracting, but no electricity is flowing through, i.e. the period of zero potential between ventricular depolarization and repolarization. The duration of the ST segment is between 0.08 and 0.12 seconds. The ST segment should be flat or have a slight positive slope, and be level with the PR segment, or the baseline (Goldberger et al., 2018). If the ST segment is elevated, it could suggest myocardial infarction, or a heart attack. If the ST segment is depressed it could indicate ischemia, a condition in which the blood flow and oxygen are restricted or reduced which could lead to heart attack, an irregular heart rhythm, or heart failure (American Heart Association, 2016).

The T wave represents when the ventricles are resetting electrically and preparing for their next muscle contraction. A normal T wave is slightly asymmetric and the peak of the wave is slightly closer to the end than the beginning of the wave. The duration of the T wave is between 0.10 to 0.25 seconds with an amplitude of less than 0.05 mV. The polarity of the T wave depends on whether the R wave or the S wave is dominant. If R is greater than S, then the T wave is positive; if S is greater than R, then the T wave is negative. As a result, the T wave is generally positive in leads I, II, aVL, V2, V3, V4, V5, and V6 (Goldberger et al., 2018). If the amplitude of the T wave is too high, then it could indicate hyperkalemia, an abnormally elevated amount of potassium in the blood which could lead to cardiac arrest and death. If the T wave is flat, then it could suggest hypokalemia, or extremely low levels of potassium in the blood which could lead to paralysis or respiratory failure (American Heart Association, 2016).

The QT interval is the time between the beginning of the QRS complex and the end of the T wave and it represents the total time for depolarization and repolarization. The duration of the QT interval is between 0.39 and 0.46 seconds (Goldberger et al., 2018). There are many causes of a prolonged QT interval including medications, arrhythmias, and hypokalemia (Albano et al, 2019).

2.2 ECG Measurements

As mentioned in the previous section, the standard clinical ECG utilizes ten electrodes to measure the physiological signal. However, there are other methods to measure an ECG signal including five-electrode, three-electrode, and two-electrode ECG circuits.

2.2.1 Five-Electrode ECG

Five-electrode ECGs are becoming increasingly more common in the medical field because the measurement is close in accuracy to a ten-electrode ECG while being less cumbersome. In a five-electrode ECG, four electrodes are placed on the torso corresponding to the limbs; the electrode that corresponds to the right lower limb (or right leg) serves as the ground electrode. The fifth electrode is used on one of the standard chest lead positions, typically the V1 location for better arrhythmia monitoring. All four limb leads can be analyzed simultaneously, but only one chest lead can be observed at a time (Francis, 2016). See Figure 6 for a diagram depicting the placement of the five leads utilized to measure a five-electrode ECG signal.

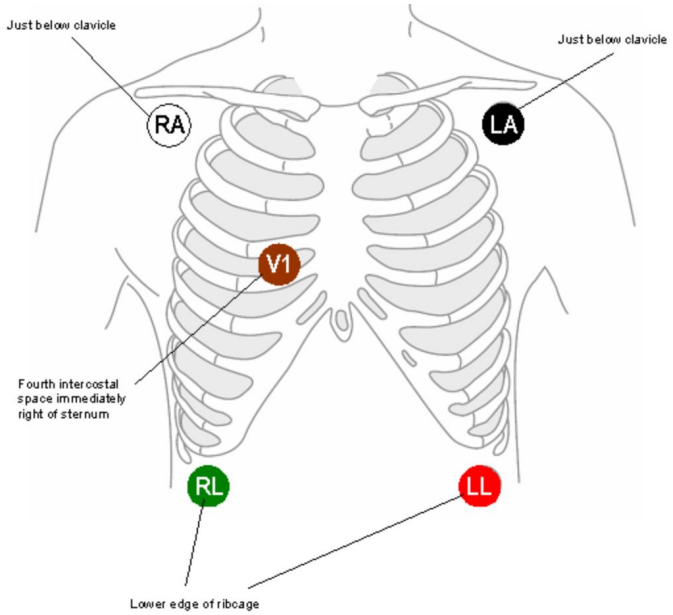

Figure 6 Placement of Leads in Five-Electrode ECG (Salinet & Silva, 2019)

2.2.2 Three-Electrode ECG

Three-electrode ECGs utilize two electrodes for active monitoring and one electrode as ground. The electrodes involved in the actual measurements can be utilized in different configurations to get lead I, II, or III. In a three-electrode ECG, there are fewer electrodes, meaning fewer leads; therefore, artifacts can only be viewed individually. For each lead being measured, the two electrodes are placed on the appropriate location of the body to acquire the desired lead, typically on the torso near the corresponding limb. The ground electrode can be placed almost anywhere on the body as long as it is not in close proximity with the other two electrodes (Francis, 2016). See Figure 7 for a diagram depicting the placement of the three leads utilized to measure a three-electrode ECG signal.

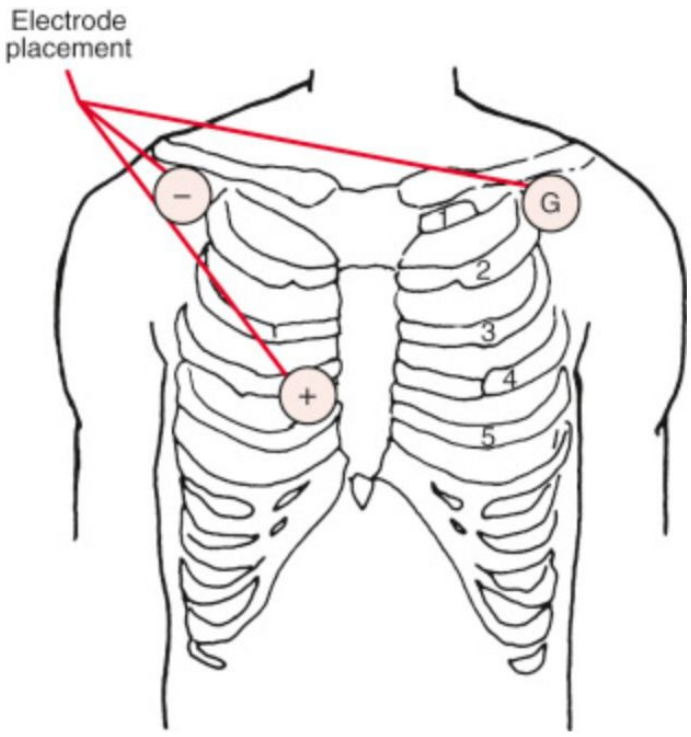

Figure 7 Placement of Leads in Three-Electrode ECG (Goldberger et al., 2018)

The circuitry for a three-electrode ECG includes three different inputs: for example, Left Arm (LA), Right Arm (RA), and Right Leg (RL), which acts as ground. LA and RA represent

the differential signal and feed into the input amplifier of the ECG circuit, while RL connects to ground and the grounded components in the ECG circuit. See Figure 8 for an example of a three-electrode ECG circuit.

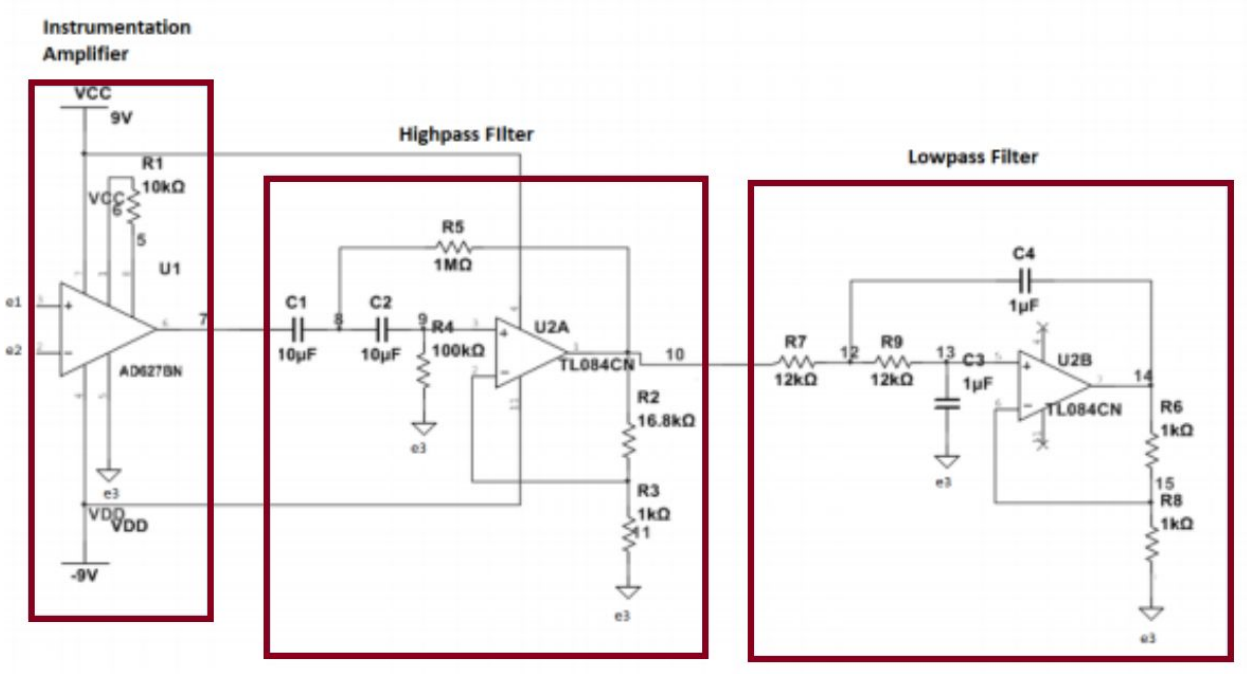

Figure 8 Example of a Three-Electrode ECG Circuit (Crowley et al., 2019)

2.2.3 Two-Electrode ECG

Two-electrode ECGs simply have two electrodes for active monitoring, LA and RA. Two-electrode ECGs do not need the RL electrode because the LA and RA electrodes connect to the input amplifier of the ECG circuit and also to high value resistors that are connected to ground. This configuration eliminates the need for an additional ground-referenced electrode, but tends to admit more powerline noise. See Figure 9 for an example of a two-electrode ECG circuit.

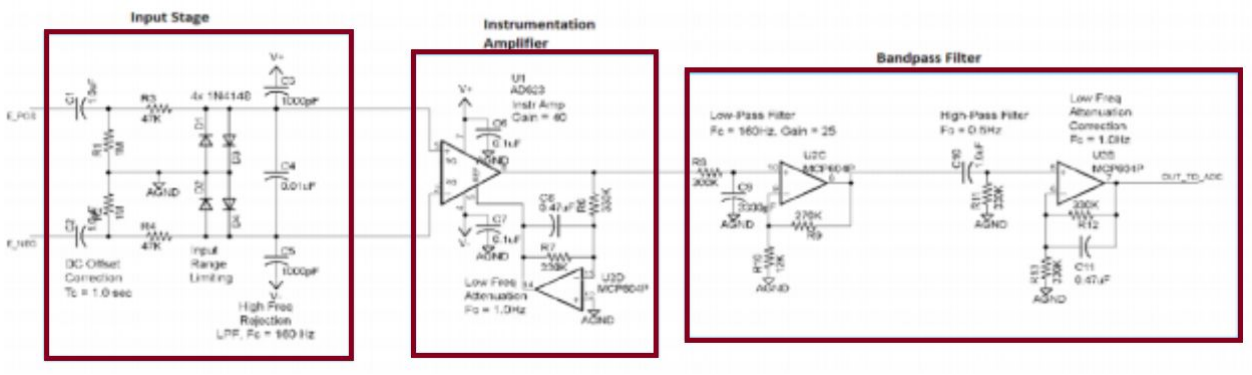

Figure 9 Example of a Two-Electrode ECG Circuit (Crowley et al., 2019)

While it is common for these electrodes to be placed on either side of the chest, the differential potential could also be measured across the two hands. Exercise machines such as treadmills and ellipticals possess metal contacts on the handles which the user could place their hands upon. Once this contact occurs, the exercise machine can detect the heart rate of the user through the surface of the skin. A trade-off for the easy access measurement of the hands is that the ECG measurements from the hands are much noisier than those from the chest. This noise is a result from motion artifacts from the user's movements, among other factors. Therefore, the most accurate way to measure an ECG signal through the hands is for the user to stand as still as possible.

2.3 ECG Analog Front End

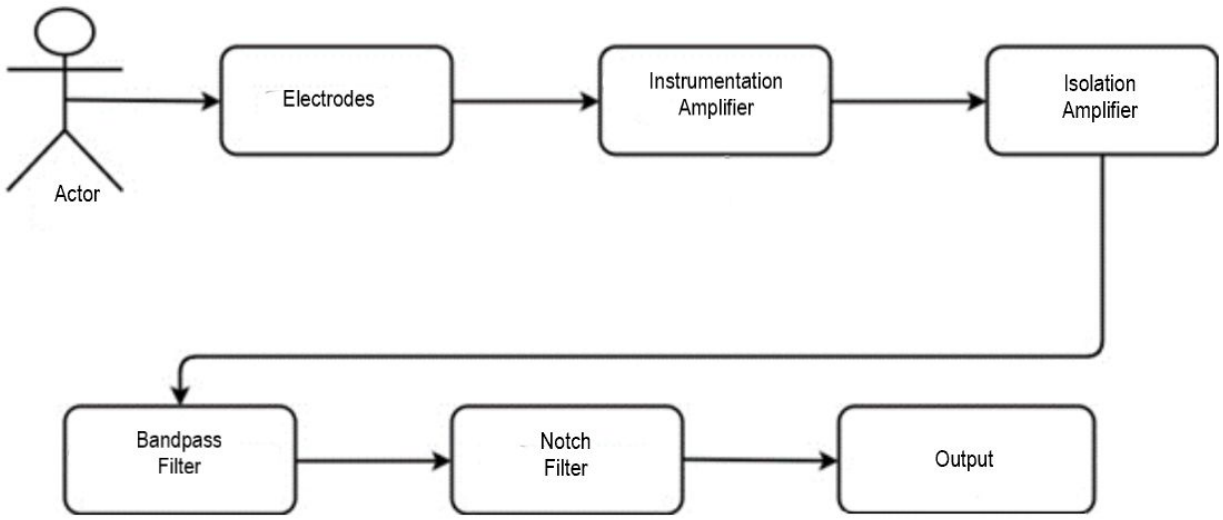

Figure 10 Block Diagram of Typical ECG Circuit (Ay et al, 2017)

2.3.1 Instrumentation Amplifier

The ECG signal will first pass through an instrumentation amplifier. An instrumentation amplifier has a high input impedance, common-mode noise rejection, differential output, and a high gain set by an external resistor. An instrumentation amplifier is comprised of non-inverting amplifying stages whose outputs act as the inputs to the differential amplifier. A differential amplifier is an inverting amplifier with negative feedback that amplifies the difference between the two input voltages. The differential amplifier will amplify the difference between the two signals being recorded and reject the common-mode voltage. The two input buffers provide a key function in the instrumentation amplifier. The ideal non-inverting amplifiers have an infinite input resistance. Therefore, the input buffers will not sink or source any current. In this stage, the differential amplifier will reject the common-mode voltage and will amplify the differential signal (Bitar et al., 2016).

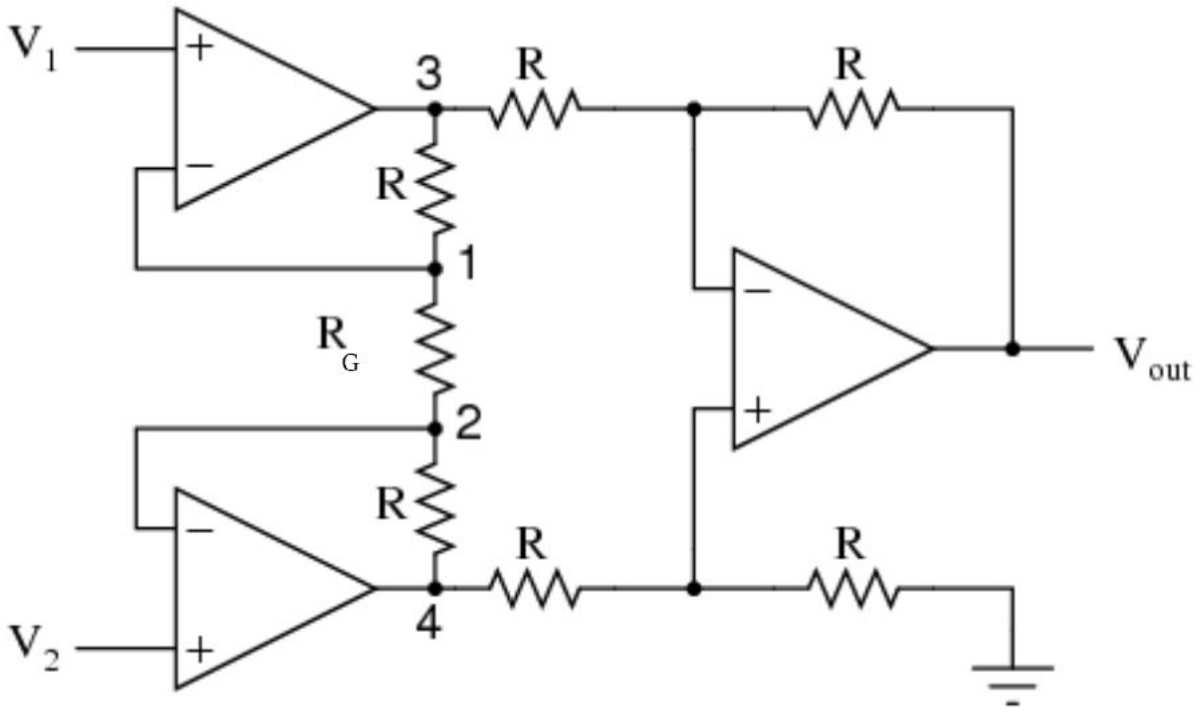

Figure 11 Model of a Basic Instrumentation Amplifier (EETech Media LLC, 2018)

We utilized an instrumentation amplifier because it allowed us to adjust the gain of the circuit by adjusting a single external resistor. Another option would have been to utilize a differential amplifier. However, we would not have had a high impedance input and we would have had to adjust multiple resistors in order to reach our desired gain. Referring to the basic instrumentation amplifier depicted in Figure 11, an instrumentation amplifier can be modeled as two buffer differential amplifiers linked by three resistors with an additional differential amplifier stage. In order to explain this circuit, we will assume all of the resistor values to be equal except for R_G. The voltage at point 1 (found above R_G) is equal to the voltage at V_1 due to the negative feedback loop of amplifier A1. In the same way, the voltage at point 2 (found below R_G) is equal to the voltage at V_2. This then causes a voltage drop across R_G thus creating a current through R_G. Due to the fact that the amplifier inputs draw no current, the only current that can travel through the resistors labeled as "R" must be the current through R_G. This current then

produces a voltage drop between points 3 and 4 (found at the top and bottom of the circuit). The equation to solve for the voltage drop between points 3 and 4 is:

$$V_{3-4} = (V_2 - V_1) * (1 + \frac{2R}{R_G})$$

The differential amplifier furthest to the right then takes this voltage drop and amplifies it by a gain of 1 (due to the fact that all of the "R" resistors in this circuit are of equal value). Therefore, the output voltage is simply the voltage drop between points 3 and 4:

$$V_{OUT} = V_{3-4}$$

To solve for the gain of a typical amplifier the following equation would be utilized:

$$A_V = (1 + \frac{2R}{R_G})$$

Equation 1 Gain Equation to solve for Gain (A_V) (EETech Media LLC, 2018)

2.3.2 Isolation Amplifier

Once the electrical signal is amplified from the instrumentation amplifier the signal will travel through the isolation amplifier, which acts as the protection stage. An isolation amplifier is an operational amplifier circuit which provides electrical isolation of one portion of a circuit from another. The protection stage is responsible for limiting the input range, rejecting high frequencies, and providing a barrier for dangerous voltages. Since the electrodes will be connected to a human body, precautions will have to be made to ensure the safety of the individuals utilizing our product. Isolation amplifiers enhance safety by preventing fault currents from flowing through the human body through a ground-referenced biopotential electrode (Kutz, 2009). We utilized an isolation amplifier in order to ensure that the human body had no direct electrical path to the earth-grounded portion of the circuit. An isolation amplifier requires two different power sources in order to pass the signal through successfully. The portion of the circuit preceding the isolation amplifier, which will be connected to the human body, needs to be powered by an isolated power supply or by batteries. The portion of the circuit following the isolation amplifier, which is earth-grounded, is powered by a non-isolated power supply. This

ensures that the only phenomenon being transferred through the isolation amplifier is the signal itself, not power (Analog Devices, 2009).

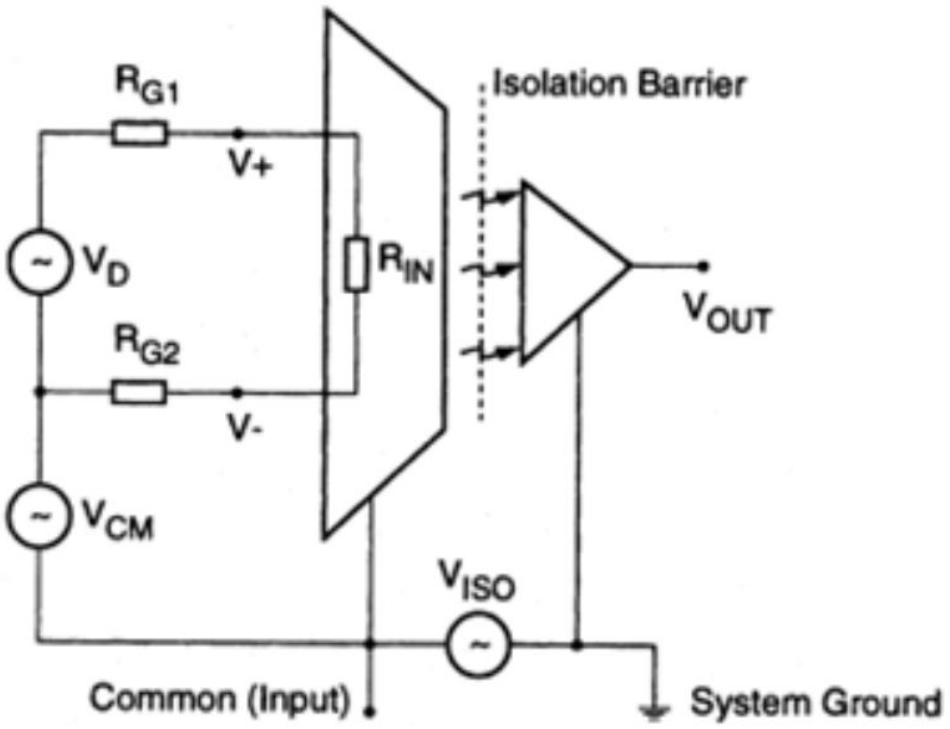

Figure 12 Isolation Amplifier Circuit Diagram (Kester, 2012)

An isolation amplifier serves as a buffer between two portions of a circuit to ensure the rightmost portion of the circuit does not influence the currents and voltages in the leftmost portion of the circuit. There are many different methods of achieving electrical isolation, but one common technique is to modulate the input signal and then demodulate to obtain the output signal. The input signal is duty-cycle modulated and then transmitted digitally across the isolation barrier. The output section of the isolation amplifier receives the duty-cycle modulated signal, converts the signal back to an analog voltage, and removes the ripple component that generated in the demodulation produced (Analog Devices, 2019). The basic concept of an isolation amplifier is visually depicted in Figure 12.

2.3.3 Bandpass Filter

To ensure the signal is smooth and contains minimal noise we needed to filter the signal by utilizing a bandpass filter. The physiological signal will contain multiple forms of noise. Noise can be produced from other muscles throughout the body, from heat in the electronics, and from the 60 Hz input power interference. A popular method used to filter out the many forms of noise is through high-pass and low-pass filtering. High-pass filters are employed to remove low-frequency components such as motion artifacts, respiratory variations, and baseline wander. Low-pass filters are employed to remove high frequency muscle artifacts and external interferences. As previously stated in Section 2.1, the frequency range of a typical ECG circuit is 0.05 Hz to 100 Hz. The ECG circuit must be able to function properly for signals ranging from 0.5 mV to 5 mV in amplitude (Beckerle et al., 2019). The bandpass filter will be comprised of a high-pass filter cascaded with a low-pass filter. A high-pass filter passes signals with frequencies higher than the cut-off frequency and rejects any signals with frequencies lower than the cut-off frequency. A low-pass filter has the exact opposite effect compared to the high-pass filter. A low-pass filter passes any signal with frequencies smaller than the cut-off frequency and rejects signals with frequencies higher than the cut-off frequency.

If a high-pass filter is cascaded with a low-pass filter, the result will be a bandpass filter (see Figure 13). Bandpass filters allow signals between two specific frequencies to pass through and rejects any signal with frequencies outside of the operating range, or passband.

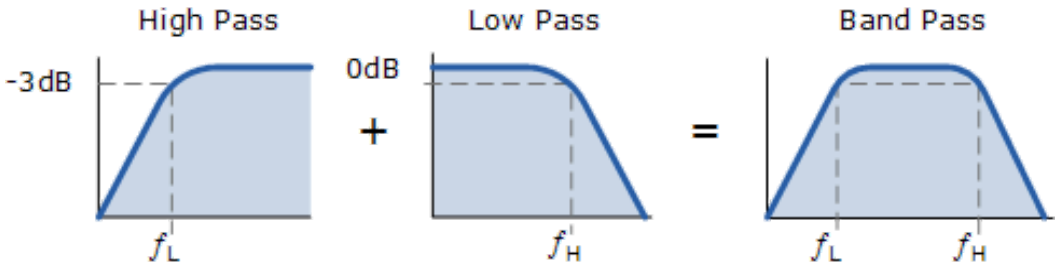

Figure 13 Bandpass Filter Comprised of High-pass and Low-pass Filters (Thompson, 2006)

Out of the many filter topologies that exist, there are two main categories: Sallen-Key and multiple feedback. The Sallen-Key topology is typically utilized in circuits which require high-gain accuracy and low Q factors, typically less than 3. A common characteristic of the Sallen-Key topology is to design the filter with equal resistances and equal capacitances. For example, a second-order Sallen-Key filter would have $R = R_1 = R_2$ and $C = C_1 = C_2$ (Carter & Mancini, 2018). However, the resistances and capacitances do not need to be equal for Sallen-Key topology. See Figure 14 for topologies of unity-gain (gain of 1) Sallen-Key second-order high-pass and low-pass filters.

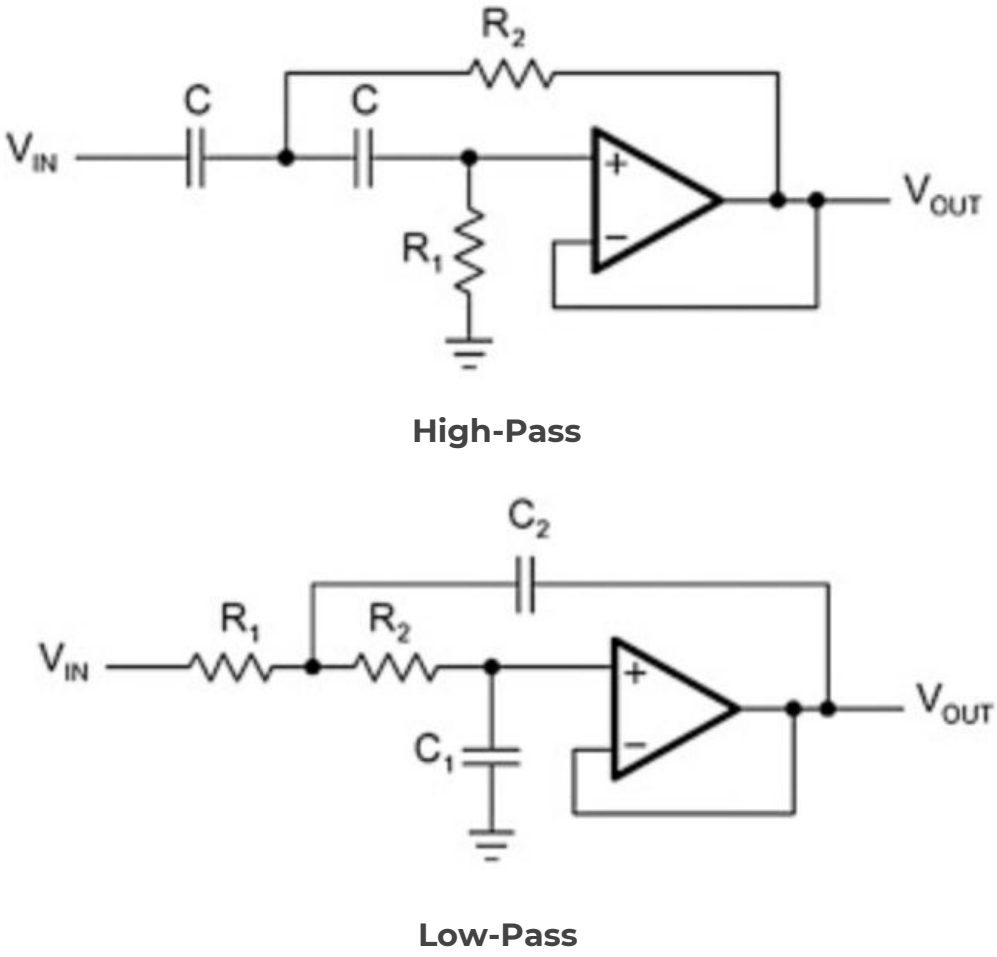

Figure 14 Unity-gain Topologies for Second-order Sallen-Key filters: High-pass (Top) & Low-pass (Bottom) (Carter & Mancini, 2018)

The multiple feedback topology is generally utilized in circuits which require high gain and high Q factors. Unlike the Sallen-key topology, multiple feedback filters have unequal resistances and capacitances. For a second-order multiple feedback high-pass filter $C_1 = C_2 \neq C_3$ and $R_1 \neq R_2$. For a second-order multiple feedback low-pass filter $R_1 \neq R_2 \neq R_3$ and $C_1 \neq C_2$ (Carter & Mancini, 2018). See Figure 15 for unity-gain multiple feedback high-pass and low-pass filters.

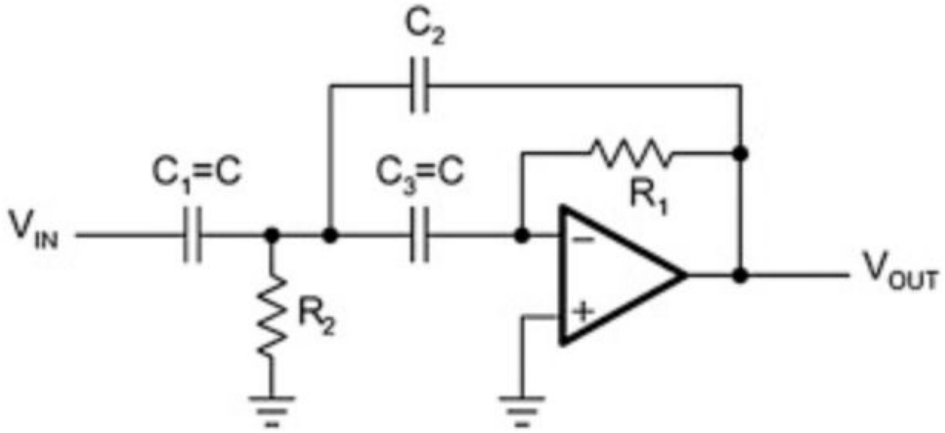

High-Pass

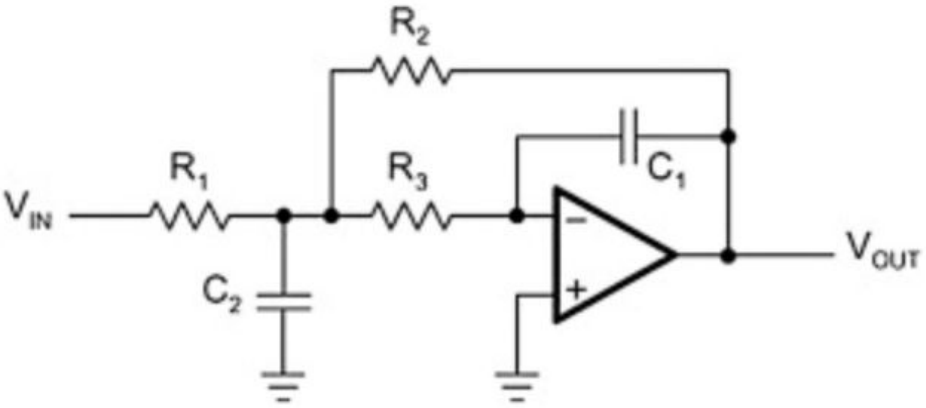

Low-Pass

Figure 15 Unity-gain Topologies for Second-order Multiple Feedback filters: High-pass (Top) & Low-pass (Bottom) (Carter & Mancini, 2018)

In a typical ECG circuit, active high-pass and low-pass filters are utilized. Out of the many forms of active filters, there are four common types: Bessel, Butterworth, Chebyshev (Type I), and Elliptic filters. Bessel filters are all-pole filters, which means that their transfer functions have no zeros. Bessel filters have no ripples in the passband and stopband in their frequency responses. The Bessel filter is optimized to obtain better transient responses due to a linear phase, or constant delay, in the passband. As a consequence, Bessel filters will have relatively poorer frequency responses, or less amplitude discrimination (Thompson, 2014). The poles of the Bessel filter can be found by locating all of the poles on a circle and separating their imaginary parts by $\frac{2}{n}$, where n is the number of poles. The distance between the top and bottom poles are determined by where the circle crosses the jω axis by $\frac{1}{n}$, or half the distance between the other poles (Zumbahlen, 2008).

Butterworth filters are also all-pole filters and their frequency responses are monotonically flat within the passbands and stopbands. The Butterworth filter is the best compromise between attenuation and phase response. To attain the Butterworth filter's ideal flatness, the filter has a relatively wide transition region from passband to stopband, with average transient characteristics (Zumbahlen, 2008). The sharpness of the roll-off from the passband to the stopband is determined by the order of the Butterworth filter. Due the square response of a Butterworth filter, there is no phase shift and the amplitude is attenuated by a factor of two at the cutoff frequency (Emery & Thomson, 2014). The poles of the Butterworth filter can be found by:

$$-\sin\frac{(2K-1)\pi}{2n} + j\cos\frac{(2K-1)\pi}{2n} \quad K = 1, 2 \ldots n$$

Equation 2 Pole Positions for Butterworth Filter (Thompson, 2014)

where K is the pole pair number and n is the number of poles. The poles are equidistant from one another, which means that the angles between the poles are equal (Thompson, 2014).

Chebyshev (Type I) filters, similar to Bessel and Butterworth filters, are also all-pole filters. However, a Chebyshev (Type I) filter's frequency response has ripples in its passband or stopband which is a trade-off for the Chebyshev (Type I) filter's smaller transition region

compared to Butterworth filters. The Chebyshev (Type I) filter minimizes the height of the maximum ripple, which is the Chebyshev (Type I) criterion. The poles of the Chebyshev (Type I) filter can be found by moving the poles of the Butterworth filter to form an ellipse. The real part of the pole is multiplied by K_r and the imaginary part of the pole is multiplied by K_I. K_r and K_I are found by utilizing the following equations:

$$K_r = \sinh A$$

Equation 3 (Zumbahlen, 2008)

$$K_I = \cosh A$$

Equation 4 (Zumbahlen, 2008)

where:

$$A = \frac{1}{n} \sinh^{-1} \frac{1}{\varepsilon}$$

Equation 5 (Zumbahlen, 2008)

where n is the filter order and:

$$\varepsilon = \sqrt{10^R - 1}$$

Equation 6 (Zumbahlen, 2008)

where:

$$R = \frac{R_{dB}}{10}$$

Equation 7 (Zumbahlen, 2008)

where R_{dB} is the passband ripple in dB. Typically, Chebyshev filters are normalized so that the edge of the ripple band is at normalized angular cut-off frequency of $\omega_o = 1$.

The 3dB bandwidth is given by:

$$A_{3dB} = \frac{1}{n} \cosh^{-1} \frac{1}{\varepsilon}$$

Equation 8 (Zumbahlen, 2008)

Now, the amplitude, step, and impulse responses of the three all-pole filters (Bessel, Butterworth, and Chebyshev (Type I)) will be compared. Figure 16 portrays the amplitude response of an eight pole 0.5dB ripple filter comparison of the Bessel, Butterworth, and Chebyshev (Type I) filters. Figure 17 portrays the step and impulse responses of the same filter. The responses have been normalized for a cut-off frequency (f_c) of 1 Hz. It is easy to see in Figure 16 that amplitude discrimination (the ability to distinguish between the desired signal from noise and other signals) increases in quality with Bessel as the poorest and Chebychev (Type I) as the best (Zumbahlen, 2008). The Bessel signal starts to attenuate at frequencies much lower than the cut-off frequency of 1 Hz, while the Chebyshev (Type I) signal seems to attenuate almost immediately at 1 Hz. The Butterworth signal attenuates only slightly before the Chebyshev (Type I) signal, which is why it is a close second.

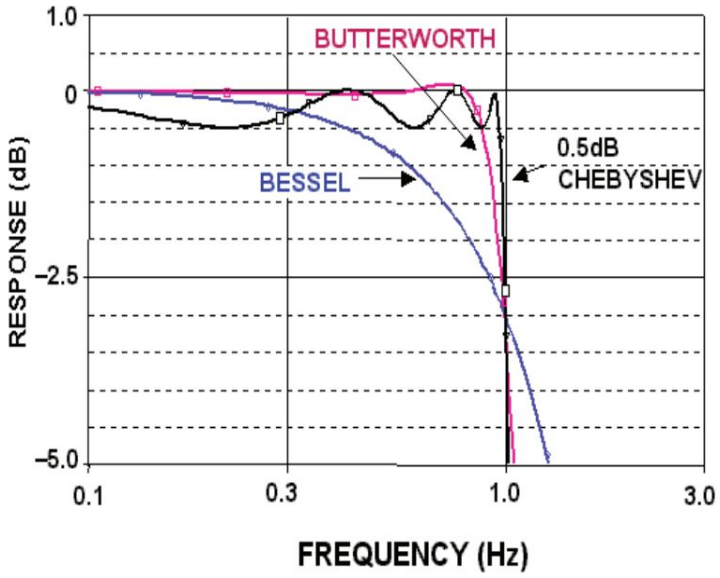

Figure 16 Comparison of Amplitude Response of Bessel, Butterworth, and Chebyshev (Type I) Filters (Zumbahlen, 2008)

Filters with better amplitude responses have poorer time responses. This trade-off phenomenon is evident in Figure 17. The transient behavior increases in quality with Chebychev (Type I) as the poorest and Bessel as the best. The left graph in Figure 17 portrays a step response comparison of all three filters. The Chebyshev (Type I) signal does not even remotely emulate a step response due to its gradual transition and multiple ripples. The Bessel signal has a very sharp transition which closely reproduces a step response. The Butterworth signal looks very similar to the Chebyshev (Type I) signal; it is only slightly better due to its decrease in ripples at a faster rate. The right graph in Figure 17 portrays an impulse response comparison of all three filters. The Bessel signal has a large, narrow initial impulse and immediately transitions into a very steady signal. The Chebyshev (Type I) signal has a smaller, wider initial impulse and has many ripples. The Butterworth signal has a slightly larger, more narrow initial impulse with fewer ripples compared to the Chebyshev (Type I) signal.

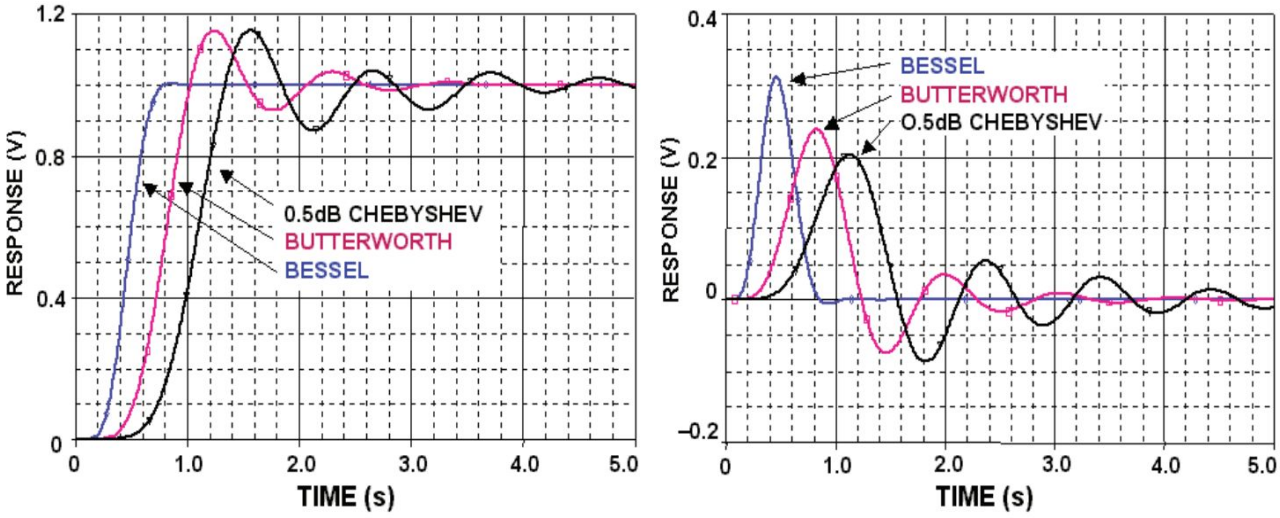

Figure 17 Comparison of Step (Left) and Impulse (Right) Responses of Bessel, Butterworth, and Chebyshev (Type I) Filters (Zumbahlen, 2008)

Elliptic filters are not all-pole filters, meaning their transfer functions contain zeros. Elliptic filters have shorter transition regions than the previously mentioned filters because there are ripples in both the passbands and stopbands. The zeros also mean that the attenuation will be very high in the stopband and "there will be some 'bounceback' of the stopband response

between the zeros" (Zumbahlen, 2008). This "bounceback" is the stopband ripple. The poles of an Elliptic filter lie on an ellipse, which means that the time domain responses are degraded, similar to Chebyshev filters. The mathematical operations behind an Elliptic filter are much more complicated than Bessel, Butterworth, and Chebyshev filters. It is not simple to solve for poles and zeros. Alternatively, the modulation angle, θ, which determines the rate of attenuation is also an alternative method to defining the filter order, n:

$$\theta = \sin^{-1} \frac{1}{F_s}$$

Equation 9 (Zumbahlen, 2008)

Another important parameter to solve for is ρ, which determines the passband ripple:

$$\rho = \sqrt{\frac{\varepsilon^2}{1 + \varepsilon^2}}$$

Equation 10 (Zumbahlen, 2008)

where ε is the ripple factor and the passband ripple is defined by:

$$R_{dB} = -10 \log(1 - \rho^2)$$

Equation 11 (Zumbahlen, 2008)

As the ripples of the Elliptic filter response increase, the value of A_{min}, the minimum attenuation in the stopband, increases as well. Also, as θ approaches 90°, the stopband frequency (F_s) approaches the cut-off frequency (F_c). When this occurs, the result is an extremely short transition region, which results in sharp rolloff. The trade-off is a lower value of A_{min}. Lastly, ρ determines the input resistance for a passive Elliptic filter, which then relates to the VSWR, or Voltage Standing Wave Ratio (Zumbahlen, 2008).

2.3.4 Notch Filter

A notch filter, also known as a bandstop filter or band-reject filter, is utilized to attenuate signals within a specific band of frequencies (stopband). All frequencies greater than or fewer than the stopband will not attenuate. Figure 18 depicts the role of a notch filter, where frequencies between f_1 and f_2 are attenuated and all frequencies less than f_1 and greater than f_2 are passed.

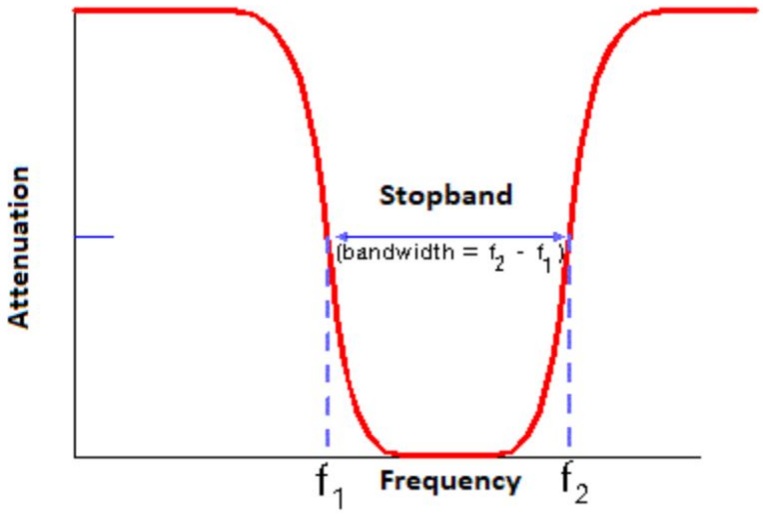

Figure 18 Example of the Role of a Notch Filter (Winder, 2008)

There are three different cases of notch filter characteristics: standard notch, high-pass notch, and low-pass notch. These cases are determined based on the relationship between the pole frequency (ω_0) and the zero frequency (ω_z). A standard notch occurs if the pole frequency is equal to the zero frequency ($\omega_0 = \omega_z$). A high-pass notch occurs if the pole frequency is greater than the zero frequency ($\omega_0 > \omega_z$). A low-pass notch occurs if the zero frequency is greater than the pole frequency ($\omega_z > \omega_0$) (Zumbahlen, 2008). Figure 19 depicts the frequency responses of the three different cases of notch filter characteristics.

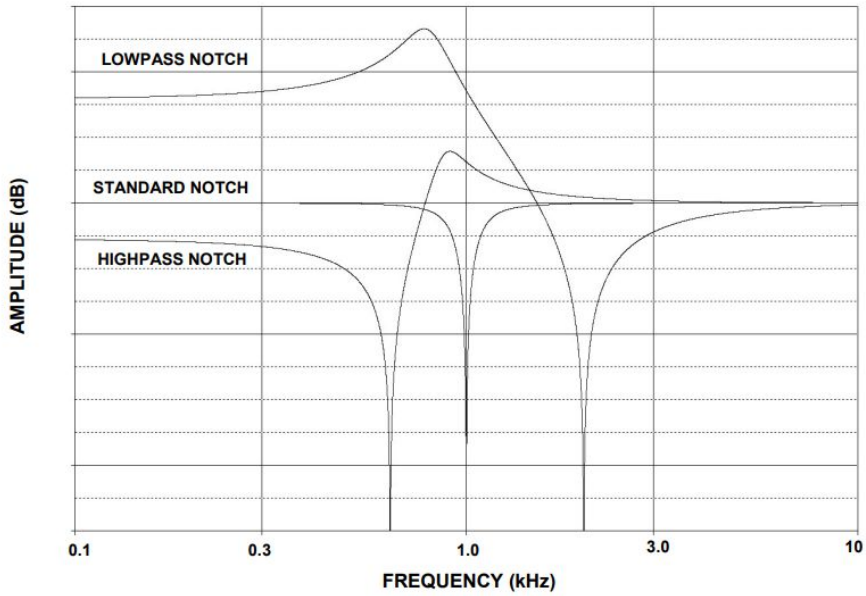

Figure 19 Comparison of Standard, High-pass, and Low-pass Notches (Zumbahlen, 2008)

Out of the many different configurations of notch filters, there are four common designs: 1 - Bandpass (1 - BP), Bainter, Boctor, and twin T. The 1 - BP notch filter is built as a bandpass filter whose output is subtracted from the input of the filter. There are two different configurations of the bandpass filter. The bandpass filter can either be inverting, similar to multiple-feedback topology (see Figure 20) or non-inverting, similar to Sallen-Key topology (see Figure 21). These configurations are important depending on which topology is being utilized to ensure that the output of the bandpass filter is being subtracted from, not added to, the input (Zumbahlen, 2008).

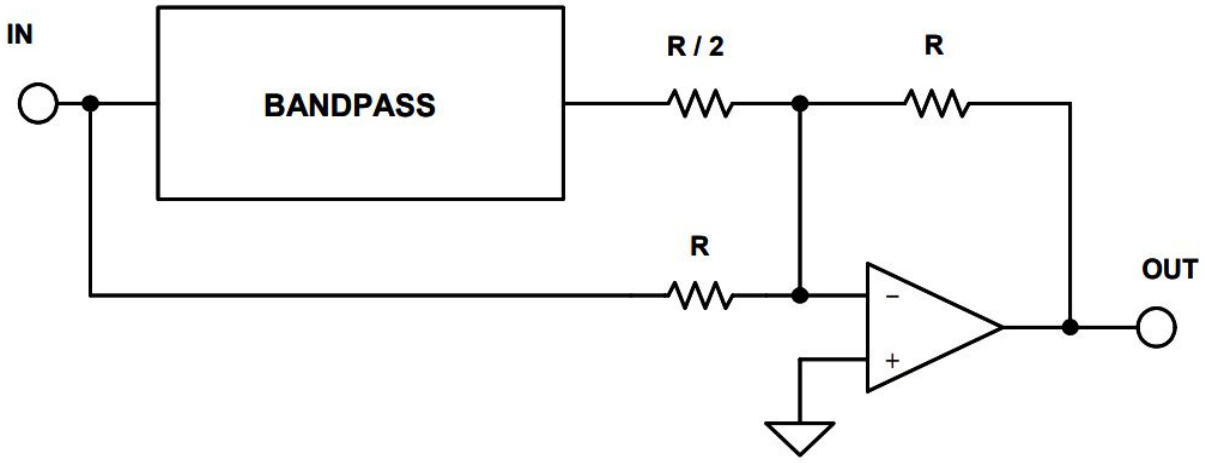

Figure 20 General Configuration for Inverting 1 - Bandpass Filter (Zumbahlen, 2008)

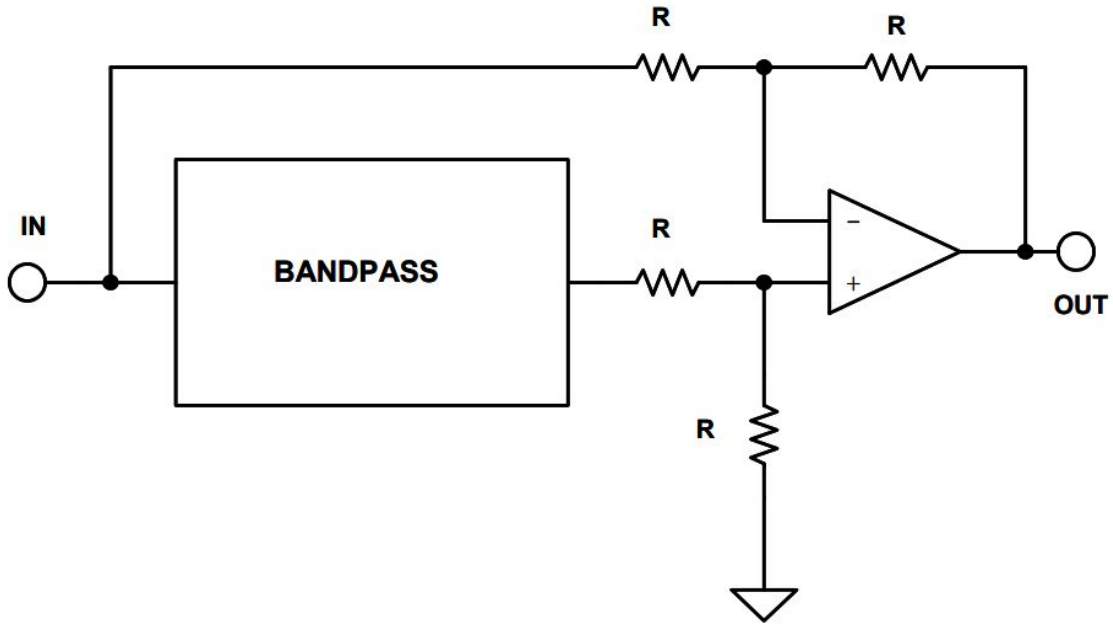

Figure 21 General Configuration for Non-inverting 1 - Bandpass Filter (Zumbahlen, 2008)

The Bainter filter is a simple notch filter which is composed of circuit blocks with two feedback loops. The Q factor of the Bainter filter is not determined by the resistance and capacitance values in the circuit, unlike other notch filters, and therefore the Bainter filter has low component sensitivity. The Q factor is dependent solely on the gains of the amplifiers in the circuit, which means that the notch depth, or amplitude of the notch, will not drift with

temperature, aging, and other environmental factors. However, the notch frequency may shift (Zumbahlen, 2008). See Figure 22 for the general configuration of a Bainer notch filter. R6 tunes the Q factor and R1 tunes the zero frequency (ω_z). Changing the value of R3 determines the ratio of pole frequency to zero frequency (ω_0 / ω_z). If R3 = R4, then the notch filter produces a standard notch. If R3 > R4, then the notch filter produces a high-pass notch, and if R3 < R4, then the notch filter produces a low-pass notch (Zumbahlen, 2008).

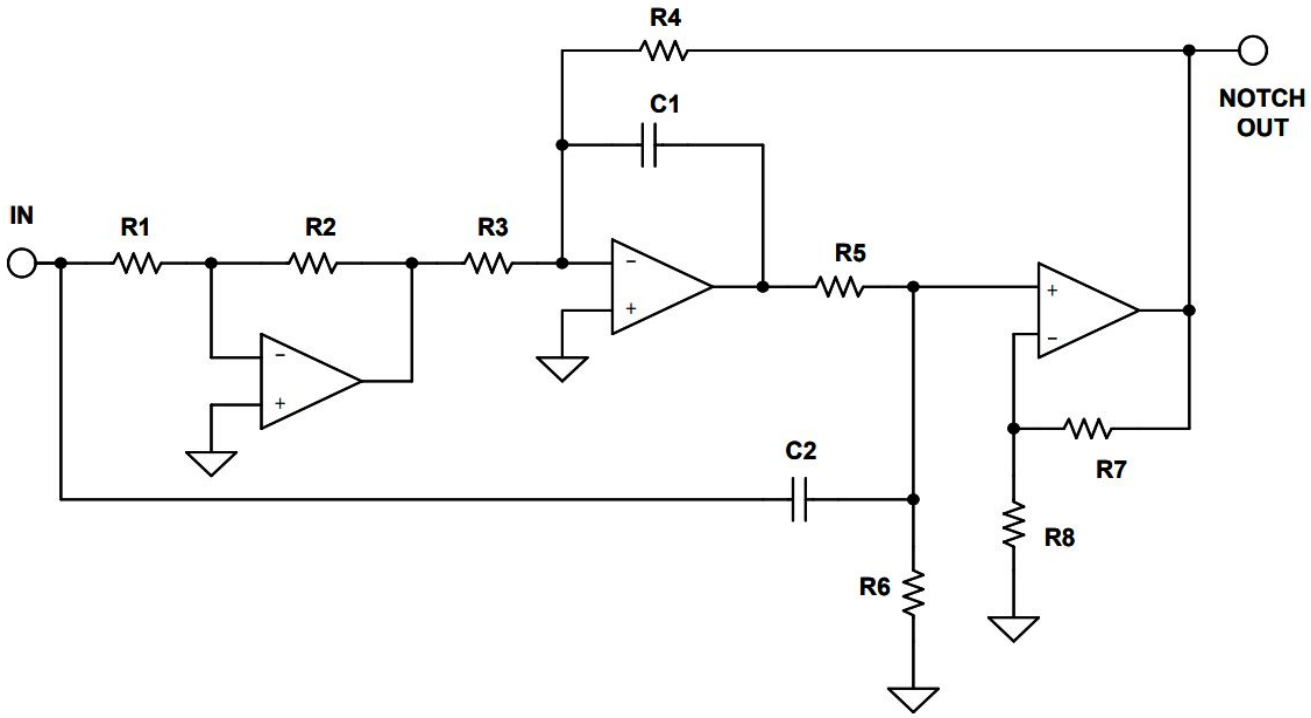

Figure 22 General Configuration of Bainter Notch Filter (Zumbahlen, 2008)

The Boctor notch filter only utilizes one operational amplifier, but has a relatively large amount of components in a moderately intricate configuration. The number of components utilized in the Boctor filter allows flexibility when it comes to component value selection. Boctor filers have low sensitivity and also possess the ability to tune the parameters of the filter independently to an extent. There are two different configurations of a Boctor filter: a high-pass notch (see Figure 23) and a low-pass notch (see Figure 24).

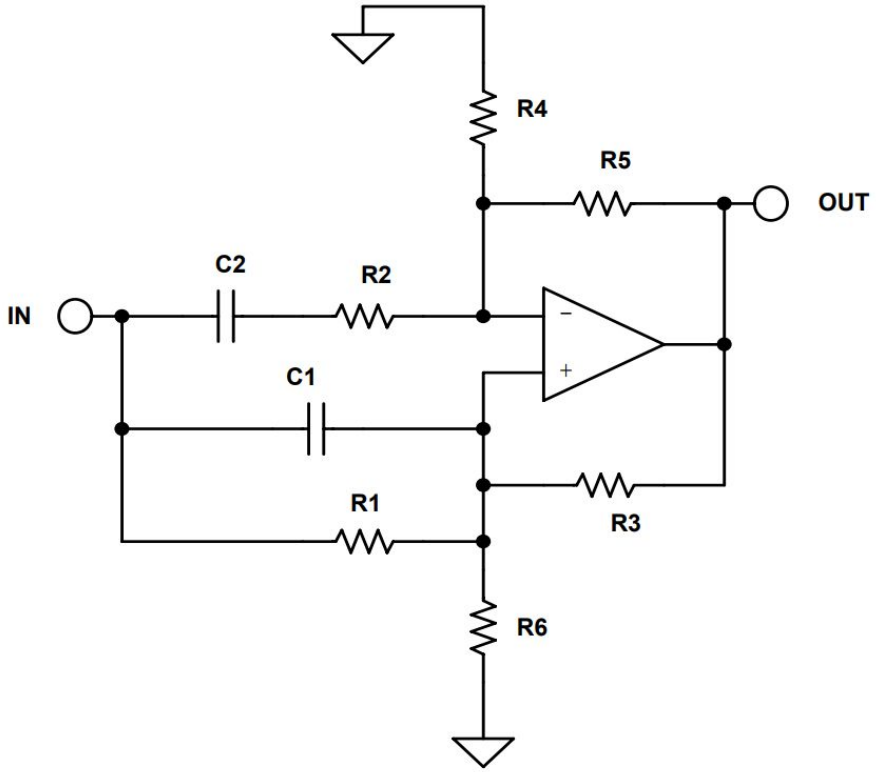

Figure 23 General Configuration of Boctor High-pass Notch Filter (Zumbahlen, 2008)

A circuit gain is required for a high-pass Boctor notch filter. The following must be true for the circuit to be considered a high-pass Boctor notch filter:

$$Q < \frac{1}{1 - \frac{\omega_z^2}{\omega_0^2}}$$

Equation 12 (Zumbahlen, 2008)

A high-pass Boctor notch filter can be comprised of only one amplifier and two capacitors, which can be the same value. The pole and zero frequencies (ω_0 and ω_z) are completely independent of the gain of the amplifier (Zumbahlen, 2008).

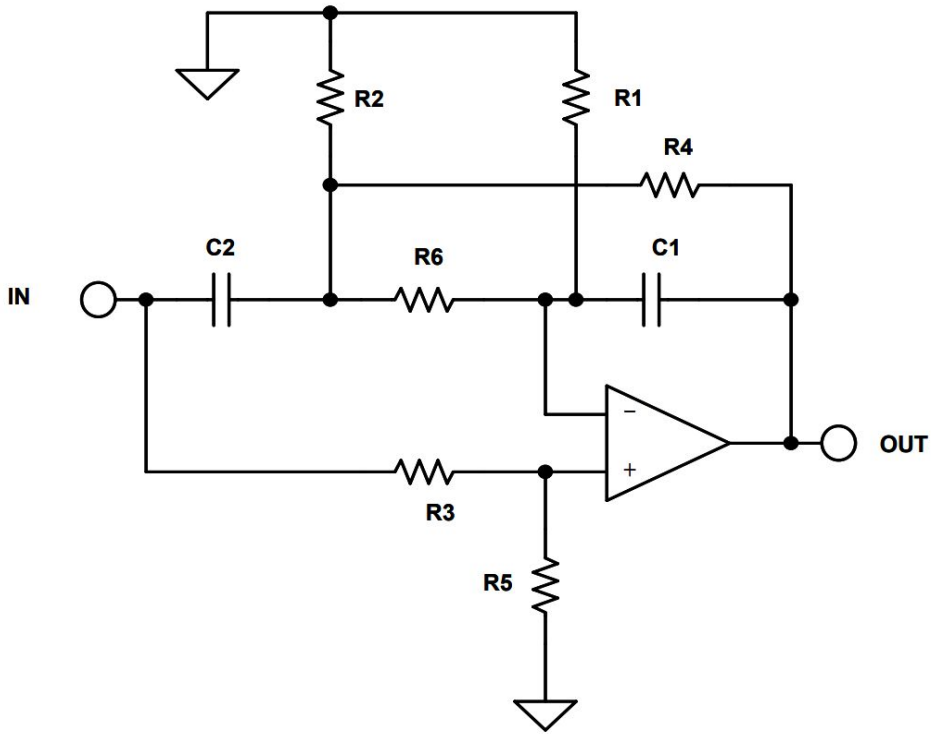

Figure 24 General Configuration of Boctor Low-pass Notch Filter (Zumbahlen, 2008)

For a low-pass Boctor notch filter, R4 tunes the pole frequency (ω_0), R2 tunes the Q factor of the poles (Q_0), R3 tunes the Q factor of the zeros (Q_z), and R1 tunes the zero frequency (ω_z) (Zumbahlen, 2008). In order for the filter to work properly with the desired components, the following must be true about parameter k1, the gain factor:

$$\frac{\omega_0^2}{\omega_z^2} < k1 < 1$$

Equation 13 (Zumbahlen, 2008)

The twin T notch filter is the most commonly utilized notch filter. A passive twin T notch filter does not have any amplifiers in its configuration, meaning there is no feedback. Passive twin T notch filters (see Figure 25) have a fixed Q factor of 0.25 (Zumbahlen, 2008).

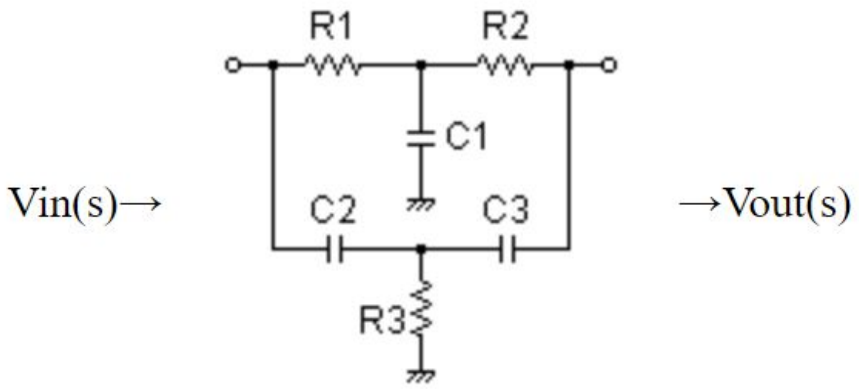

Figure 25 General Configuration of a Passive Twin T Notch Filter (Okawa Electric Design, 2019)

An active twin T notch filter contains positive feedback to the reference node. Unlike the passive twin T notch filter, the active configuration has a variable Q factor, which is determined by the ratio R4/R5. This ratio also determines the notch depth of the filter signal. To reach a maximum notch depth, resistors R4, R5, and the associated operational amplifier can be eliminated. If this were to happen, then the node connecting R3 and C3 would be directly connected to the output. See Figure 26 for a general configuration of an active twin T notch filter.

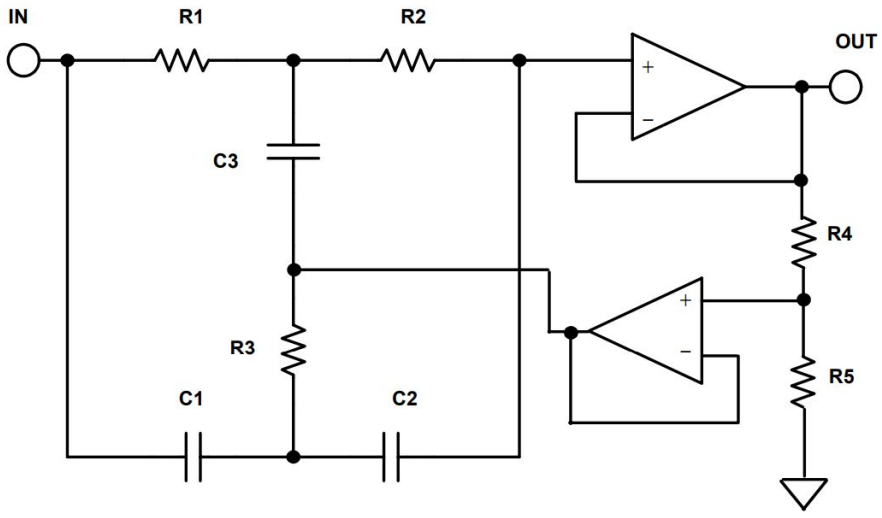

Figure 26 General Configuration of an Active Twin T Notch Filter (Zumbahlen, 2008)

3. Methods

3.1 Display

The "Touch Tomorrow" event is a free, educational event hosted by WPI for community partners, supporters, or individuals with a passion for science to assist in inspiring the next generation of problem solvers. This event is an opportunity for individuals to display their work and/or nifty, interactive exhibits to students from grades K-12 with the purpose of sparking interest in the STEM fields, as shown in Figure 27 (Worcester Polytechnic Institute, 2019).

Figure 27 WPI's Touch Tomorrow Event Spring of 2019 (Worcester Polytechnic Institute, 2019)

Our team plans to feature our project at this event to depict how biomedical instrumentation and electrical and computer engineering overlap within the STEM fields through an interactive project with which children of all ages can participate. Our team created custom parts from Elenco Electronics Snap-Circuit components to produce a simple ECG circuit, shown in Figure 28. Students at the event will be able to recreate the circuit by using the available snap-circuit pieces on display. Once the students complete their circuit, they will have the opportunity to measure their own ECG and view the signal which will be displayed on an oscilloscope.

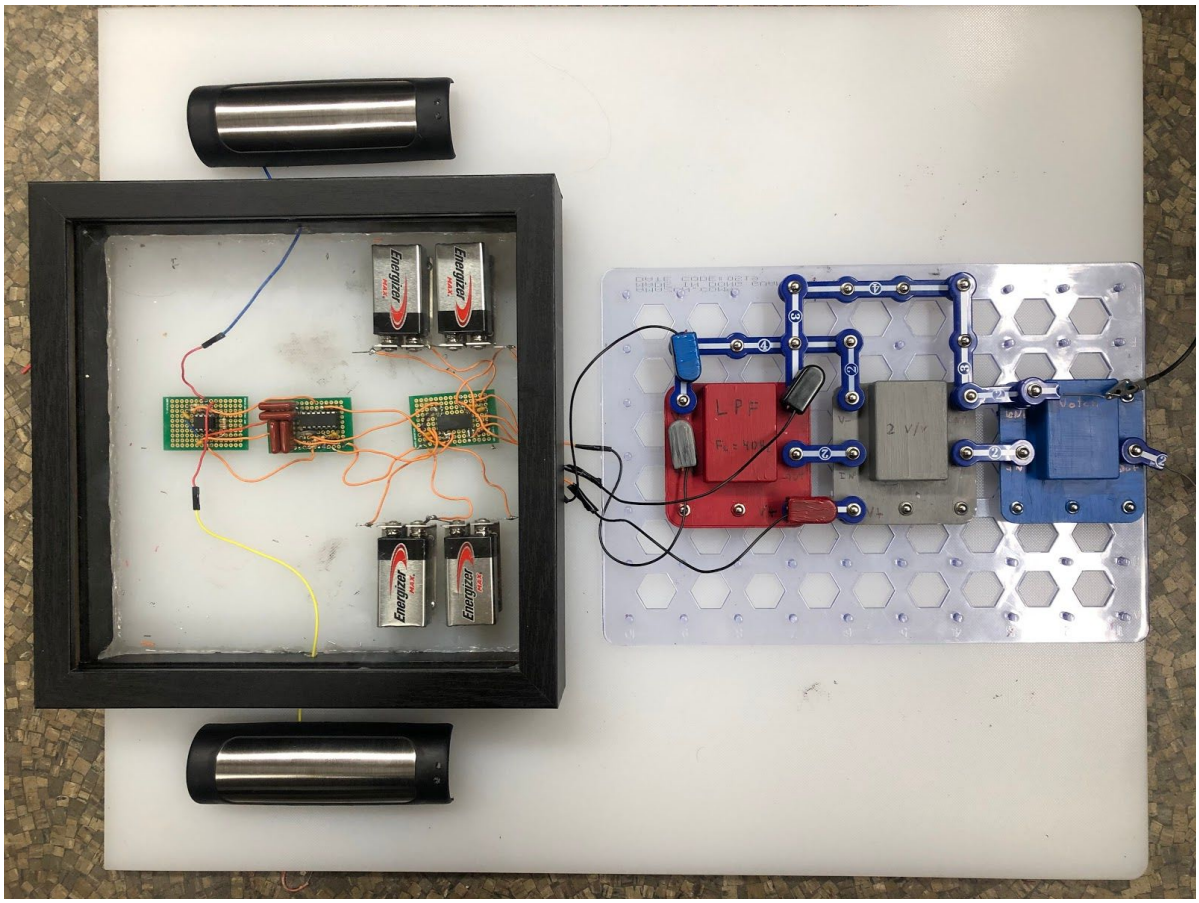

Figure 28 Completed ECG Snap Circuit

3.2 ECG Circuit Design

The main goal of the "Touch Tomorrow" event is to provide interesting, interactive projects to excite and inspire the participants. To ensure our display was interactive, we provided different values for certain stages of our ECG circuit for participants to choose from, which let them have the freedom to create their own semi-custom ECG circuit. Referencing Figure 29, there are two different portions of the ECG circuit we designed. The isolated section of the circuit (instrumentation amplifier, high-pass filter, and isolation amplifier) will be hardwired and enclosed in a clear case to prevent participants from altering the circuitry. The interactive portion will consist of the earth-grounded components (low-pass filter, gain stage, and notch filter). These stages will be enclosed within Elenco Electronics Snap-Circuit pieces for participants to place sequentially to complete the ECG circuit.

To make the display even more interactive, we provided three low-pass filter modules with different cut-off frequencies (100 Hz, 70 Hz, and 40 Hz) as well as two gain stage modules with different gain settings (3 V/V and 2 V/V). For the schematic of our final ECG circuit (see Figure 30) we chose the low-pass module with a cut-off frequency of 40 Hz and the gain stage module with a gain of 2 V/V.

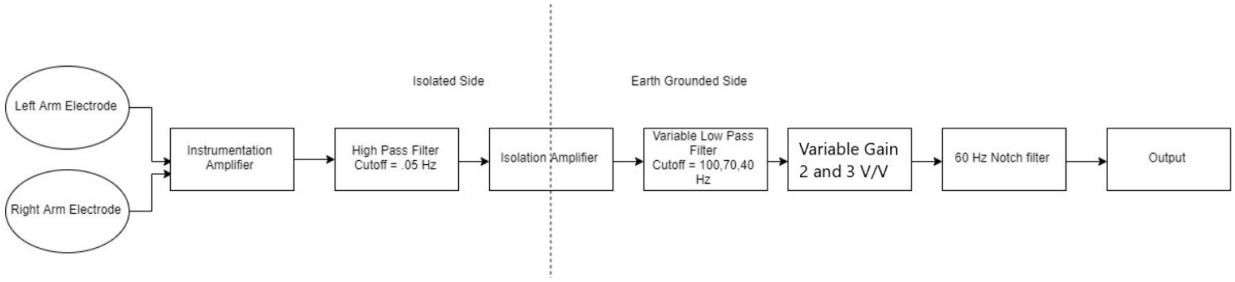

Figure 29 Block Diagram of Final ECG Circuit

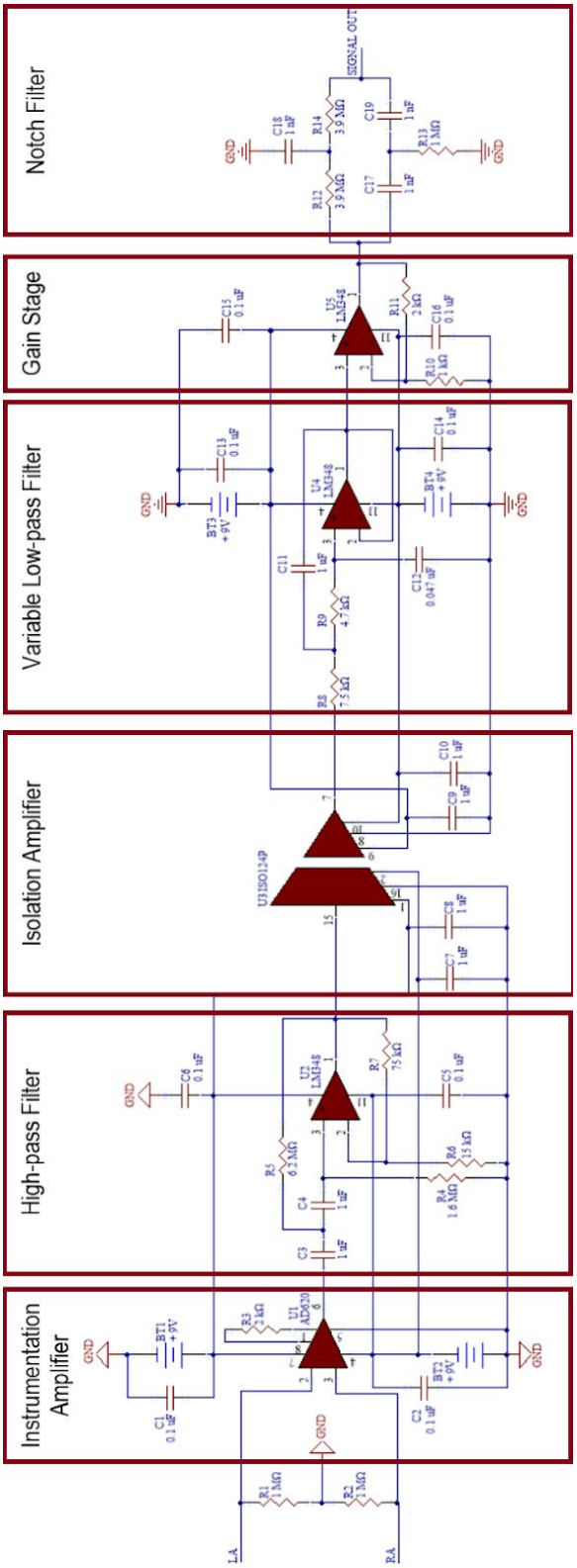

Figure 30 Schematic of Final ECG Circuit

3.2.1 Electrode Handles

In order for the participants to view their ECG signal, we provided electrodes that would transmit their signal to the ECG circuit we developed. To do so, we designed two separate iterations of electrodes for the ECG display.

First Iteration: Adhesive Electrodes

For the first iteration of our handles we utilized adhesive electrodes, similar to the electrodes featured in Figure 31, that were provided to us by our advisor Professor Edward A. Clancy. We decided to design a two-electrode ECG circuit, which would make the application of the electrodes much simpler. While three-electrode ECGs typically contain less noise, we made a compromise to ensure our product would be easy and efficient to utilize at the "Touch Tomorrow" event. Adhesive electrodes were most beneficial during testing because they were easy to implement in our circuit; we simply needed to connect the adhesive end of each electrode to the corresponding wrist (LA or RA) of the user and connect wire portions of the electrodes into each of the two inputs of the instrumentation amplifier. In terms of our display for the "Touch Tomorrow" event, we knew adhesive electrodes would be inefficient. Adhesive electrodes are not reusable which means that WPI would need to purchase the electrodes in bulk to accomodate all visitors of the event, and even then it is possible for the event to run out of them. Adhesive electrodes can also be uncomfortable to remove and this could be a possible issue when working with young children.

Figure 31 Example of Adhesive Electrodes (Farnsworth, 2019)

Second Iteration: Exercise Handle Electrodes

For our second design iteration we utilized exercise handles from an elliptical exercise machine, shown in Figure 32. These handles worked effectively as electrodes, so we utilized them in our final display. We secured these exercise handles with screws to a plastic non-conducting cutting board which we utilized as the base of our isolated front end circuitry (see Figure 29). We believed providing stationary handles for individuals to rest their hands on would be a more kid-friendly and a more efficient method of measuring ECG signals. The stationary handles would limit possible inconveniences with measuring the ECG signals compared to the adhesive electrodes.

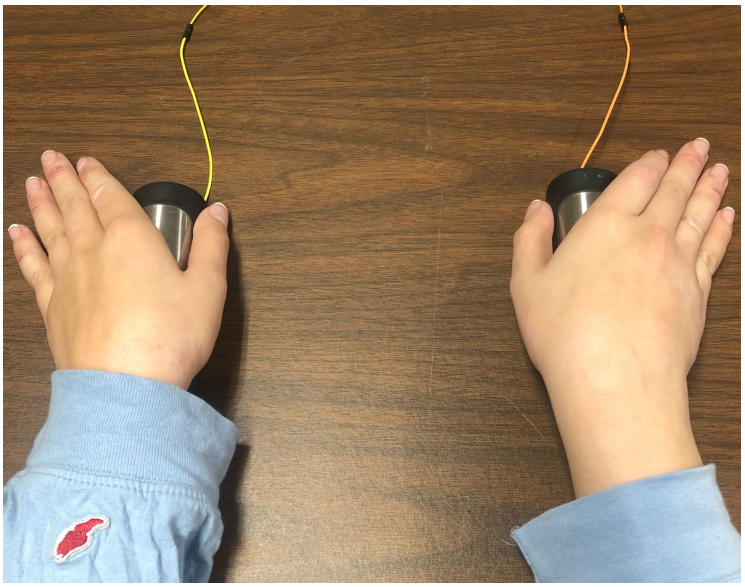

Figure 32 Exercise Handle Electrodes in Use

3.2.2 Instrumentation Amplifier Stage

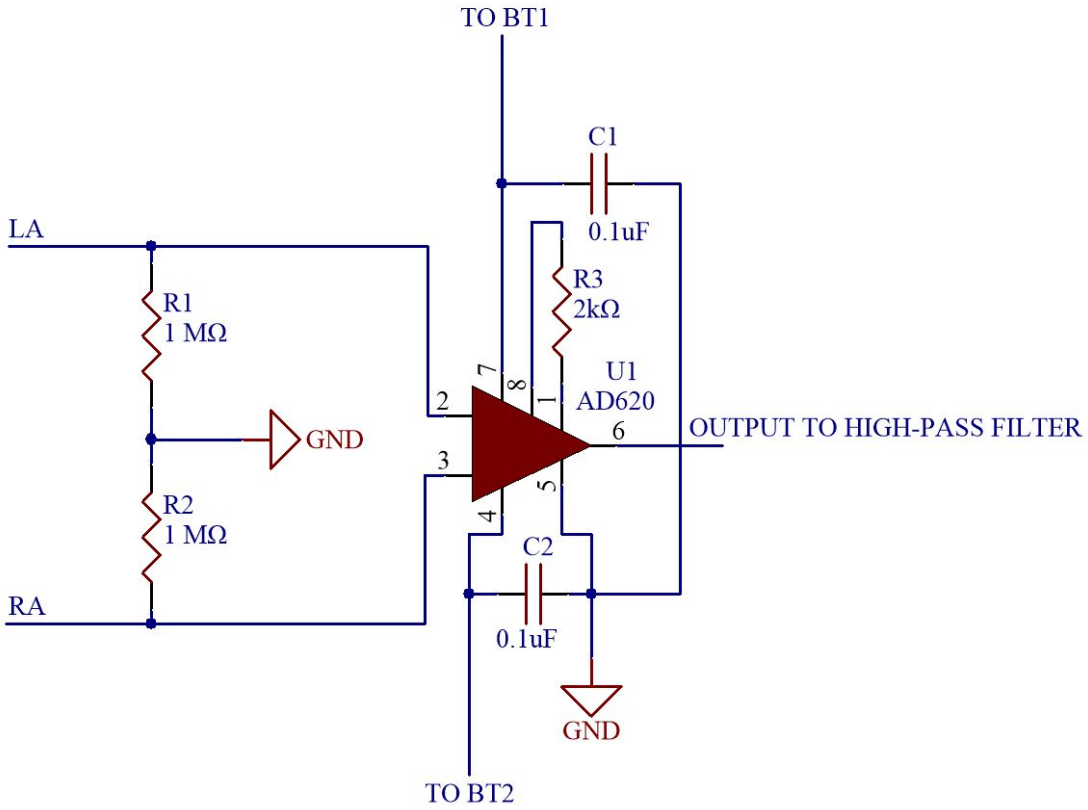

Figure 33 Schematic of Instrumentation Amplifier Stage

The instrumentation amplifier module is the first stage in the ECG circuit we created, as depicted in Figures 29 and 30. As previously mentioned in Section 3.2.1, the ECG circuit we designed was a two-electrode ECG. To design the two-electrode ECG circuit, we needed to account for the missing RL electrode, which is present in a three-electrode ECG circuit. The RL electrode represents the common ground point on the patient's body and acts as a reference for the instrumentation amplifier. Although this point is referred to as “ground” it is actually a floating voltage point on the body. In a two-electrode circuit this point is removed and instead this reference voltage is derived from the two measured potentials on the body. Referring to Figure 33, resistors R1 and R2, which connect to the instrumentation amplifier, split the voltage across the potential difference of the ECG signal and create a center reference that is the virtual driven ground point. R1 and R2 are relatively high resistor values in order to limit the current entering the ground. The ground point that is created between the junction of R1, R2, and virtual ground represents the missing third electrode and is used as a reference for the active components in the circuit.

As a team we decided to utilize an AD620 instrumentation amplifier because it has a wide power supply voltage range of $\pm$ 2.3 V to 18 V, a maximum supply current of 1.3 mA, and is capable of providing a maximum bandwidth of 120 kHz at a gain of 100 (Analog Devices). For our project we did not require the full bandwidth of 120 kHz in order to capture the signal, nor the power supply range provided. However, we preferred to employ an amplifier that could utilize additional bandwidth in addition to the fact that the amplifier was inexpensive and easily accessible.

With these parameters in mind, we utilized two 9 V batteries to create a $\pm$ 9 V dual power supply to power the AD620. In addition, we added two 0.1 μF decoupling, or bypass, capacitors to the power rails of the instrumentation amplifier (one capacitor connected from +9V (+) to ground (-) and one capacitor connected from -9V (-) to ground (+). The values of these bypass capacitors were determined by the data sheet for the AD620 (Analog Devices, 2019). The role of bypass capacitors are to short AC signals to ground to ensure that any AC noise present in DC

signals are removed. Essentially, decoupling capacitors filter out AC noise so that clean, pure DC signals travel through the circuit without any AC ripple (Kester, 2012).

After the decoupling capacitors were added to the circuit, the gain of the instrumentation amplifier needed to be determined. The gain of the AD620 was based on many factors, but mainly on the trade-off between noise reduction and amplification of the signal. We needed to apply a large enough gain in the instrumentation stage, which reduces the system's bandwidth, to diminish the noise in subsequent stages of the circuit (Gerstenhaber et al., 2015). However, there is a point at which the gain has no effect on the voltage noise, which is evident in Figure 34.

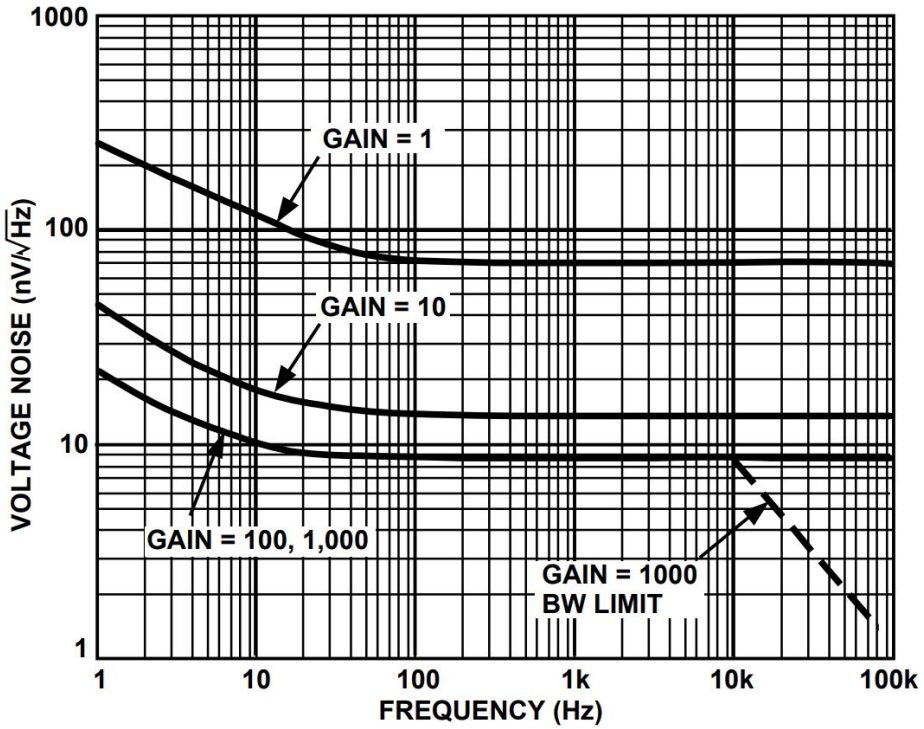

Figure 34 Voltage Noise Spectral Density vs. Frequency (G = 1 - 1000) (Analog Devices)

The increase in gain from 1 to 10 results in a great reduction in voltage noise. However, the increase in gain from 10 to 100 as well as 1,000 is the exact same. This means that as the gain increases to higher values, the voltage noise reduction gradually slows until the voltage noise reaches a point where it is constant. Based on Figure 34, we decided that we needed to choose a gain between 10 and 100 to achieve adequate noise reduction in our ECG circuit. In order to determine the gain of the AD620, we needed to take into account the voltage limitations

set by the power rails of the amplifier, ± 9V. However, due to a diode voltage drop of ± 0.7 V, the maximum voltage supplied to the circuit is

$$\pm 9\text{V} - \pm 0.7\text{ V} = \pm 8.3\text{ V}$$

We also needed to take into account the direct current (DC) offset voltage from the skin-electrode contact, which is a maximum of ± 300 mV.

We utilized the maximum DC offset voltage in our calculations to ensure that the ECG signal would never saturate, i.e., never exceed ± 8.3 V. We also had to take into account the dynamic range of an ECG signal which is 0.5 mV to 5 mV. We utilized the maximum differential voltage of an ECG signal, 5 mV, along with the maximum DC offset to calculate for the maximum input voltage into the instrumentation amplifier, which will be 305 mV. The instrumentation amplifier is powered by two 9 V batteries, which means that the maximum gain the instrumentation can hold is:

$$\frac{8.3\ V}{305\ mV} = 27.21\text{ V/V}$$

We wanted to utilize standard values based on the AD620 data sheet, therefore we utilized Equation 14 to choose a gain of 25.7 for the instrumentation stage, which is less than the maximum allowable gain of 27.21. Based on the previously mentioned equation and table, the resistor value which corresponds with a gain of 25.7 is a 2 kΩ resistor.

$$A_V = (1 + \frac{49.4k\Omega}{R_G})$$

Equation 14 Equation to solve for Gain (A_V) using an AD620 (Analog Devices)

In order to analyze the instrumentation amplifier we utilized Figure 35 in conjunction with Kirchhoff's Voltage Law, Kirchhoff's Current Law, and Ohm's Law. We utilized an input differential voltage of 5 mV plus a 300 mV DC offset in our calculations to ensure that the output signal of the instrumentation amplifier would not saturate. This input voltage represents the voltage across R_G, or v_G plus the DC offset.

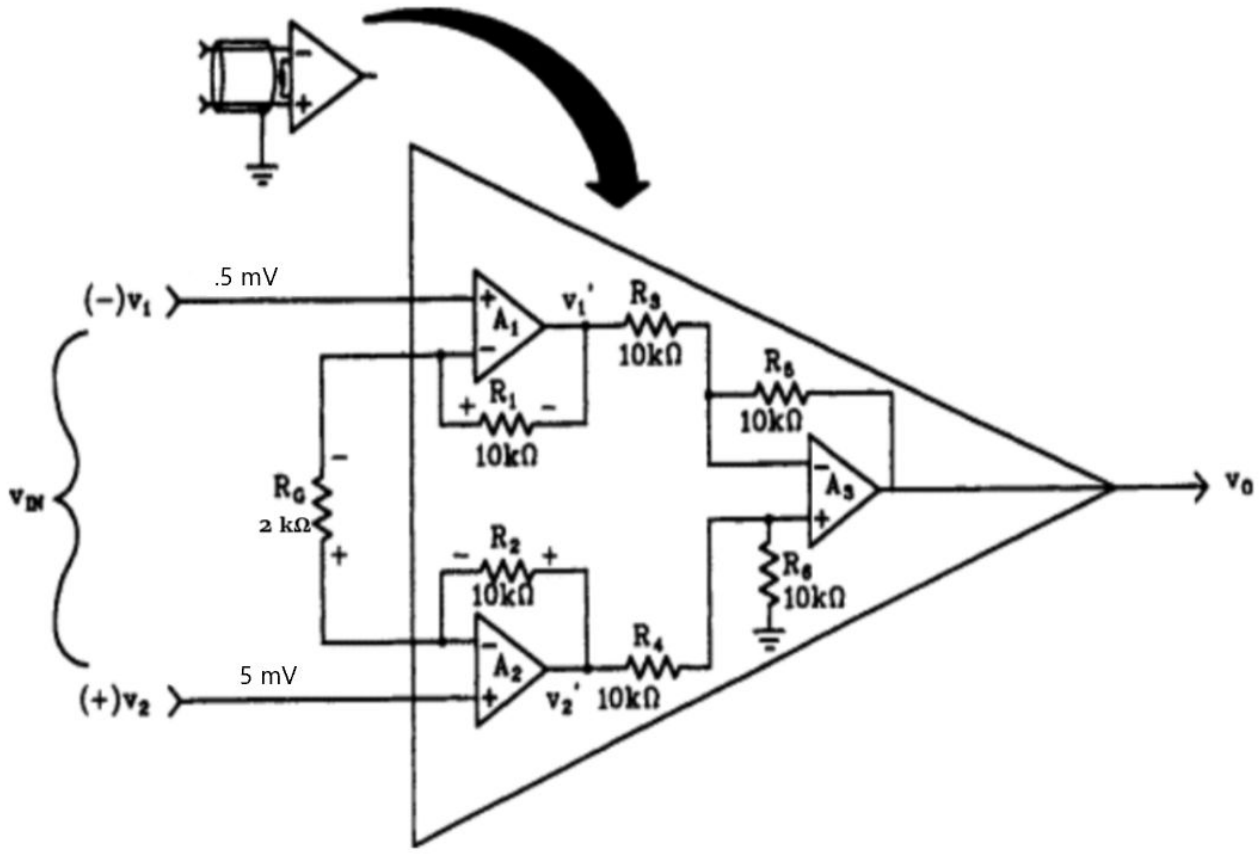

Figure 35 Basic Instrumentation Amplifier used for Numerical Analysis (Terrell, 1996)

We then utilized the values we found for R_G and v_G to calculate the current through R_G utilizing Ohm's Law for the worst-case scenario:

$$i_G = \frac{v_G}{R_G} = \frac{(5\ mV + 300\ mV)}{2\ k\Omega} = 152.5\ \mu A$$

After the current travels through the gain resistor, it must flow through the feedback resistors of amplifiers A_1 and A_2 because current cannot flow in or out of ideal amplifier inputs. We utilized Ohm's law to determine the resulting voltage drop across the feedback resistors:

$$v_{R1} = v_{R2} = i_G * R_1 = 152.5\ \mu A * 24.7\ k\Omega = 3.76675\ V$$

We then solved for the voltage at the output of A_1 and A_2 by utilizing Kirchkoff's Voltage Law. The DC offset was added to each of the input voltages, v_1 and v_2:

$$v'_1 = v_1 - v_{R1} = (0\ \text{mV}) - 3.76675\ \text{V} = -3.76675\ \text{V}$$

$$v'_2 = v_2 + v_{R2} = (300\ \text{mV} + 5\ \text{mV}) + 3.76675\ \text{V} = 4.07175\ \text{V}$$

These voltages are then fed into a differential amplifier. The output of a differential amplifier is simply the difference of the two inputs:

$$v_o = (v'_2 - v'_1) = 4.07175\ \text{V} - (-3.76675\ \text{V}) = 7.8385\ \text{V}$$

In order to support the output voltage we calculated utilizing Equation 3, we utilized algebraic manipulations to determine the equation for the voltage gain of the instrumentation amplifier:

$$v'_1 = v_1 - v_{R1}$$

$$v'_2 = v_2 + v_{R2}$$

$$i_G = \frac{v2 - v1}{R_G}$$

$$v_{R1} = i_G * R_1 = \frac{(v2 - v1) * R1}{R_G}$$

$$v_{R2} = i_G * R_2 = \frac{(v2 - v1) * R2}{R_G}$$

$$v_o = v'_2 - v'_1$$

We then utilized substitution in order to get the following equations:

$$v_o = (v_2 + v_{R2}) - (v_1 - v_{R1})$$

$$= \left[v_2 + \frac{(v2 - v1) * R2}{R_G} \right] - \left[v_1 + \frac{(v2 - v1) * R1}{R_G} \right]$$

$$= \left[(v_2 - v_1) + \frac{(R1 + R2) * (v2 - v1)}{R_G} \right]$$

Since R1 = R2, we can replace (R1+R2) = 2R:

$$v_o = (v_2 - v_1) + \frac{2R * (v2 - v1)}{R_G} = \frac{R_G (v2 - v1) + 2R * (v2 - v1)}{R_G}$$

$$= \frac{(v2 - v1) * (2R + R_G)}{R_G} = (v_2 - v_1) * \frac{(2R + R_G)}{R_G}$$

$$= (v_2 - v_1) * \left(\frac{2R}{R_G} + \frac{R_G}{R_G} \right) = (v_2 - v_1) * \left(1 + \frac{2R}{R_G}\right)$$

The equation we derived above matches the universal equation for the output of instrumentation amplifiers and we utilized the values we measured and calculated to determine the output of our instrumentation amplifier:

$$v_o = (v_2 - v_1) * \left(1 + \frac{2R}{R_G}\right)$$

$$= (300 \text{ mV} + 5 \text{ mV}) * \left(1 + \frac{2 * (24.7\ k\Omega)}{2\ k\Omega}\right) = 7.8385 \text{ V}$$

We were able to support that the equation we derived and the mathematical operations we computed through Kirchhoff's Voltage Law, Kirchhoff's Current Law, and Ohm's Law resulted in the same output of $v_o = 7.8385$ V.

Once we had a finalized design for our instrumentation amplifier stage, we were able to build a perforated breadboard prototype to be utilized in the analog front end of the finalized ECG circuit (see Figure 36).

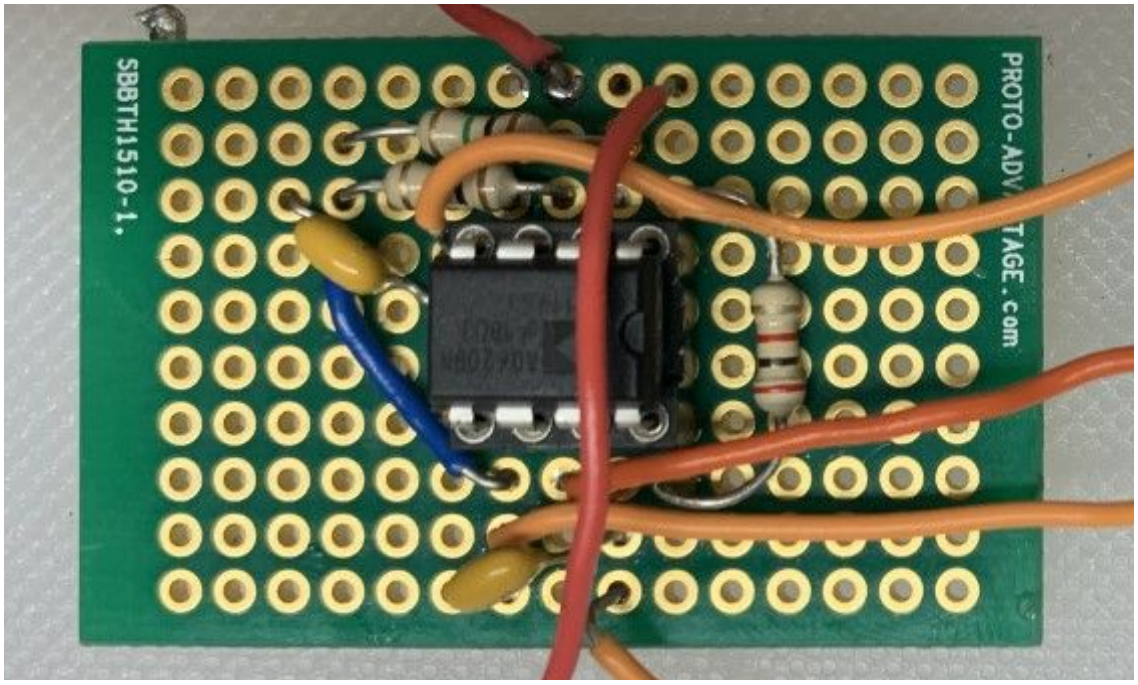

Figure 36 Physical Implementation of Instrumentation Amplifier Stage

3.2.3 High-pass Filter

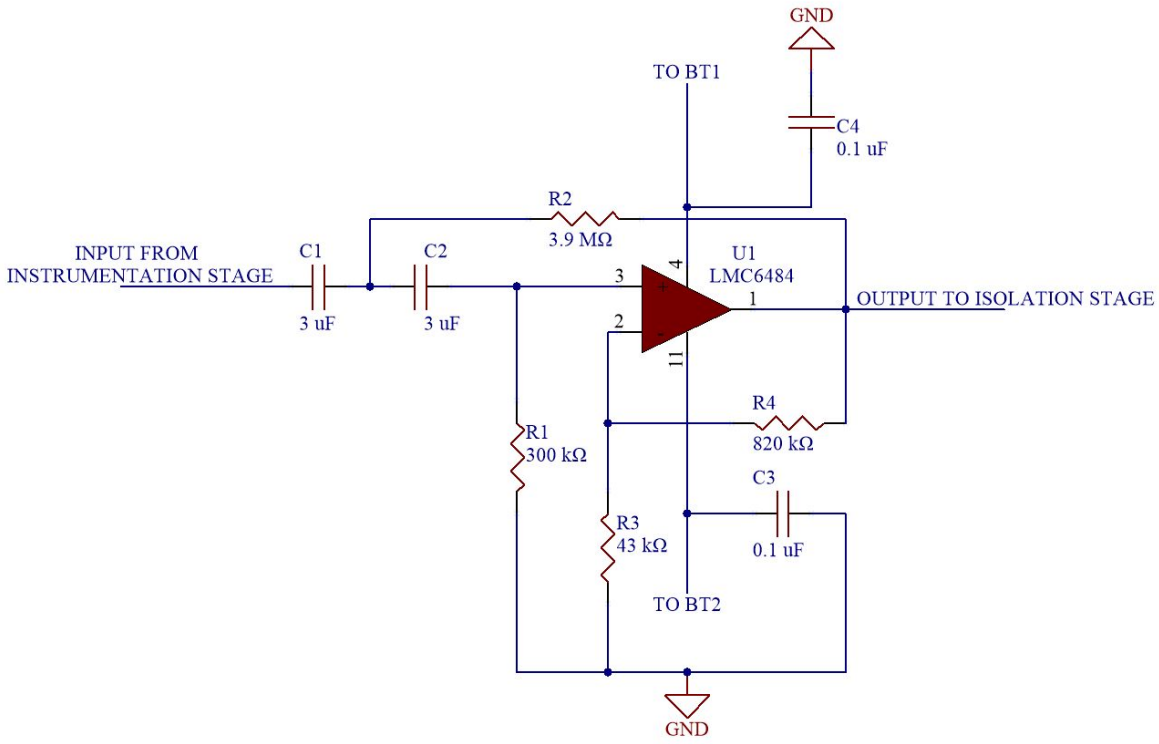

Figure 37 Schematic of High-pass Filter Stage

Following the instrumentation amplifier in our ECG circuit is the high-pass filter. To build the high-pass filter stage, we utilized an LM348 operational amplifier, which contains four independent, high-gain, internally compensated, low power operational amplifiers (Texas Instruments, 2015). We chose to utilize this operational amplifier due to functionality as well as convenience. The LM348 operational amplifier has a maximum supply current of 2.4 mA and a dual power supply range of ± 4V to 18V. Our analog front end is powered by two 9 V batteries, which means this operational amplifier can accommodate our power supply. The LM348 has a maximum input offset voltage of 1 mV, which is a minute value and does not need to be considered in gain calculations since it is so insignificant. Utilizing the LM348 was also convenient for us because the lab we were working with had multiple in stock, which reduced cost. Similar to the instrumentation amplifier, we utilized two 0.1 µF decoupling capacitors which matched the specifications of the LM348 data sheet.

Referencing Figures 29 and 30, only the first stage of the bandpass filter is placed before the isolation amplifier. This choice was made for the purpose of noise rejection. We placed the majority of the gain in the beginning of the circuit, i.e. mainly in the instrumentation amplifier and high-pass filter. If these two stages contain a large percentage of the circuit's total gain, then the noise that is also amplified with the signal in these stages will be filtered through the high-pass filter before it travels through the isolation amplifier, which also provides a considerable amount of noise. The noise produced by the isolation amplifier will then be reduced through the low-pass filter, which is the final stage of the bandpass filter, which will be discussed further in Section 3.2.4.

One of the most important roles of the high-pass filter was to remove the DC offset. As discussed in Section 3.2.2, the maximum DC offset of the skin-electrode contact is 300 mV. After the amplified signal leaves the instrumentation amplifier, it flows into the high-pass filter, which removes the amplified DC offset component of the ECG signal. We calculated the total output voltage of the instrumentation amplifier to be v_o = 7.8385 V. The maximum DC offset portion of this output voltage can be calculated as follows:

$$v_{o(DC)} = 300 \text{ mV} * 25.7 = 7.71 \text{ V}$$

meaning that the voltage of the ECG signal entering the high-pass filter can be as large as:

$$7.8385 \text{ V} - 7.71 \text{ V} = 128.5 \text{ mV}$$

We utilized this voltage value to determine an appropriate gain for the high-pass filter stage. The maximum allowable gain that can be utilized in the high-pass filter stage can be calculated as such:

$$\frac{8.3V}{128.5\,mV} = 64.59 \text{ V/V}$$

We designed our circuit to contain variable gain stages between the low-pass filter and the notch filter. Therefore, we did not want to choose too high of a gain in the high-pass filter to ensure the ECG signal would not saturate. Therefore, with a maximum allowable gain of 64.59

in the high-pass stage, we chose a gain of 20. This ensures that the maximum allowable gain of the variable gain stage is 3.2295 V/V and we utilized this value to design our gain modules, which will be discussed later in Section 3.3.6. The total circuit gain at the point of the output of the high-pass filter is as follows:

$$25.7 \text{ V/V} * 20 \text{ V/V} = 514 \text{ V/V}$$

We decided to design the high-pass filter to be a second-order Sallen-Key Butterworth filter. Referencing Section 2.3.3, we decided the Sallen-Key topology was most applicable to the ECG circuit we were designing due to the circuit's low Q factor and need for high-quality gain. Our team chose to apply the Butterworth characteristics to our high-pass filter because of the filter's maximally flat response in both the passband and stopband. In addition, we preferred the Butterworth filter's steep transition between the passband and stopband dependent on the order of the filter. The higher the order of the filter, the steeper the transition, as depicted in Figure 38. As shown, as the order increases the response of the Butterworth filter begins to resemble a nearly ideal response. For our purposes, we designed a second-order Butterworth filter because the overall circuit was simple to build and the frequency response was sufficient.

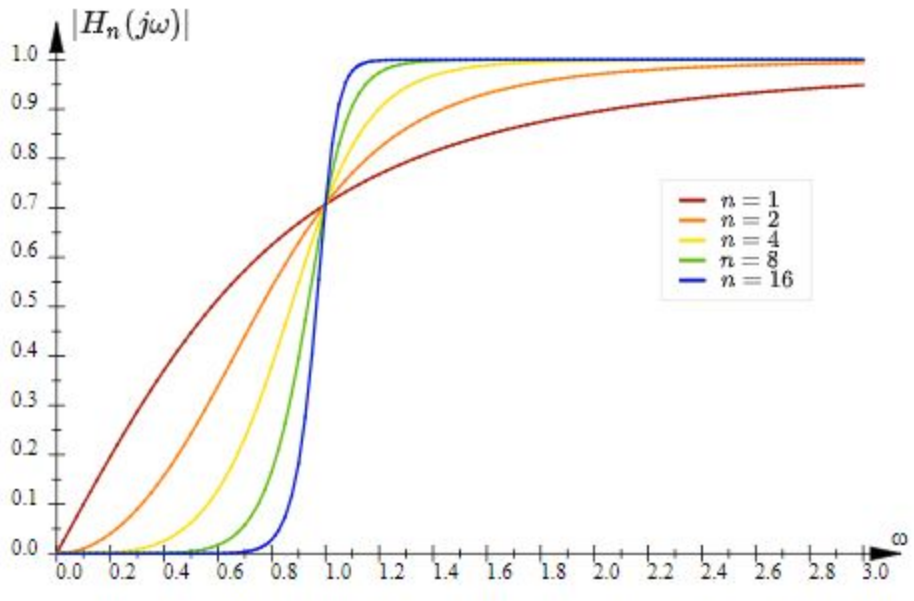

Figure 38 Frequency response of normalized Butterworth high-pass filter with different orders (Pieter, 2018)

In order to derive the transfer function of a second-order Sallen-Key high-pass filter, we utilized the unity gain topology. The gain of the high-pass filter is determined by resistors R3 and R4 which are not necessary for deriving the transfer function. We utilized Figure 39 as a reference and derived the transfer function of a second-order Sallen-Key high-pass filter using KCL at node V_X.

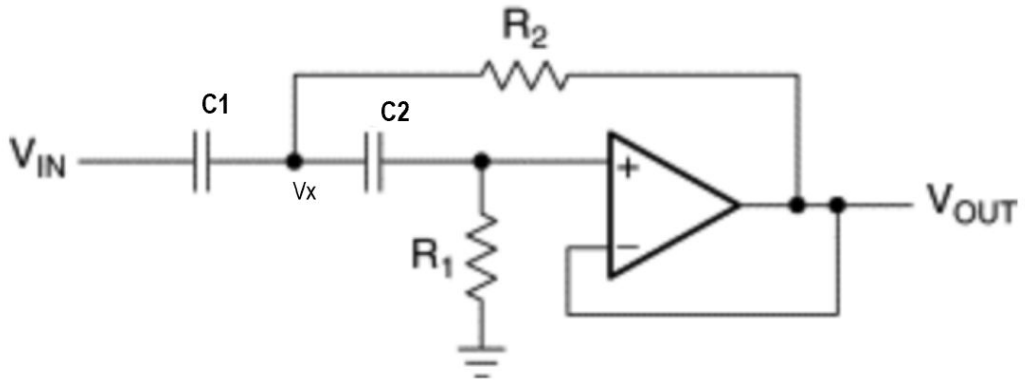

Figure 39 Second-order Sallen-key High-pass Unity Gain Filter for Transfer Function Derivation (Kugelstadt, 2009)

We utilized KCL to state that the current through C_1 is equal to the sum of currents through C_2 and R_2. From this conclusion we can create the following equation:

$$\frac{v_{IN} - v_X}{\frac{1}{C_1 s}} = \frac{v_X - v_{OUT}}{R_2} + \frac{v_X - v_{OUT}}{\frac{1}{C_2 s}}$$

We then utilized KCL to state that the current through C_2 is equal to the current through R_1. From this conclusion we can create the following equation:

$$\frac{v_X - v_{OUT}}{\frac{1}{C_2 s}} = \frac{v_{OUT}}{R_1}$$

The equation above can be rewritten as:

$$v_x = v_{OUT}\left(\frac{\frac{1}{C_2 s}}{R_1} + 1\right)$$

We then substituted the above equation into the following:

$$\frac{v_{IN} - v_X}{\frac{1}{C_1 s}} = \frac{v_X - v_{OUT}}{R_2} + \frac{v_X - v_{OUT}}{\frac{1}{C_2 s}}$$

$$\frac{v_{IN} - v_{OUT}\left(\frac{\frac{1}{C_2 s}}{R_1} + 1\right)}{\frac{1}{C_1 s}} = \frac{v_{OUT}\left(\frac{\frac{1}{C_2 s}}{R_1} + 1\right) - v_{OUT}}{R_2} + \frac{v_{OUT}\left(\frac{\frac{1}{C_2 s}}{R_1} + 1\right) - v_{OUT}}{\frac{1}{C_2 s}}$$

Rearranging the previous equation results in the transfer function:

$$\frac{v_{OUT}}{v_{IN}} = \frac{R_2 R_1}{\frac{1}{C_1 s}\frac{1}{C_2 s} + R_2\left(\frac{1}{C_1 s} + \frac{1}{C_2 s}\right) + R_2 R_1}$$

Finally, after utilizing algebraic operations, we were able to simplify the equation above to derive a finalized transfer function for a second-order high-pass Sallen-Key filter:

$$\mathrm{H(s)} = \frac{s^2 R_1 R_2 C_1 C_2}{s^2 R_1 R_2 C_1 C_2 + s R_2 (C_1 + C_2) + 1}$$

Deriving the transfer function allowed us to design our filter properly. To ensure the values we implemented were correct we utilized a calculator by Okawa Electric Design. When we utilized the calculator, we simply needed to enter the filter type (Butterworth), our desired cut-off frequency, and our desired capacitor values. The appropriate bandwidth of an ECG signal ranges from 0.05 Hz to 100 Hz, which is why we chose to design the high-pass filter to have a cut-off frequency of 0.05 Hz. The actual cut-off frequency of the filter we designed was 0.049046265646272 Hz. We utilized Equation 15 to determine the error percentages of our desired values compared to our actual values:

$$\%\ Error = \frac{|Calculated\ Gain - Theoretical\ Gain|}{Theoretical\ Gain} \cdot 100\%$$

Equation 15 Equation for Percent Error (University of Iowa Department of Physics and Astronomy, 2017)

We found that our calculated cut-off frequency only had an error percentage of 1.9% from our desired cut-off frequency. We also chose to utilize 3 µF capacitors for both C_1 and C_2.

While these values may seem high, we had to compromise to ensure the resistor values would not be too high as well, which we found to be R_1 = 300 kΩ and R_2 = 3.9 MΩ. The transfer function of the high-pass filter is the following:

$$H(s) = \frac{20.06976744186\, s^2}{s^2 + 0.59232756907176s + 0.094966761633428}$$

We aimed to design the filter to have a Q factor of 0.707, a characteristic of a Sallen-key filter. However, the actual Q factor of the filter we designed was 0.52026411021796, which was a 26.41% error. At first we were concerned with the error percentage, however when we plotted the step response of the high-pass filter with the Okawa Electric Design calculator (see Figure 40) we found the result to be very satisfactory and the high-pass filter to be stable. The filter enters a steady state after approximately 15 seconds. This means, after 15 seconds there are no longer any transients, or oscillations, occurring in the signal.

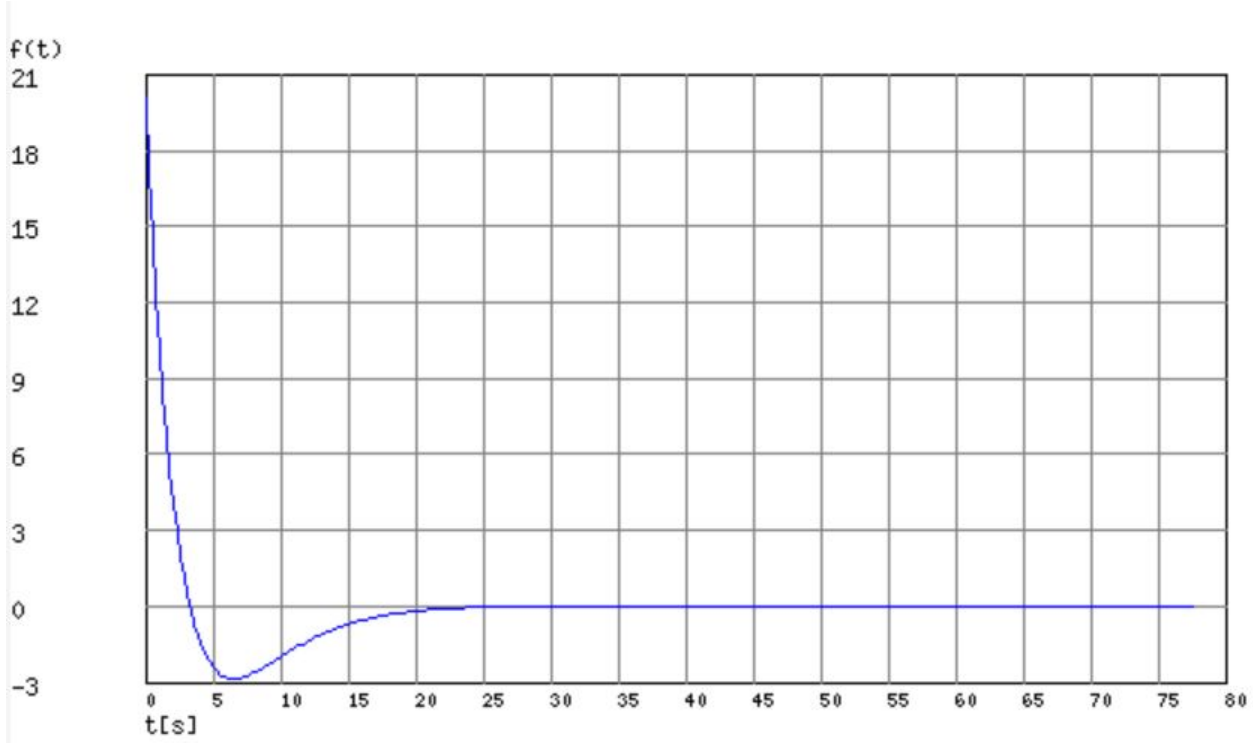

Figure 40 Transient Response of High-pass Filter (Okawa Electric Design, 2019)

After our high-pass filter was designed, we then utilized the Okawa Electric Design calculator to determine if the filter we designed possessed typical high-pass characteristics. We

also utilized these tests to compare our results from the tests we conducted on the actual high-pass filter circuit we built. A bode plot is used as an intuitive way to understand the frequency response of a filter by comparing the frequency response to both the phase delay and magnitude of the signal. The bode plot depicted in Figure 41 represents how we expected our high-pass filter to handle the signal being processed. Referring to the first plot, the y-axis represents the magnitude of the gain of the signal in decibels [dB] and the x-axis depicts the frequency. From the first plot, we can determine that the filter passed all frequencies after 0.05 Hz. This can be inferred by the horizontal line occupying frequencies ranging from 0.05 Hz and on. For the frequencies smaller than 0.05 Hz the line is attenuated, and steadily inclines until it reaches the cut-off frequency 0.05 Hz. This is because our high-pass filter was built to attenuate, or reject, frequencies smaller than 0.05 Hz. If we refer to the second plot, we can infer that at approximately 0.05 Hz the signal begins to experience phase delay. At the cut-off frequency of 0.05 Hz we can expect to have a delay of approximately 100°. To convert the delay from degrees to seconds we utilized Equation 14, where $\varphi\circ$ represents the phase angle and f represents the frequency, and found the time delay to be 5.6 seconds at 0.05 Hz.

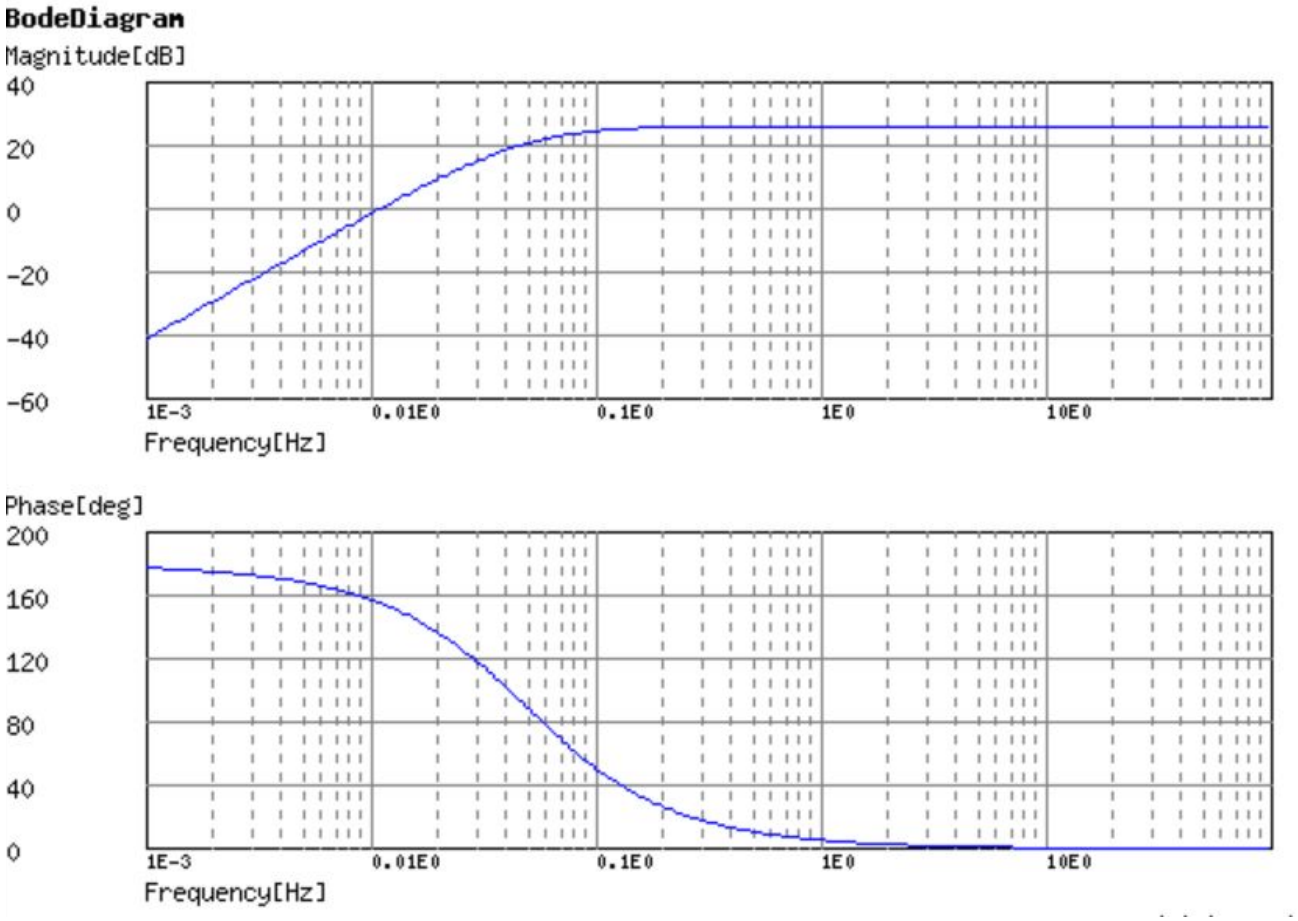

Figure 41 Theoretical Bode Plot of the 0.05 Hz High-pass Filter (Okawa Electric Design, 2019)

$$\Delta t = \frac{\varphi^{\circ}}{360 \cdot f}$$

Equation 16 Time Delay Equation

Visually, one could expect this delay to look similar to Figure 42.

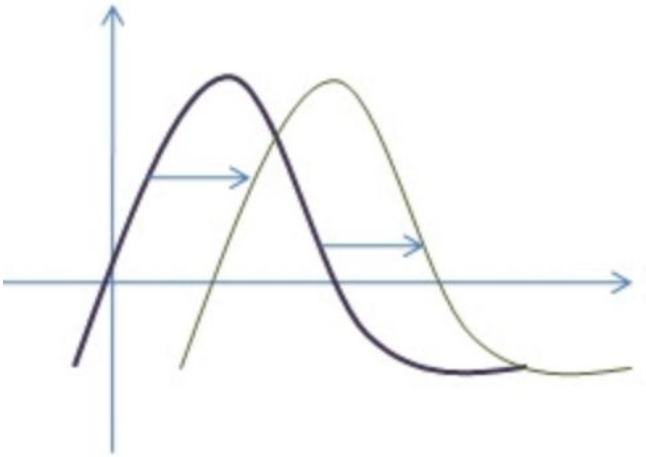

Figure 42 Example of a Delayed Signal (Science Direct)

Once we had a finalized design for our high-pass filter stage, we built a prototype to be utilized in the analog front end of the finalized ECG circuit (see Figure 43).

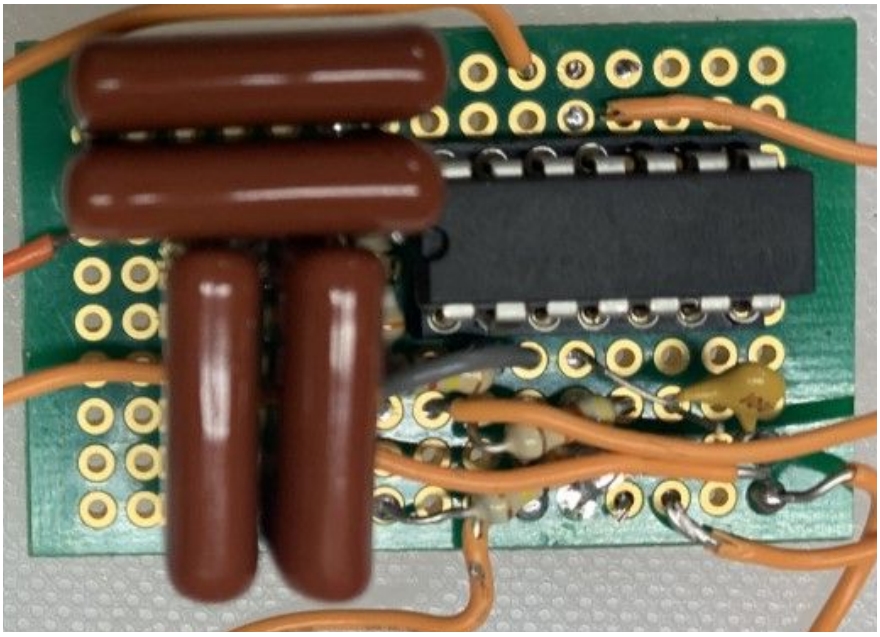

Figure 43 Physical Implementation of High-pass Filter Stage

3.2.4 Isolation Amplifier

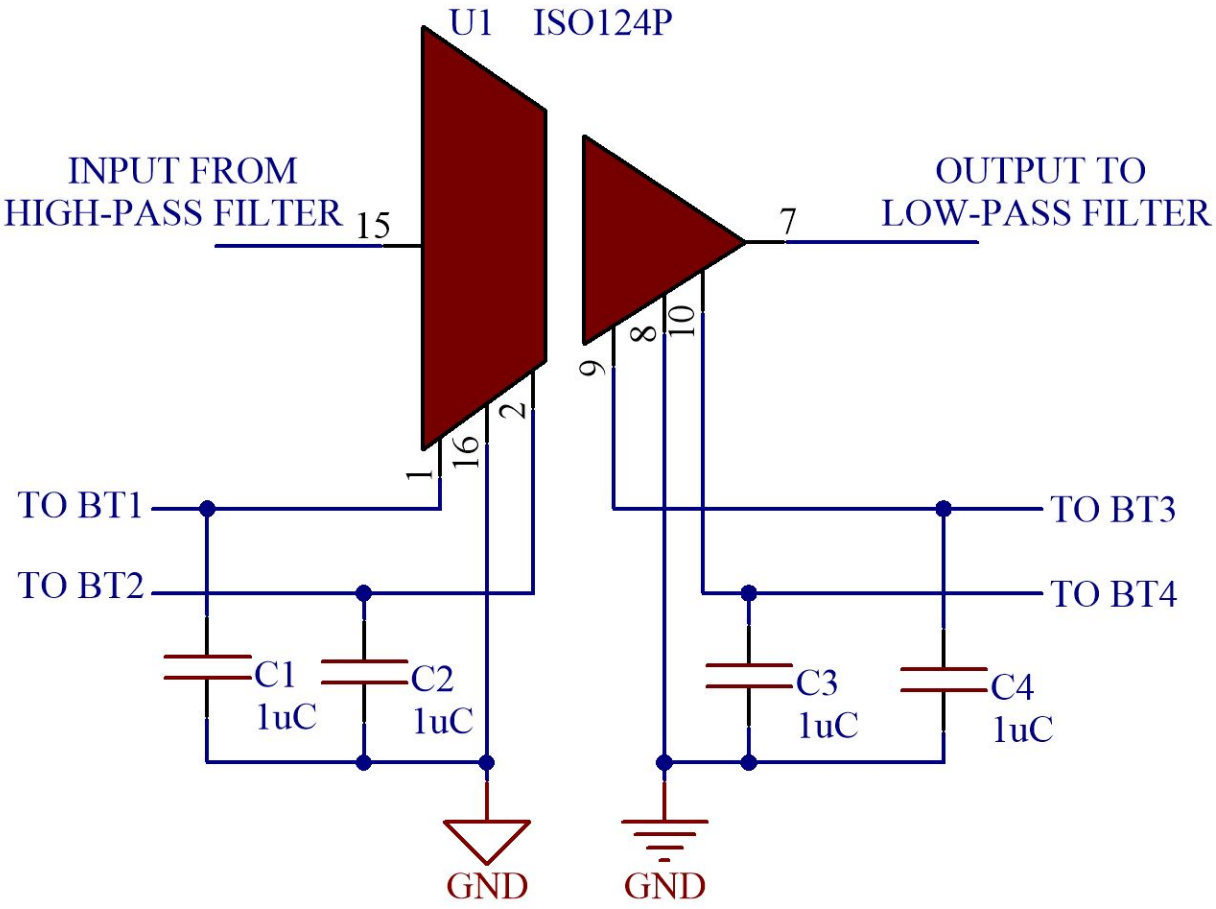

Figure 44 Schematic of Isolation Stage

After the high-pass filter in our ECG circuit, we implemented an isolation amplifier. We utilized an ISO124 amplifier produced by Texas Instruments. This amplifier is a precision isolation amplifier that incorporates a novel duty cycle modulation-demodulation technique. In simpler terms, the amplifier has an input and an output section that is galvanically isolated by matched 1 pF isolating capacitors built into the plastic package, as depicted in Figure 45. The input is duty-cycle modulated and transmitted digitally across the capacitive barrier. The output section then receives the modulated signal and converts it back to an analog voltage. In doing so, it removes the ripple component inherent in the demodulation (Texas Instruments).

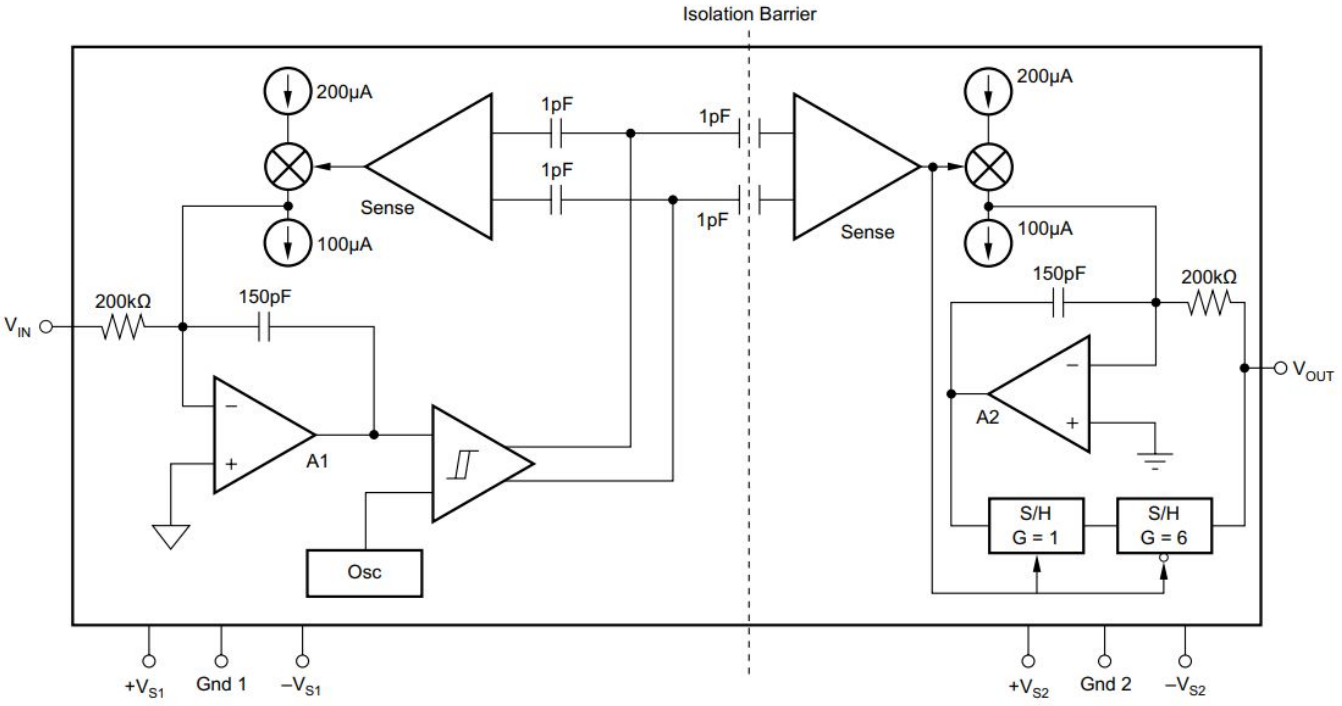

Figure 45 ISO124 Functional Block Diagram (Texas Instruments)

We were attracted to the ISO124 amplifier for its excellent linearity (0.010% maximum nonlinearity), 50 kHz signal bandwidth and maximum voltage rating at the input of 100 V with a recommended power supply range of ±4.5 V to ±18 V. It was important we utilized an isolation amplifier that maintained linearity (proportionality between the output and input signal) to ensure the analog output waveform, the user's ECG signal, would not be distorted due to fluctuation in gain. We were also attracted to the ISO124 for its power supply range because each side of the isolation amplifier will be powered by two 9 V batteries. For this stage we also utilized two 1µF decoupling capacitors on each side of the isolation amplifier for a total of four bypass capacitors.

Once we had a finalized design for our isolation stage, we built a prototype to be utilized in the analog front end of the finalized ECG circuit (see Figure 46).

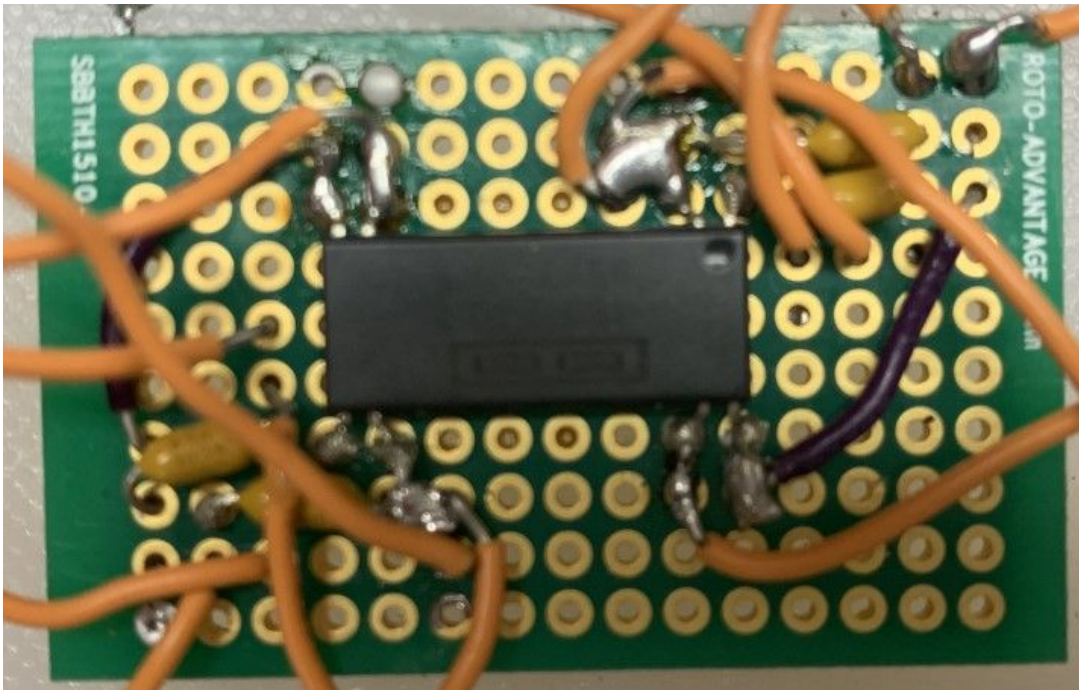

Figure 46 Physical Model of Isolation Amplifier Stage

The beginning portion of our circuit, i.e., the instrumentation amplifier and high-pass filter, will be isolated powered, which means the power ports of the amplifiers will connect to $+V_{S1}$ and $-V_{S1}$ of the isolation amplifier (see Figure 45). This portion of the circuit, along with the isolation amplifier, will not be integrated into the Elenco Snap Circuit pieces, rather it will be hardwired into the display and will not be allowed to be accessed by the public. This ensures that the circuitry remains intact and as well as protects individuals by securing the isolation amplifier so it can function properly. Figure 47 portrays the isolated portion of our ECG circuit.

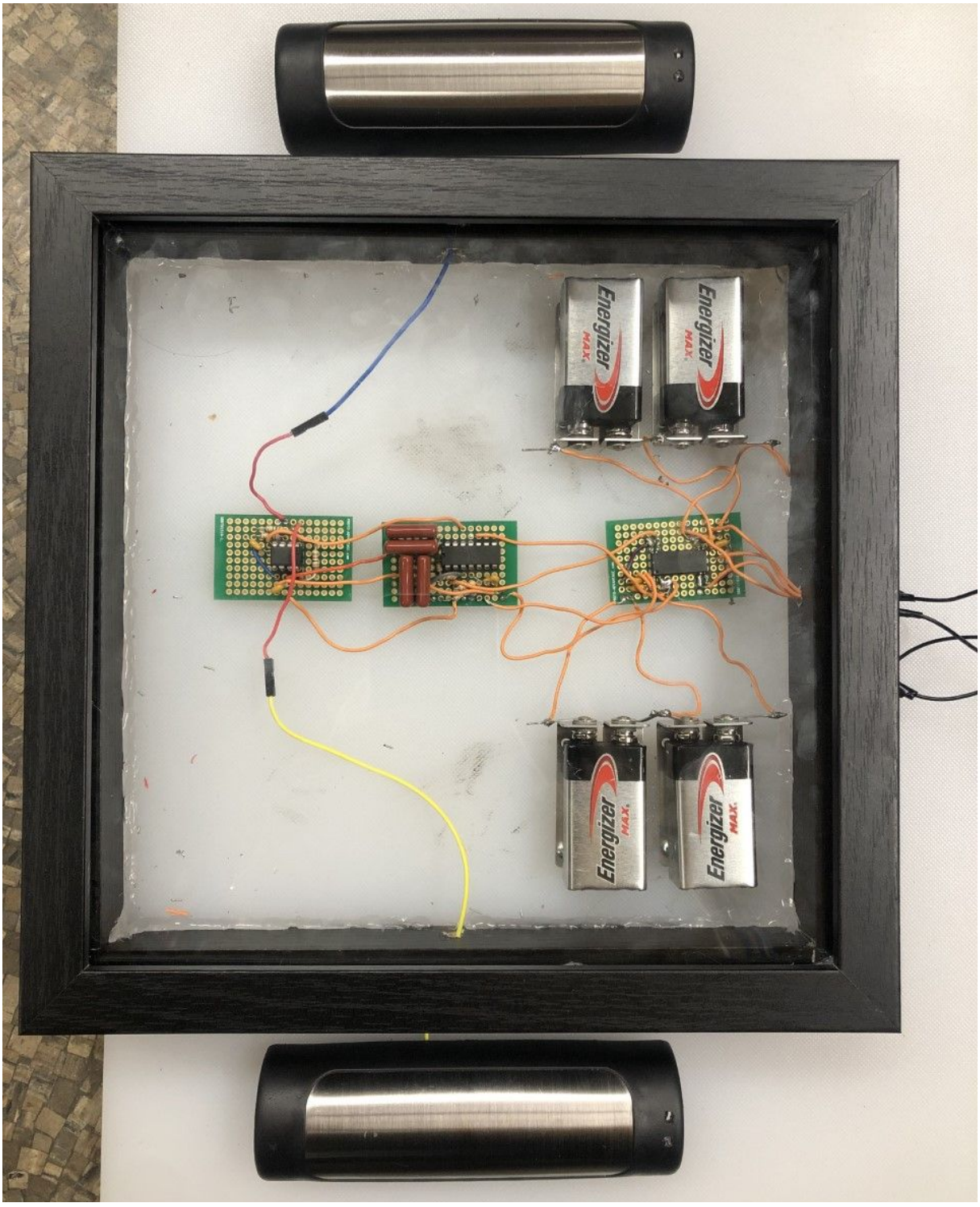

Figure 47 Isolated Portion of ECG Circuit

The portion of the circuit that follows the isolation amplifier is the earth-grounded side. The power rails on each amplifier on the earth-grounded side will connect to $+V_{S2}$ and $-V_{S2}$ of the isolation amplifier (see Figure 45). Each module on this side of the circuit will be encased in Elenco Snap Circuit pieces; this includes the low-pass filter, the gain stage, and the notch filter. Figure 48 portrays the earth-grounded portion of our ECG circuit.

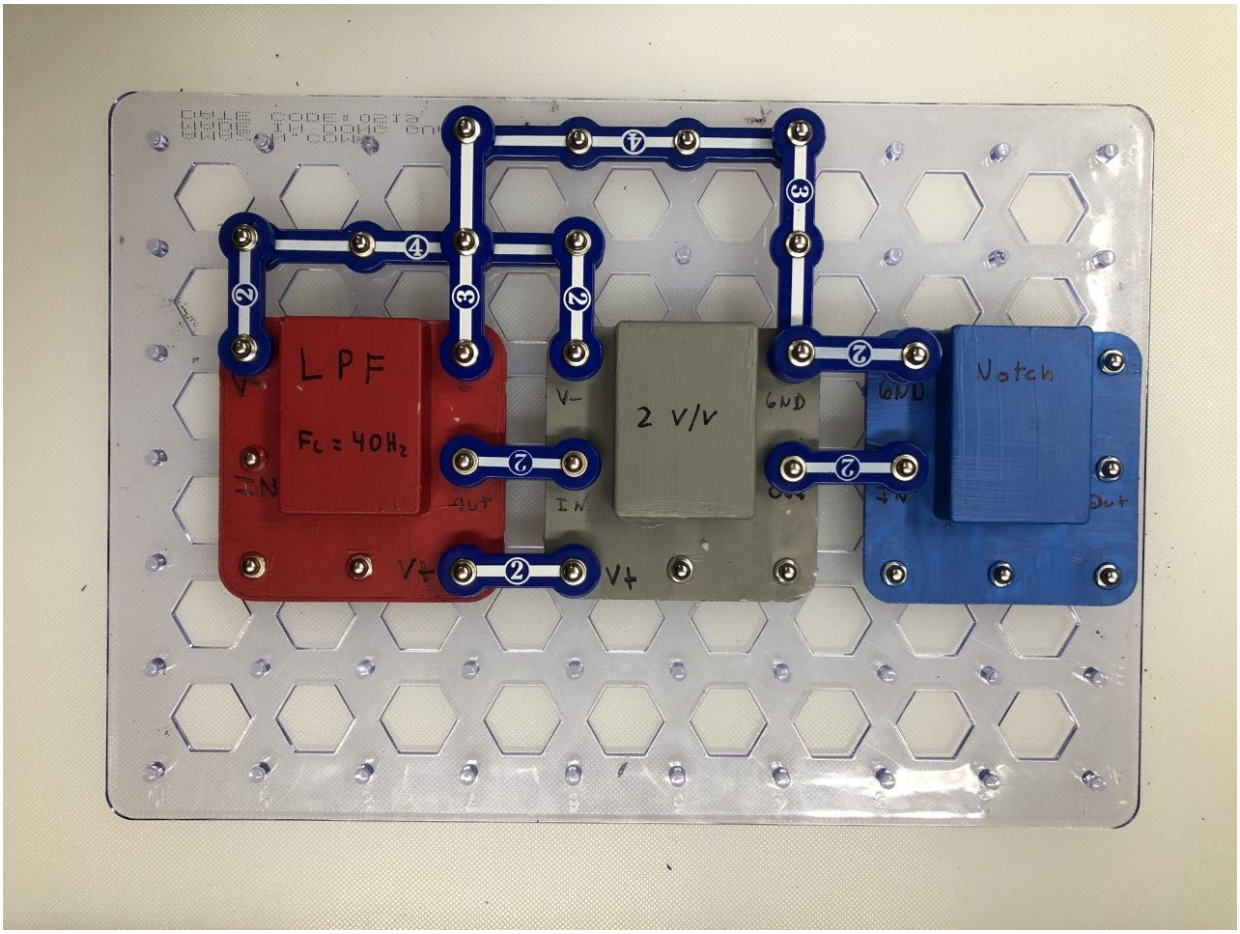

Figure 48 Earth-grounded Portion of ECG circuit

3.2.5 Low-pass Filter

Once the ECG signal passes through the isolation amplifier it enters the low-pass filter, which completes the bandpass filtering stage. We utilized the same operational amplifier in the low-pass filter that we did for the high-pass filter, an LM348 because both filters had the same

specifications. The operational amplifier is powered by two 9 V batteries and we again utilized two 0.1 µF decoupling capacitors.

We utilized a second-order Sallen-Key Butterworth filter for the low-pass filter, which is the same topology as we utilized for the high-pass filter, only the locations of the resistors and capacitors were reversed. We then utilized Figure 49 as a reference and derived the transfer function of a second-order Sallen-Key low-pass filter using KCL at node V_X.

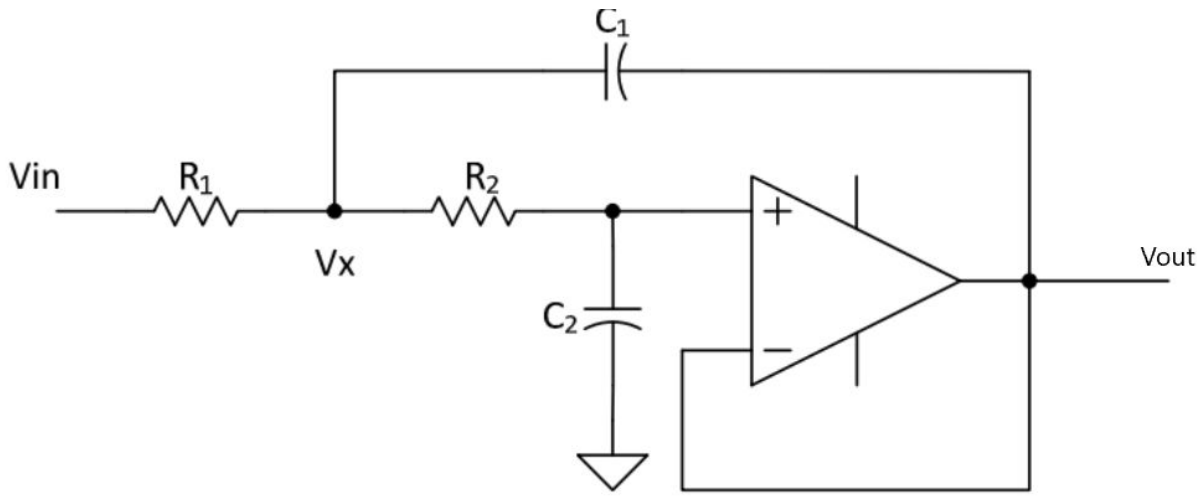

Figure 49 Sallen-Key Unity Gain Low-pass Filter Schematic (Science Direct)

We utilized KCL to state that the current through R_1 is equal to the sum of currents through R_2 and C_1. From this conclusion we can create the following equation:

$$\frac{v_{IN} - v_X}{R_1} = \frac{v_X - v_{OUT}}{\frac{1}{C_1 s}} + \frac{v_X - v_{OUT}}{R_2}$$

We then utilized KCL to state that the current through R_2 is equal to the current through C_2 . From this conclusion, we can create the following equation:

$$\frac{v_X - v_{OUT}}{R_2} = \frac{v_{OUT}}{\frac{1}{C_2 s}}$$

The equation above can be rewritten as:

$$v_x = v_{OUT}\left(\frac{R_2}{\frac{1}{C_2 s}} + 1\right)$$

We then substituted the above equation into the following:

$$\frac{v_{IN} - v_X}{\frac{1}{C_1 s}} = \frac{v_X - v_{OUT}}{R_2} + \frac{v_X - v_{OUT}}{\frac{1}{C_2 s}}$$

$$\frac{v_{IN} - v_{OUT}\left(\frac{R_2}{\frac{1}{C_2 s}} + 1\right)}{R_1} = \frac{v_{OUT}\left(\frac{R_2}{\frac{1}{C_2 s}} + 1\right) - v_{OUT}}{\frac{1}{C_1 s}} + \frac{v_{OUT}\left(\frac{R_2}{\frac{1}{C_2 s}} + 1\right) - v_{OUT}}{R_2}$$

Rearranging the previous equation results in the transfer function:

$$\frac{v_{OUT}}{v_{IN}} = \frac{\frac{1}{C_1 s}\frac{1}{C_2 s}}{R_2 R_1 + \frac{1}{C_1 s}(R_2 + R_1) + \frac{1}{C_1 s}\frac{1}{C_2 s}}$$

Finally, after utilizing algebraic operations, we were able to simplify the equation above to derive a finalized transfer function for a second-order high-pass Sallen-Key filter:

$$H(s) = \frac{1}{s^2 C_1 C_2 R_1 R_2 + s C_2 (R_1 + R_2) + 1}$$

Low-Pass Filter with Cut-off Frequency of 100 Hz

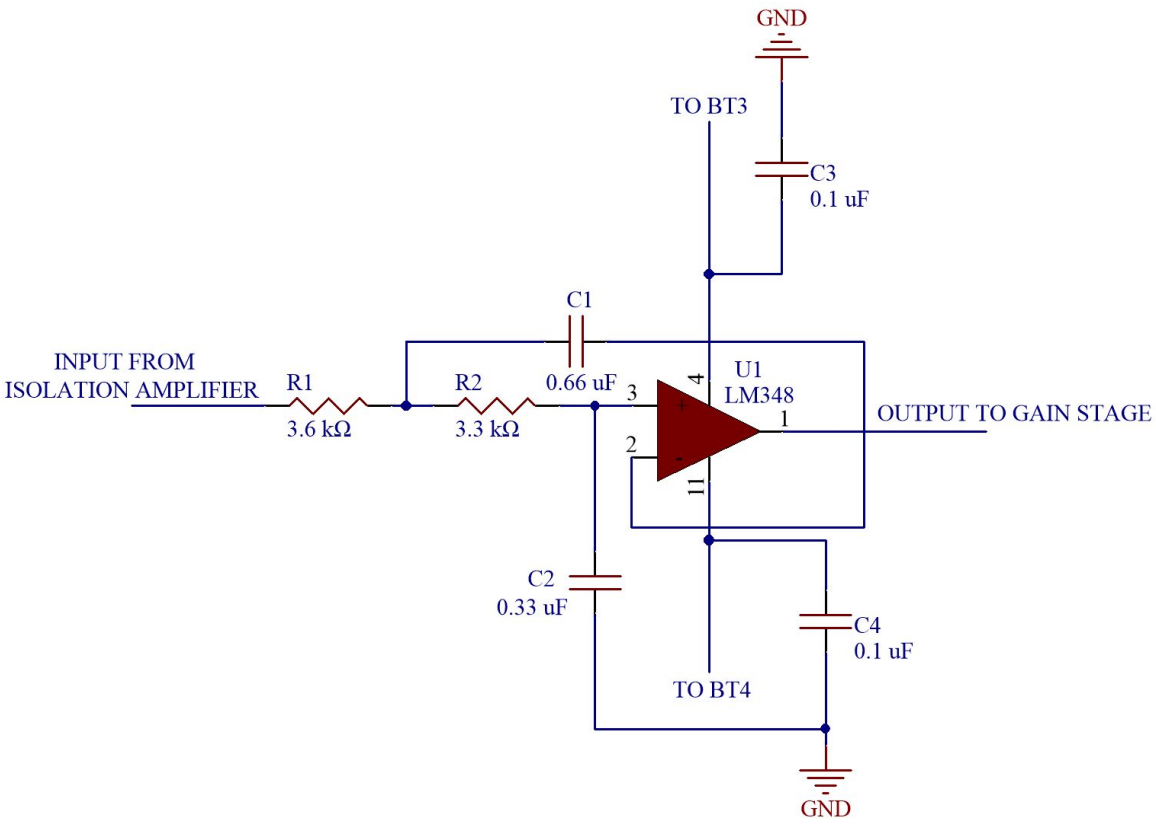

Figure 50 Schematic of Low-pass Filter with Cut-off Frequency of 100 Hz

Deriving the transfer function allowed us to design our low-pass filters properly. To ensure the values we implemented were correct we utilized the Okawa Electric Design calculator again. As mentioned in Section 3.2.3, the appropriate bandwidth of an ECG signal ranges from 0.05 Hz to 100 Hz, which is why we chose to design the low-pass filter to have a cut-off frequency of 100 Hz. The actual cut-off frequency of the filter we designed was 98.942521423799 Hz. We utilized Equation 15, referenced in Section 3.2.3, to again determine the error percentage of our desired values compared to our actual values. We found that our calculated cut-off frequency had an error percentage of 1.05%. For our low-pass filter with a cut-off frequency of 100 Hz, we chose to utilize a 0.66 µF capacitor for C_1 and a 0.33 µF capacitor for C_2. We decided to use these capacitor values in order to produce a low-pass filter that should have a Q factor of 0.707, a property of a Butterworth filter. In order to achieve a Q

factor of 0.707, R_1 was set to 3.6 kΩ and R_2 was set to 3.3 kΩ. The transfer function of the low-pass filter is the following:

$$G(s) = \frac{386478.80704}{s^2+880.01224364s+386478.80704}$$

We were pleased to find that the actual Q factor of the filter we designed was 0.70643812214226 which produced an error of 0.08%. We then reviewed the step response of the low-pass filter with the Okawa Electric Design calculator (see Figure 51) and were satisfied to find a stable low-pass filter. The transient analysis of the low-pass filter with a cut-off frequency of 100 Hz was very satisfactory. The low-pass filter enters a steady state after approximately 0.01 seconds. This means, after 0.01 seconds there are no longer any transients, or oscillations, occurring in the signal.

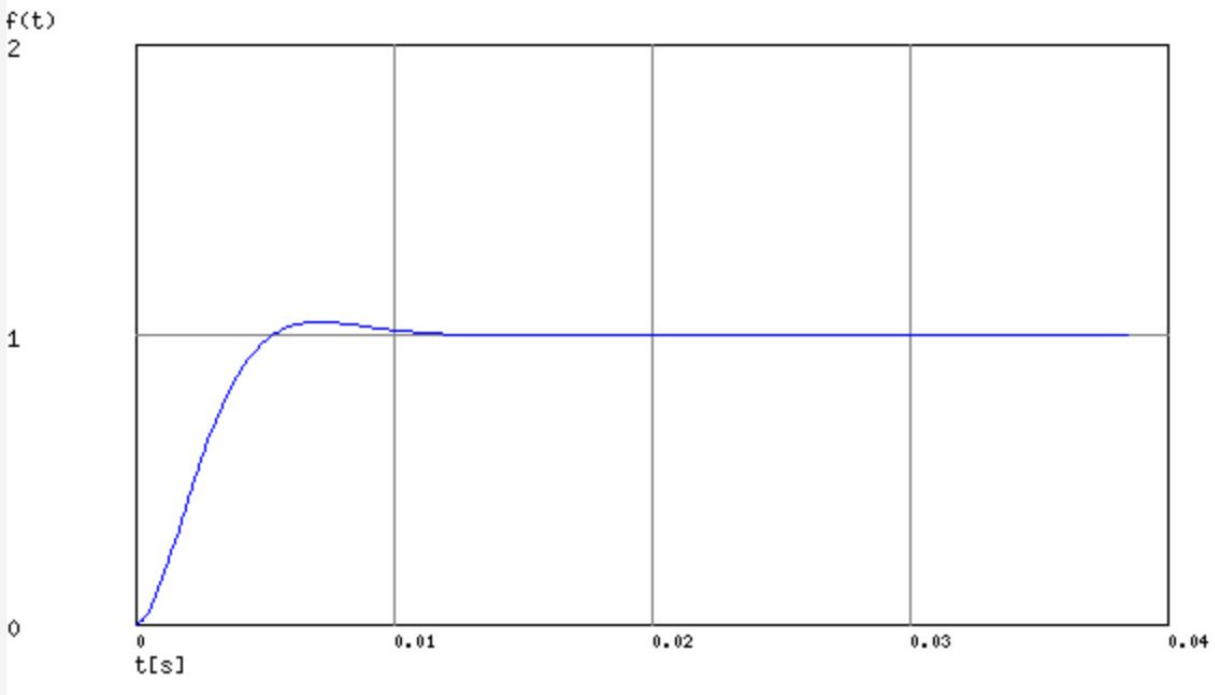

Figure 51 Transient Response of the Low-pass Filter with Cut-off Frequency of 100 Hz (Okawa Electric Design, 2019)

We then followed the same process as we did in Section 3.2.3 to determine if the filter we designed possessed typical low-pass filter characteristics. In addition, we utilized these tests to

compare our results from the tests we conducted on the actual low-pass filter circuit we built. Figure 52 is the theoretical bode plot Okawa Electric Design produced depicting the behavior of the low-pass filter.

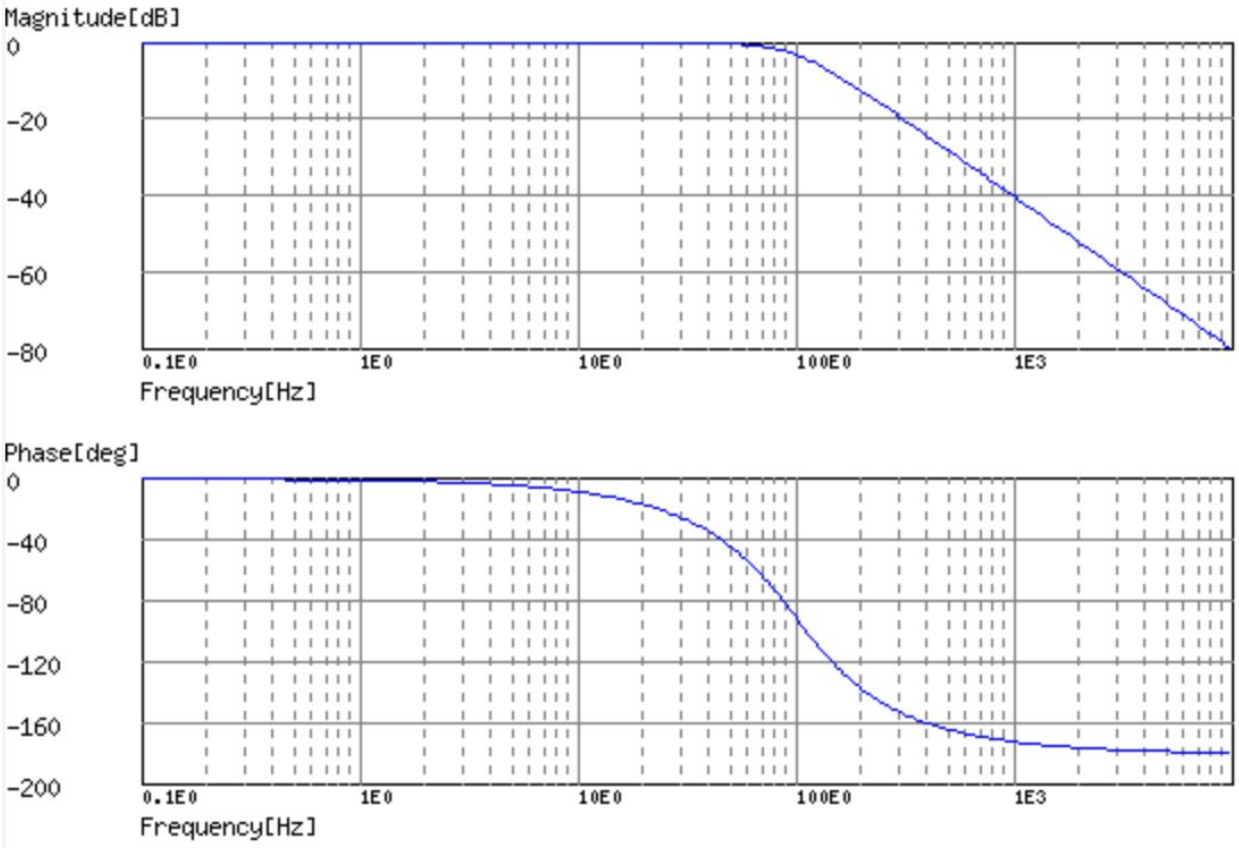

Figure 52 Theoretical Bode Plot of the Low-pass Filter with Cut-off Frequency of 100 Hz (Okawa Electric Design, 2019)

Referring to the top plot depicted in Figure 52, the y-axis represents the magnitude of the gain of the signal in decibels [dB] and the x-axis depicts the frequency. From this plot, we can determine that the filter passed all frequencies up until approximately 100 Hz ($100*10^0$). This can be inferred by the horizontal line occupying frequencies ranging from 0.1 Hz to 100 Hz. For the frequencies larger than 100 Hz the line is attenuated, steadily declining. This is because our low-pass filter was built to pass all frequencies smaller than 100 Hz. If we refer to the bottom plot, we can infer that at approximately 10 Hz the signal begins to experience phase delay. At the

cut-off frequency of 100 Hz we can expect the signal to have a delay of approximately -80°. To convert the delay from degrees to seconds we utilized Equation 14, referenced in Section 3.2.3, and found the time delay to be 0.002 seconds at 100 Hz.

Once we had a finalized design for our low-pass filter with a cut-off frequency of 100 Hz, we built a prototype to be utilized in the analog front end of the finalized ECG circuit (see Figure 53). The image on the left is the low-pass filter circuit that we soldered to a perforated breadboard. We connected the inputs and outputs to the "snaps" (the small metal pins that are used to connect snap-circuit components together). The image on the right portrays the completed snap-circuit building block with the inputs and outputs clearly labeled.

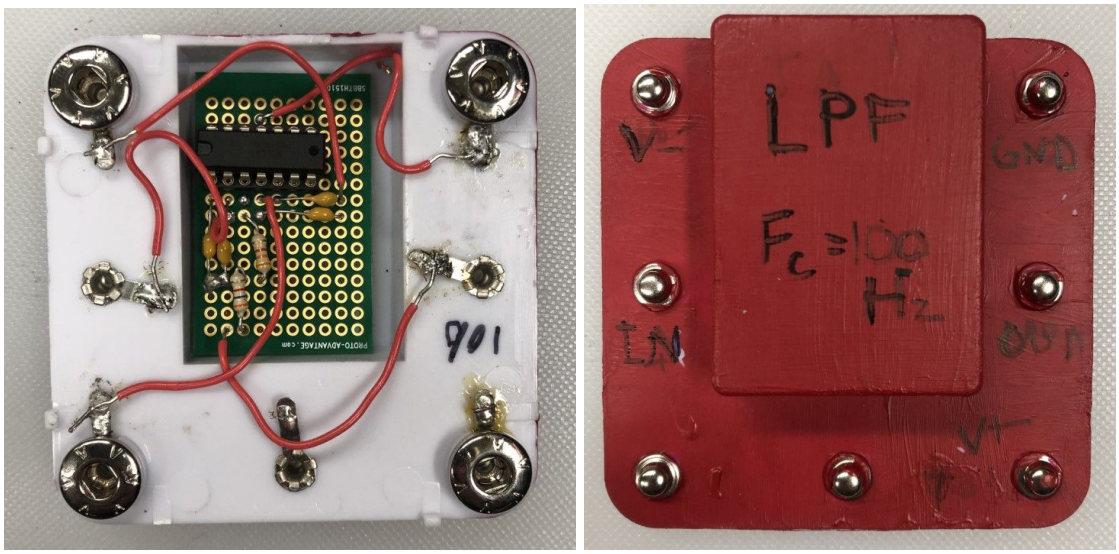

Figure 53 Physical Implementation of the Low-pass Filter with a Cut-off Frequency of 100 Hz

This process was then repeated twice more for two other low-pass filter modules with different cut-off frequencies. For educational purposes, we created additional pieces so students could visualize how their ECG signal would be altered by different cut-off frequencies at this stage in the circuit. Since the appropriate bandwidth of an ECG ranges from 0.05 Hz to 100 Hz, we decided the second cut-off frequency should be 70 Hz because it is close to 60 Hz, which is the frequency that the notch filter we implemented attenuates.

Low-Pass Filter with Cut-off Frequency of 70 Hz

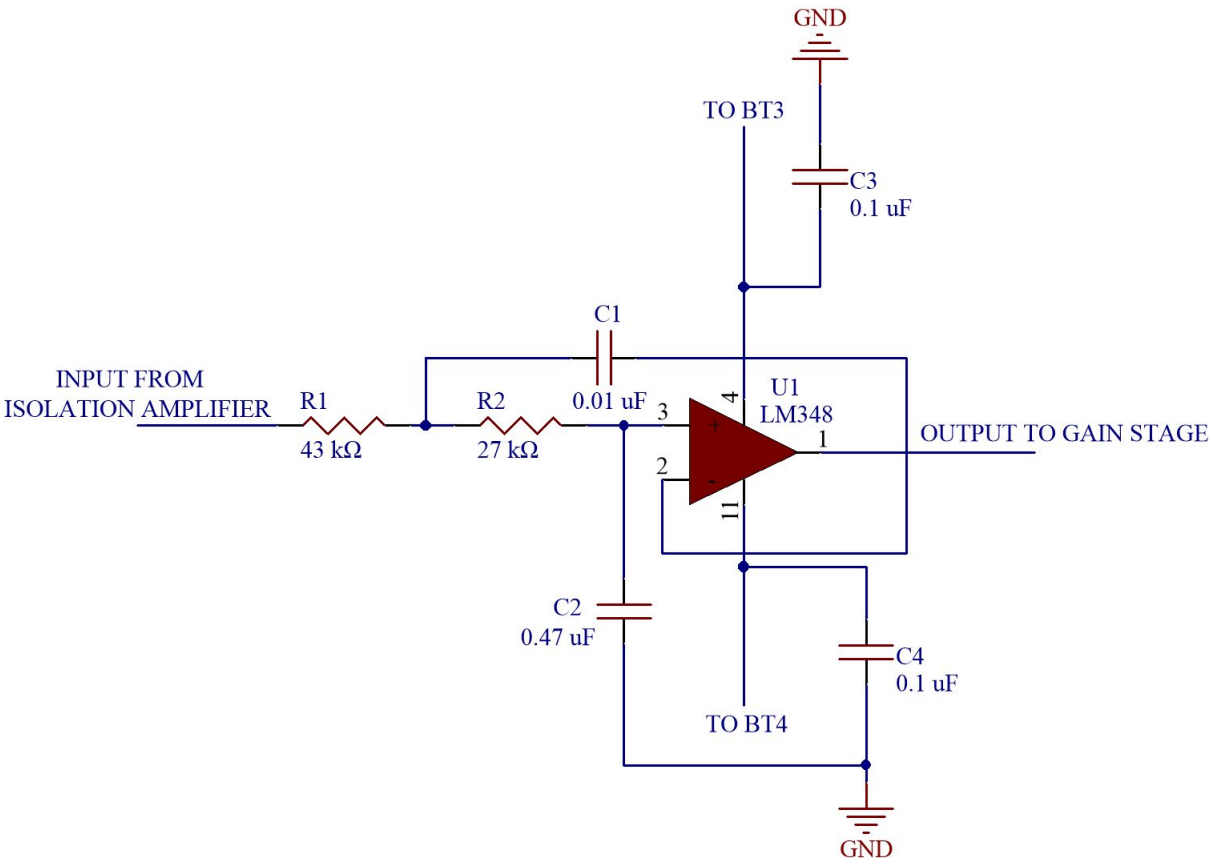

Figure 54 Schematic of Low-pass Filter with Cut-off Frequency of 70 Hz

The actual cut-off frequency of the low-pass filter with a desired cut-off frequency of 70 Hz we designed was 68.132620471314 Hz. We again utilized Equation 15 to determine the error percentage of our desired values compared to our actual values, which we found to be only 2.7%. For this low-pass filter, we chose to utilize a 0.01 µF capacitor for C_1 and a .047 µF for C_2. In choosing to use these values, we found R_1 had to be 43 kΩ and R_2 had to be 27 kΩ in order to build a low-pass circuit with respect to the Butterworth characteristics. The transfer function of this low-pass filter with a cut-off frequency of 70 Hz is the following:

$$G(s) = \frac{183260.94525996}{s^2+6029.2850990525s+183260.94525996}$$

We again aimed to design the filter to have a Q factor of 0.707. However, the actual Q factor of the filter we designed was 0.271001764363784, which produced an error of 61.7%. We were concerned with the high error percentage, but found that the step response plot is very close to an ideal step response of a low-pass filter. The low-pass filter enters a steady state after approximately 0.2 seconds. This means, after 0.2 seconds there are no longer any transients, or oscillations, occurring in the signal.

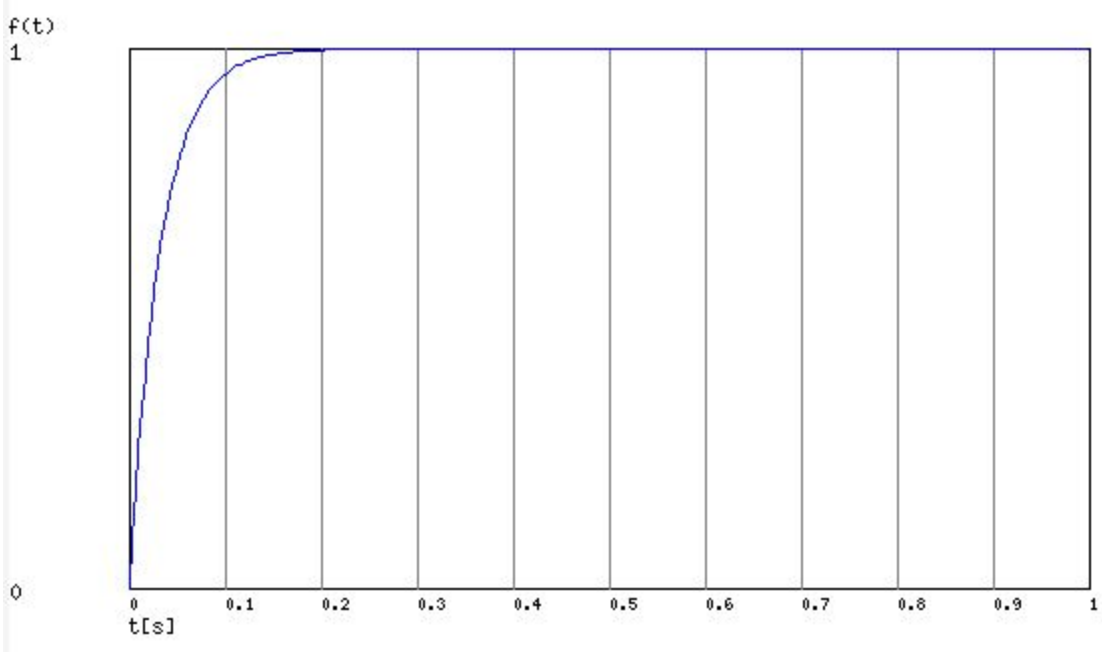

Figure 55 Transient Response of the Low-pass Filter with Cut-off Frequency of 70 Hz (Okawa Electric Design, 2019)

To determine if the 70 Hz low-pass filter we designed possessed typical low-pass characteristics we again utilized the Okawa Electric Design calculator to analyze the filter's bode plot. Figure 56 depicts how we expected the low-pass filter to handle the signal being processed. Referring to the top plot in Figure 56, we can see that the filter begins to gradually attenuate at approximately 20 Hz, which is much earlier than expected. We were not extremely concerned with these results, as they were expected after solving for such a high error percentage and analyzing the transient response of the filter. If we refer to the bottom plot in the figure, we can infer that multiple phase delays occur in the signal. Neither plot portrayed the characteristics of an optimal low-pass filter with a cut-off frequency of 70 Hz, but the filter still served its purpose,

as it was still attenuating frequencies larger than 70 Hz, and would produce a noisier signal at the output for students to compare and contrast to other two cut-off frequencies (100 Hz and 40 Hz).

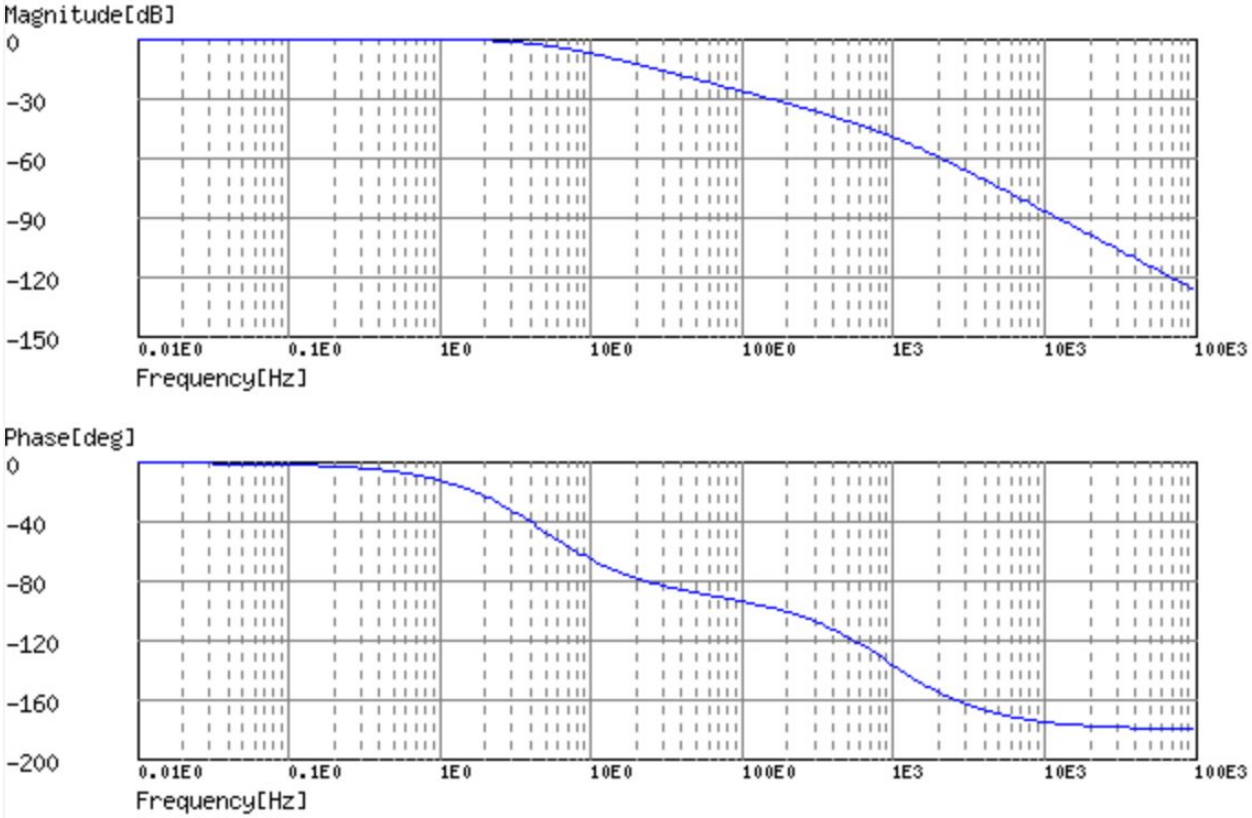

Figure 56 Theoretical Bode Plot of the Low-pass Filter with Cut-off Frequency of 70 Hz (Okawa Electric Design, 2019)

Once we had a finalized design for our low-pass filter with a cut-off frequency of 70 Hz, we built a prototype to be utilized in the analog front end of the finalized ECG circuit (see Figure 57).

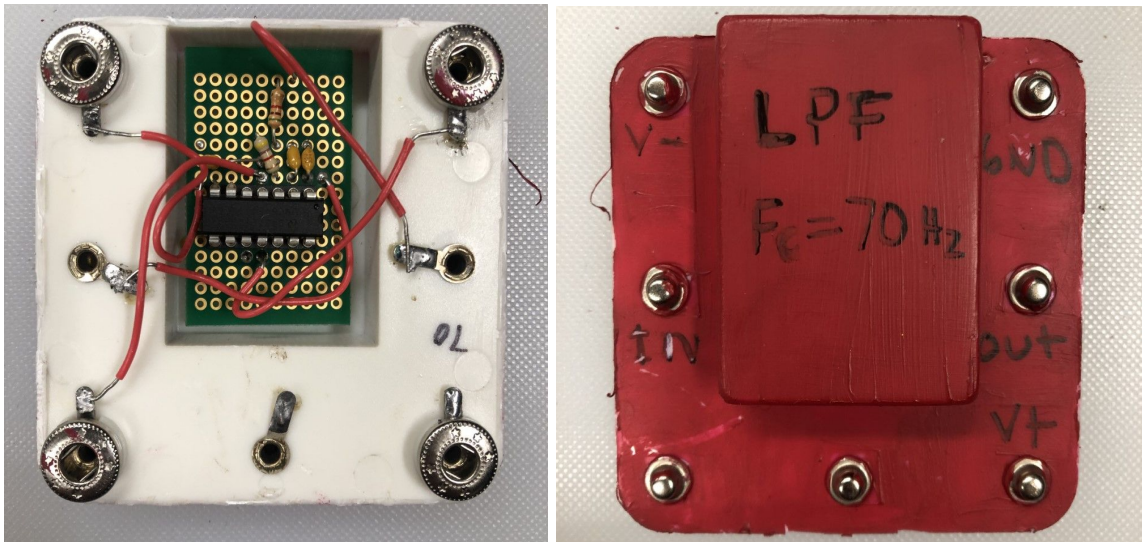

Figure 57 Physical Implementation of the Low-pass Filter with a Cut-off Frequency of 70 Hz

Low-Pass Filter with Cut-off Frequency of 40 Hz

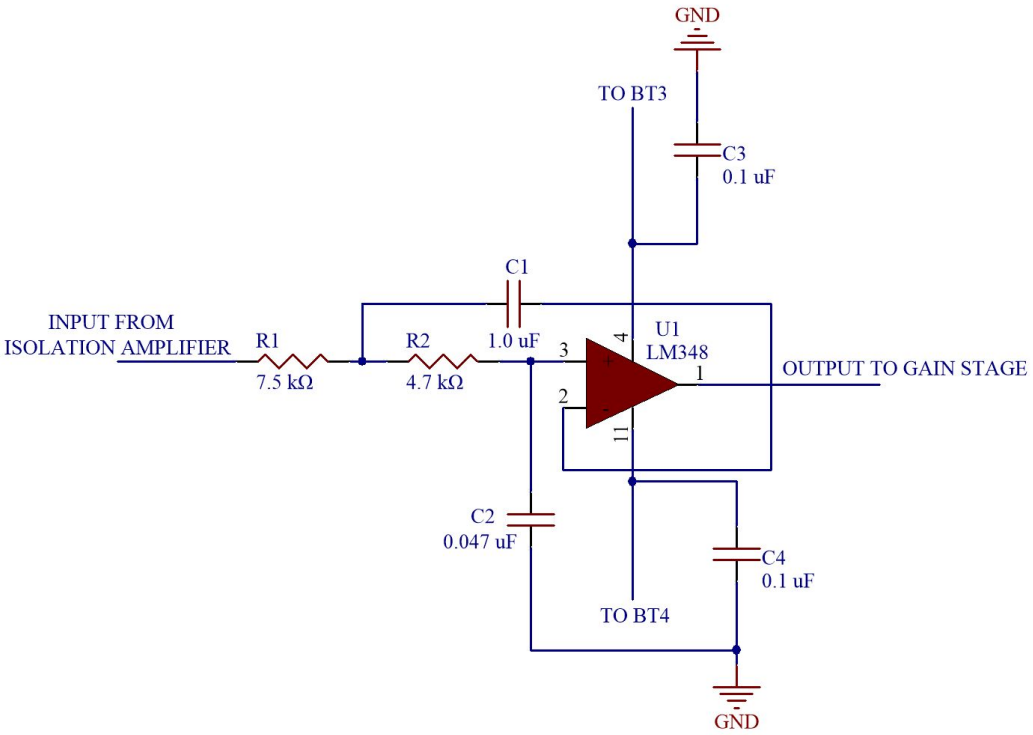

Figure 58 Schematic of Low-pass Filter with Cut-off Frequency of 40 Hz

This process was repeated for the last time with a low-pass filter designed with a cut-off frequency of 40 Hz. The actual cut-off frequency of the filter we designed was 39.101340100836 Hz. We again utilized Equation 15 to determine the error percentage of our desired values compared to our actual values, which we found to be 2.2%. For this low-pass filter, we chose to utilize a 1.0 μF capacitor for C_1 and a 0.047 μF for C_2. In choosing to use these values, we found R_1 had to be 7.5 kΩ and R_2 had to be 4.7 kΩ. The transfer function of this low-pass filter with a cut-off frequency of 40 Hz is the following:

$$G(s) = \frac{60359.136864343}{s^2+346.09929078014s+60359.136864343}$$

We again aimed to design the filter to have a Q factor of 0.707. However, the actual Q factor of the filter we designed was 0.7098568883479, which produced an extremely low error of 0.4%. We were extremely pleased with this result, and found that the filter's step response was extremely satisfactory. As shown in Figure 59, the filter enters a steady state after approximately 0.03 seconds.

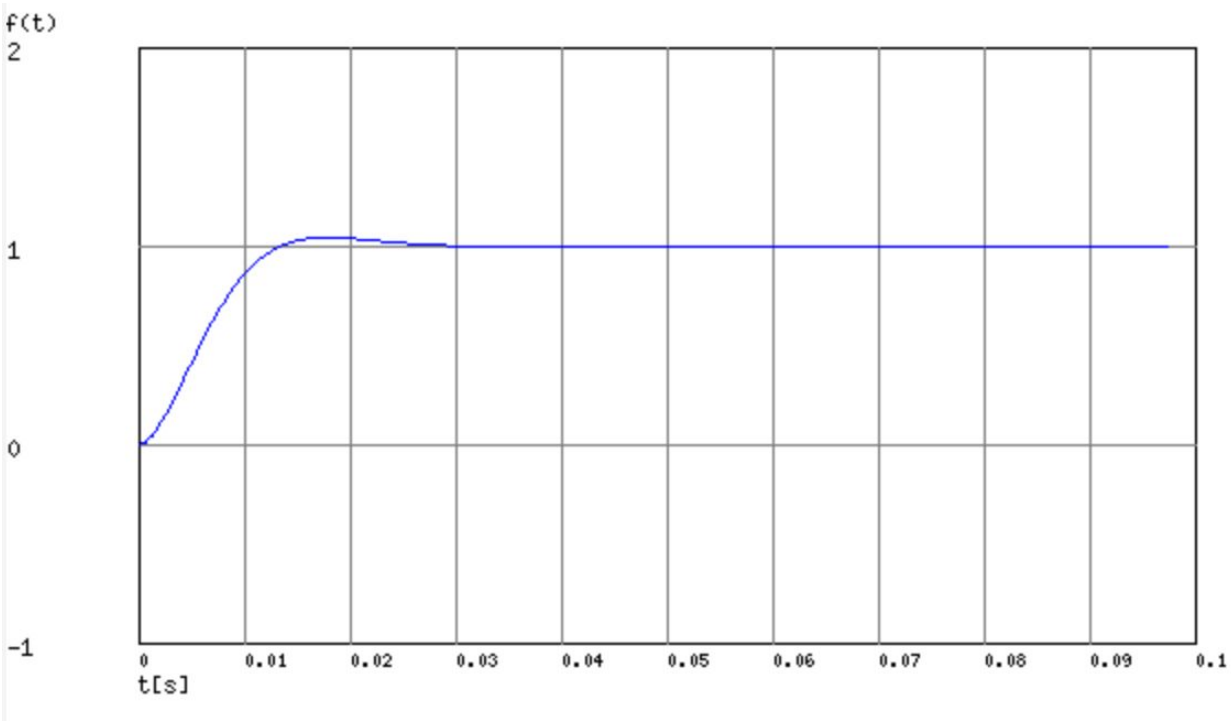

Figure 59 Transient Response of 40 Hz Low-pass Filter (Okawa Electric Design, 2019)

To ensure this filter possessed typical low-pass filter characteristics we analyzed the filter's bode plot. Figure 60 depicts how the low-pass filter with a cut-off frequency of 40 Hz handled the signal being processed.

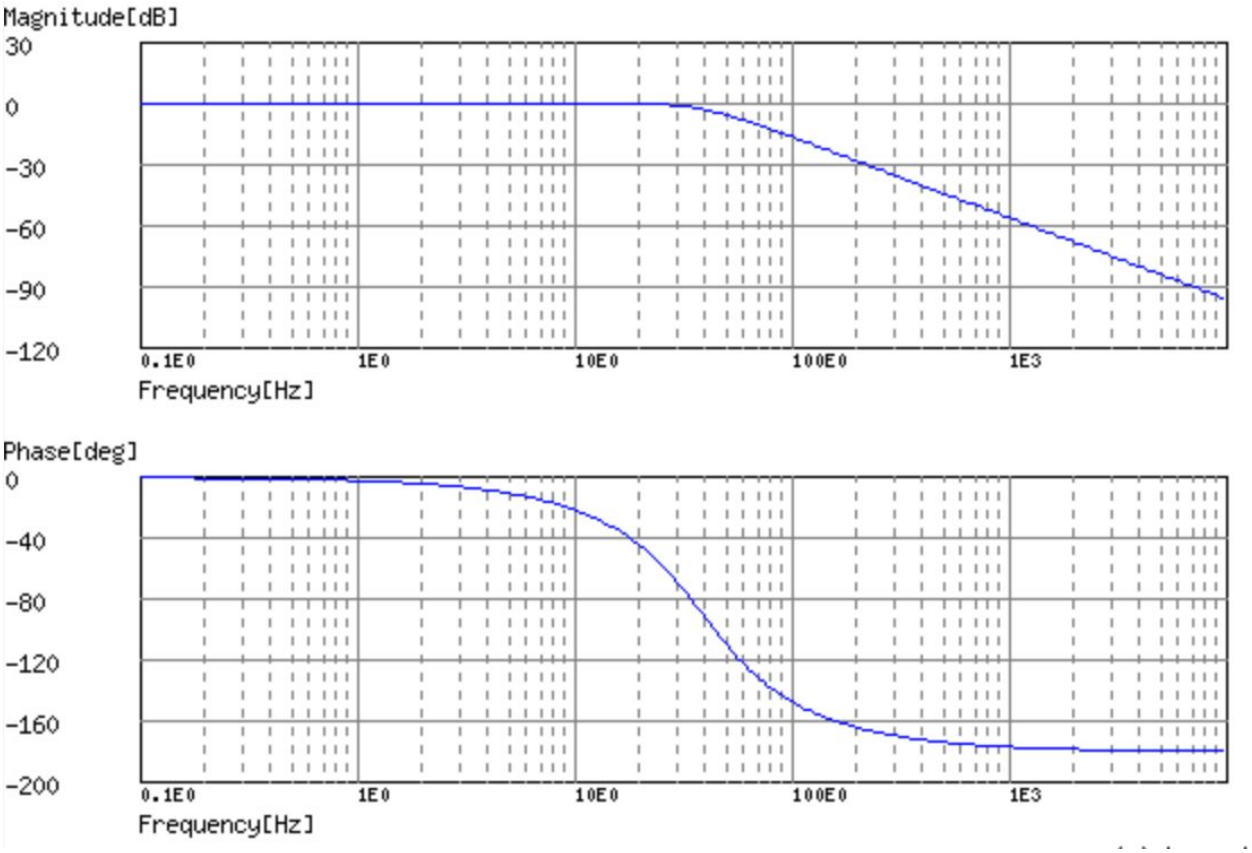

Figure 60 Theoretical Bode Plot of the 40 Hz Low-pass Filter (Okawa Electric Design, 2019)

Referring to the top plot depicted in Figure 60, we can determine that the filter passed all frequencies up until approximately 40 Hz. This can be inferred by the horizontal line occupying frequencies ranging from 0.1 Hz to 40 Hz. For the frequencies larger than 30 Hz the line is attenuated, steadily declining. This is because our low-pass filter was built to pass all frequencies smaller than 40 Hz. If we refer to the bottom plot, we can infer that at approximately 5 Hz the signal begins to experience phase delay. At the cut-off frequency of 40 Hz we can expect the signal to have a delay of approximately -100°. To convert the delay from degrees to seconds we can utilize Equation 14, referenced in Section 3.2.3, and find that the time delay to be 0.007 seconds at 40 Hz.

Once we had a finalized design for our low-pass filter with a cut-off frequency of 40 Hz, we built a prototype to be utilized in the analog front end of the finalized ECG circuit (see Figure 61).

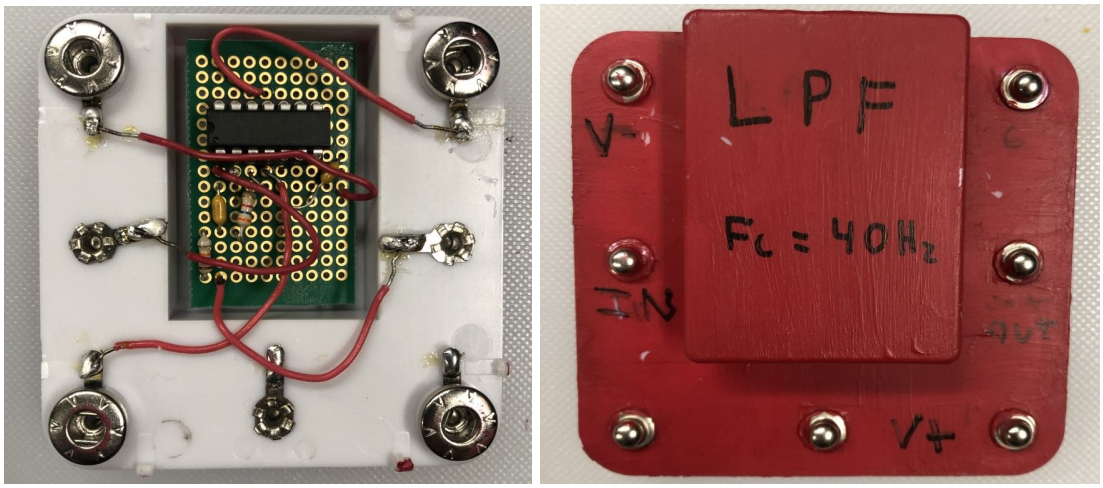

Figure 61 Physical Implementation of the Low-pass Filter with a Cut-off Frequency of 40 Hz

3.2.6 Gain Stage

After the signal passes through one of the low-pass filters, the user will then choose a gain. The next portion of the snap circuits that needed to be designed was the selectable gain stages. Our team decided upon two different gains that can be placed into the circuit. The two different gain modules we designed were 2 V/V and 3 V/V. We determined that the highest possible gain that could be implemented to avoid saturation was 3.2295 V/V. The method for determining this value is explained in section 3.2.3. Our team chose a non-inverting topology for the gain pieces. This topology is similar to the Sallen-Key topology that is used in both the high-pass and low-pass stages, without the filtering. To create the non-inverting amplifiers, we utilized an LM348 operational amplifier, similar to the high-pass and low-pass stages. We again utilized two 0.1 µF decoupling capacitors to limit the current.

Gain Stage of Gain of 2 V/V

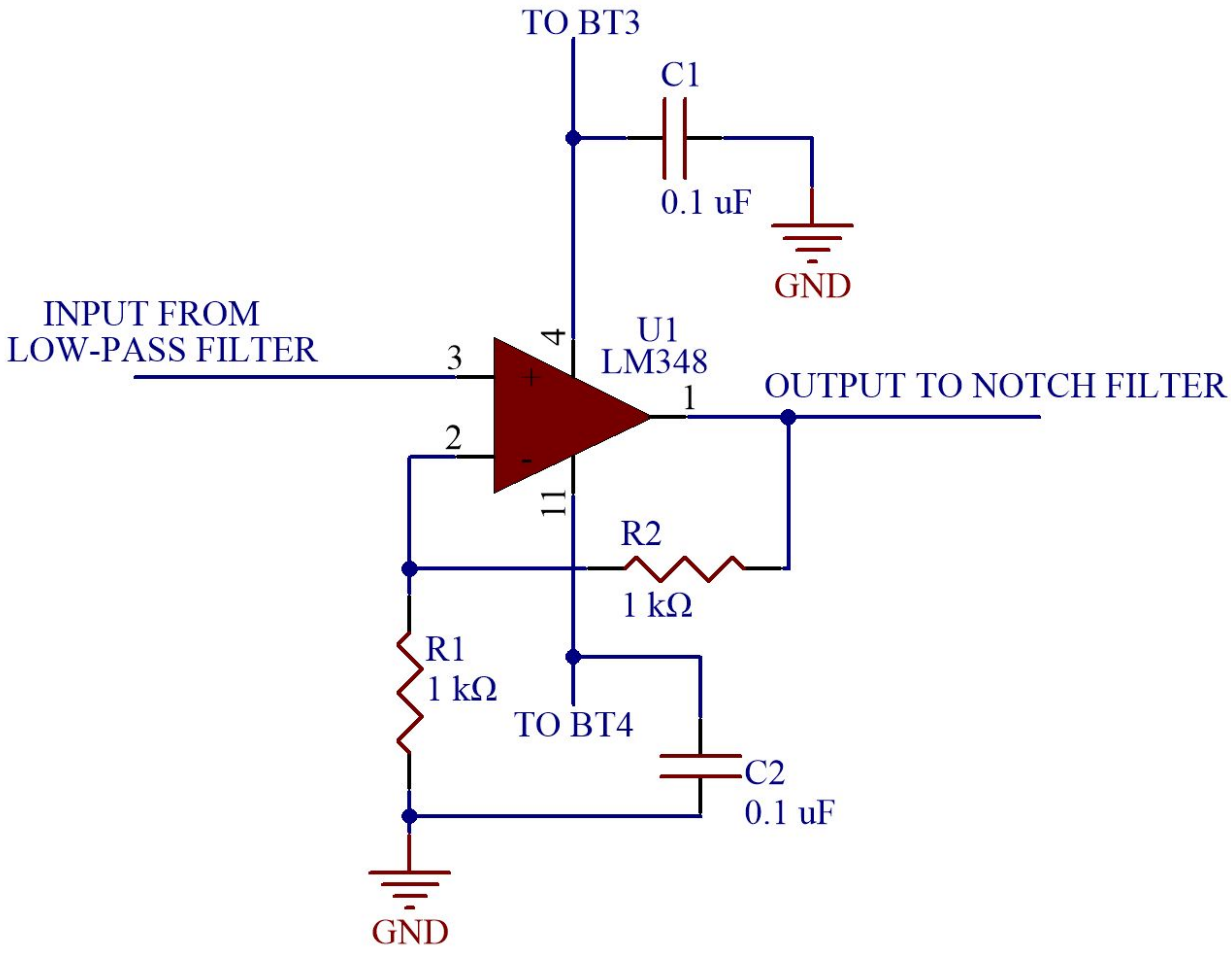

Figure 62 Schematic Gain Stage with Gain of 2 V/V

To calculate the gain for the gain stage of 2 V/V, we utilized Equation 16, which portrays the equation for determining the gain of a non-inverting amplifier circuit, while Figure 63 shows the topology for a non-inverting operational amplifier with a gain feedback loop.

$$A_V = (1 + \frac{R_2}{R_1})$$

Equation 17 Gain Equation for a Non-inverting Amplifier

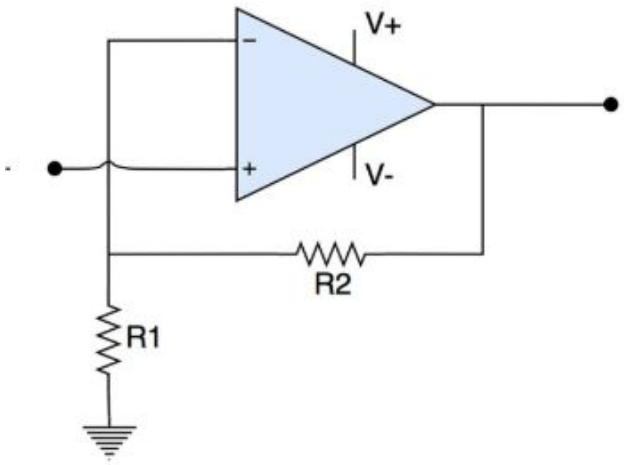

Figure 63 Non-Inverting Gain Stage Topology

For simplicity, R_1 was set to 1 kΩ and R_2 was used to control the gain. Therefore, to calculate for a gain of 2 V/V, R_1 = 1 kΩ and R2 = 1 kΩ as well:

$$A_V = (1 + \frac{1\,k\Omega}{1\,k\Omega}) = 2\,V/V$$

After the signal passes through the gain stage of 2 V/V, the total gain of the ECG circuit would be as follows:

$$A_{TOTAL} = 25.7\ V/V * 20\ V/V * 2\ V/V = 1028\ V/V$$

The snap circuits had the same pin connections as the low-pass filters that were designed. There are 5 connections on the snap circuit. The three power connections, +9V, -9V and ground. It also has a connection for the input and output signal. The photos of the physical implementations of the gain stage for a gain of 2 V/V are shown in Figure 64.

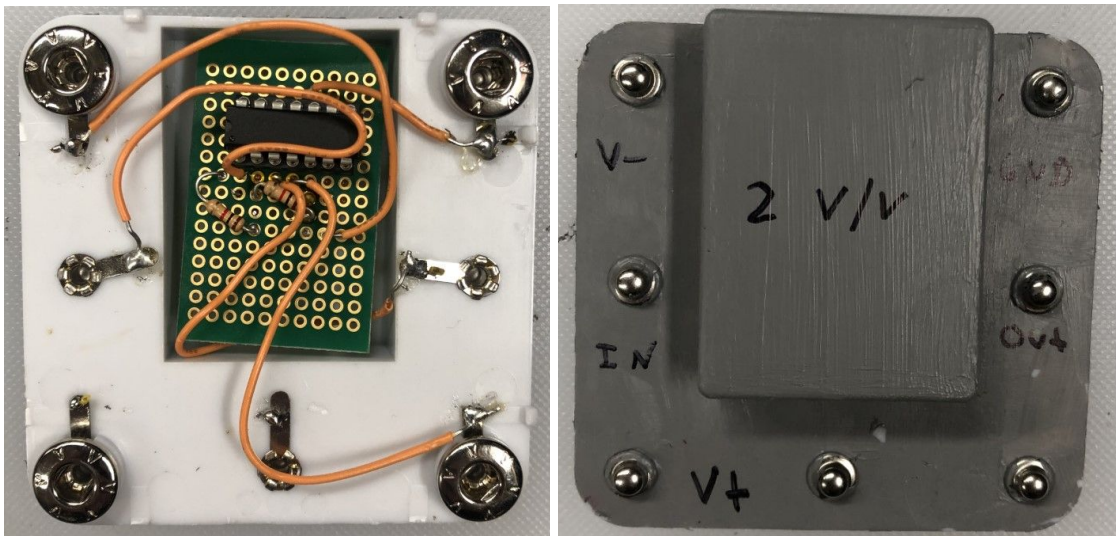

Figure 64 Physical Implementation of the Gain Stage with a Gain of 2 V/V

Gain Stage of Gain of 3 V/V

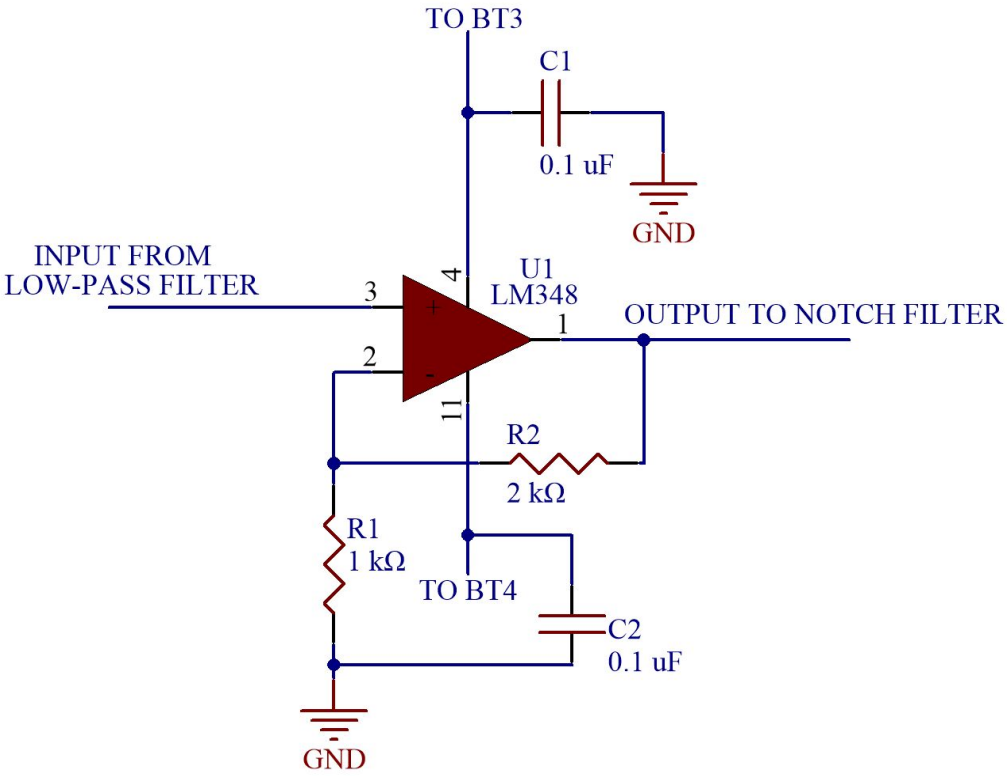

Figure 65 Schematic of Gain Stage with Gain of 3 V/V

To calculate the gain for the gain stage of 3 V/V, we again utilized Equation 16. R_1 was set to 1 kΩ and R_2 was used to control the gain similar to the 2 V/V gain stage. Therefore, to calculate for a gain of 3 V/V, R_1 = 1 kΩ and R2 = 3 kΩ as well:

$$A_V = (1 + \frac{2\,k\Omega}{1\,k\Omega}) = 3\,V/V$$

After the signal passes through the gain stage of 3 V/V, the total gain of the ECG circuit would be as follows:

$$A_{TOTAL} = 25.7\ V/V * 20\ V/V * 3\ V/V = 1542\ V/V$$

Once we had a finalized design for our gain stage with a gain of 3 V/V, we built a prototype to be utilized in the analog front end of the finalized ECG circuit (see Figure 66).

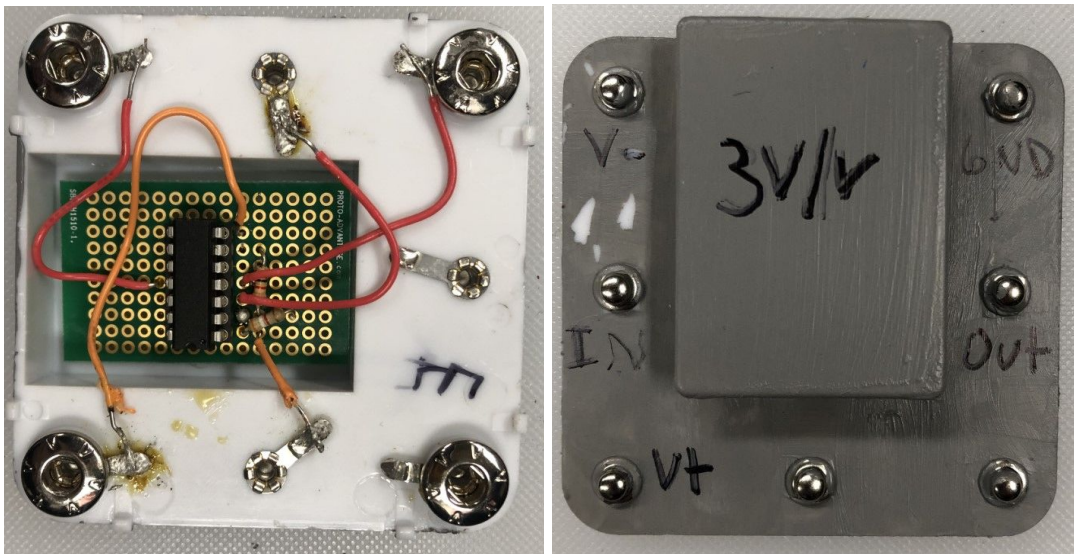

Figure 66 Physical Implementation of the Gain Stage with a Gain of 3 V/V

3.2.7 Notch Filter

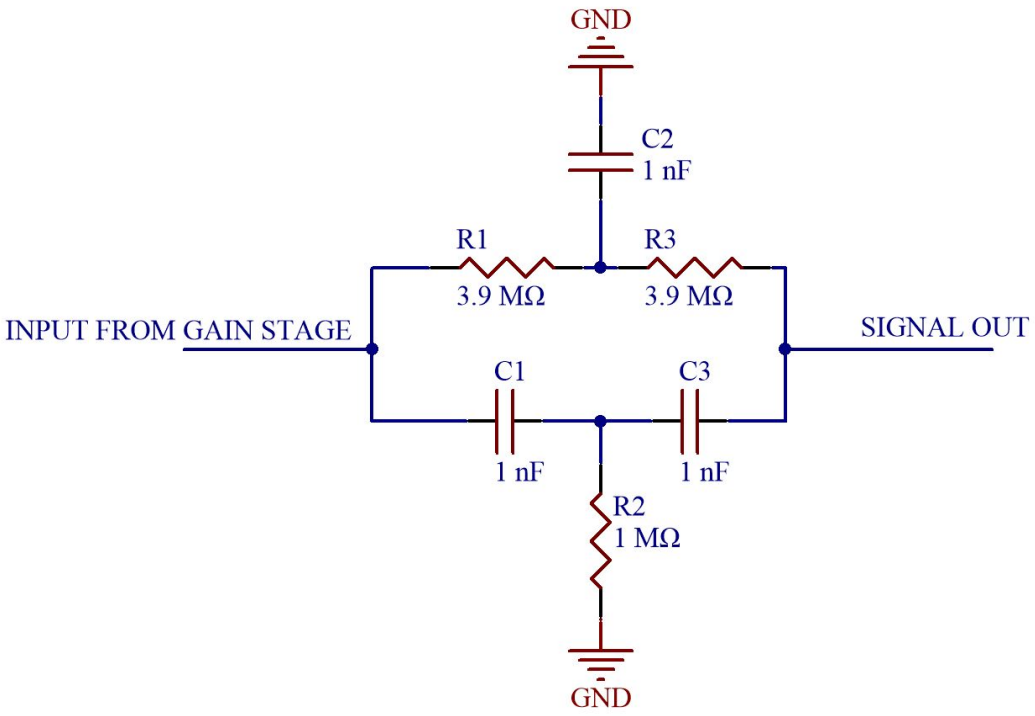

Figure 67 Schematic of Notch Filter with Stopband at 60 Hz

To design the notch filter correctly, we utilized the Okawa twin T notch filter design tool. We chose to implement a passive twin T notch filter because it is commonly utilized in ECG circuits and it was very simple to construct. The resistor and capacitor values for the notch filter were determined using the Okawa calculator. Our team tested the filter design against a pre-existing reference design and found that the passive circuit worked well in removing 60 Hz noise from the signal. The designed filter is shown in Figure 67, where the signal is input on the left side and output on the right side.

In order to ensure the notch filter performed properly we conducted the same tests as for the bandpass filter, without the step response. From Figure 68 we can determine that the notch filter should attenuate at 60 Hz as depicted by the large drop in-between 10 Hz and 100 Hz.

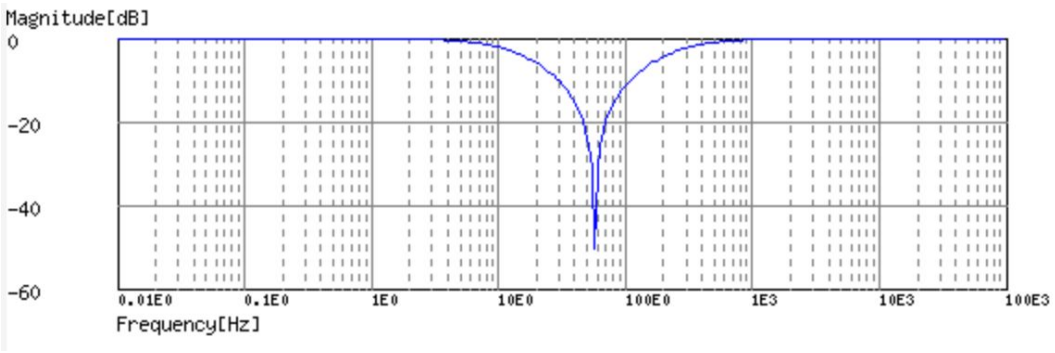

Figure 68 Theoretical Bode Plot of the Notch Filter (Okawa Electric Design)

A snap circuit piece was designed to implement this circuit. Since this module did not require any power, there were only 2 inputs and 1 output to the module. The two inputs were the signal and ground and the output pin was the signal output. This snap circuit piece is optional for the user. If it is used, it serves the function of being the last snap circuit module and the oscilloscope will be connected to it. Figure 69 portrays the final implementation of the notch filter module.

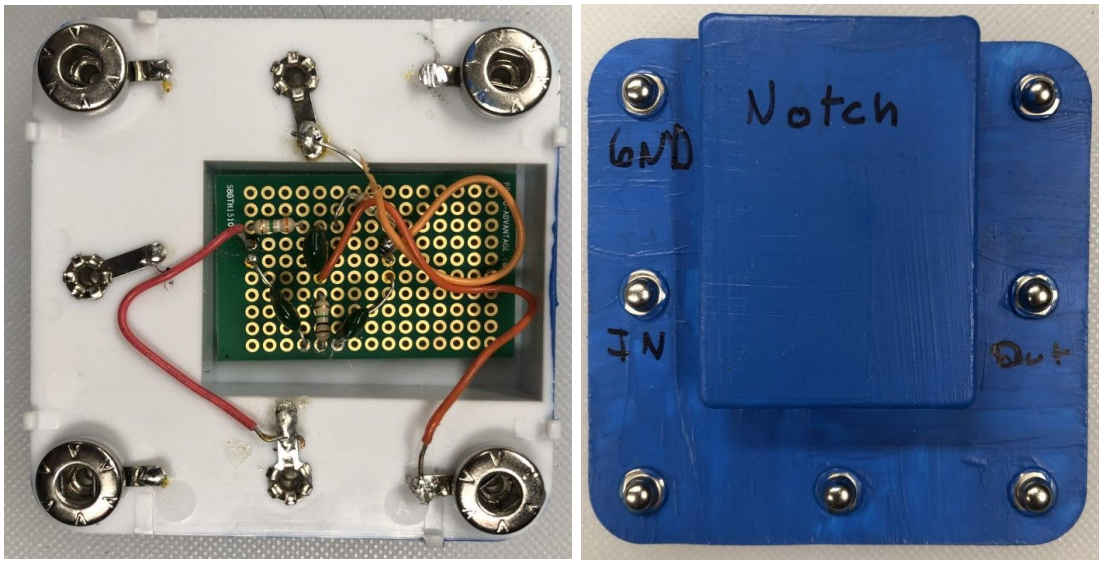

Figure 69 Physical Implementation of the Gain Stage with a Gain of 3 V/V

4. Results

4.1 Instrumentation Amplifier Stage

4.1.1 Gain Testing

	Instrumentation Amplifier
Theoretical	25.7 V/V
Measured	30.2 V/V
Vin	20 mV pk-pk
Vout	0.604 V pk-pk
Error	17.5%

Table 1 Comparison of Theoretical to Measured Gain Values for Instrumentation Amplifier

To verify the gain we expected to produce at the instrumentation amplifier stage we measured the amplitude of a 50 Hz sine wave at the output of each stage. We used a 50 Hz sine wave to measure the values because 50 Hz is within the passband of our filters and would not attenuate. As depicted in Table 1, we were pleased to find the theoretical values we solved for closely resembled the values we measured. For precision purposes, we solved for the percent error of our stage gains.

4.1.2 Common Mode Rejection Ratio

Common Mode Rejection Ratio (CMRR) is measured by evaluating the common mode gain and differential gain over the ECG signal's passband (0.05 Hz to 100 Hz). To find the common mode rejection ratio we connected the two input pins of the AD620 and applied a 5

Vpk-pk sine wave. Ideally, the instrumentation amplifier would recognize the same signal at both inputs and perfectly subtract one from the other to create an output of zero. The frequency of the input sine wave was varied from 1 Hz to 250 Hz incrementing by 10 Hz. At the output pin of the instrumentation amplifier we measured the amplitude of the output signal at each frequency and calculated for the common mode gain by utilizing Equation 18.

$$CMG = \frac{Output\ Amplitude}{Input\ Amplitude} = \frac{V_{OUT}}{5\ V}$$

Equation 18 Equation for Common Mode Gain

We found that the measured amplitude of the common mode output voltage ranged from 0.28 mV pk-pk at 1 Hz to 1.24 mVpk-pk at 250 Hz. We would like to note that while measuring the common mode output signal dropped to a very low magnitude that was difficult to measure reliably using the available lab, though we were not concerned because a small output indicates low common-mode gain.

$$CMRR\ (dB) = 20log_{10}(\frac{differential\ gain}{common\ mode\ gain})$$

Equation 19 Equation for Common Mode Rejection Ratio

Ideally, the output of the instrumentation amplifier would be 0 V. The measured output of the instrumentation amplifier was 2.8 mV. The common mode gain was then calculated by dividing the output of the instrumentation amplifier by the input voltage, 5 V. This gave a common mode gain of 0.56 mV/V. To calculate the common mode rejection ratio in dB, we divided the measured differential gain of the amplifier, 30.2 V/V by the common mode gain and converted the value into dB. This gave a common mode gain of 94.64 dB. This was repeated over the range of frequencies that we wanted to test. The results are shown in the graph below. In order for our circuit to attenuate 60 Hz noise from the body, the common mode rejection ratio would need to be at least 89 dB. Our circuit had a common-mode rejection ratio higher than 89 dB for frequencies less than 230 Hz. Since this extends the dynamic frequency range of the ECG

signal, our circuit worked within the required specifications. See Figure 70 for a plot of CMRR vs. Frequency.

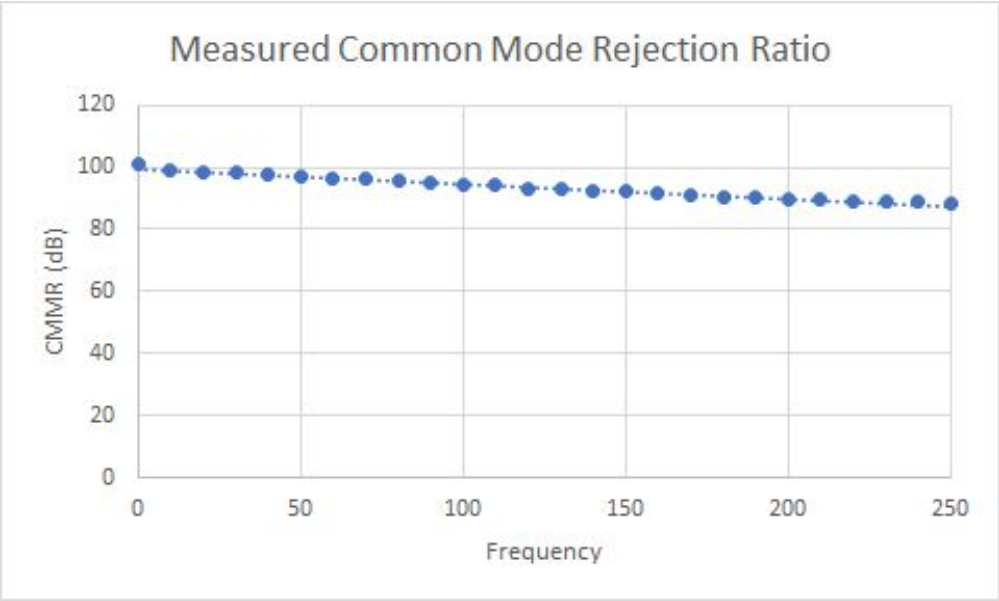

Figure 70 Common Mode Rejection Ratio

4.1.3 Input Offset Voltage

After we tested the gain and common mode rejection of the instrumentation amplifier, we then measured the input offset voltage, which should have been a maximum of 50 μV based on the specifications sheet of the AD620 (Analog Devices, 2019). To find this value, we had to connect the inputs of the instrumentation amplifier to ground to ensure the only voltage being passed through was the offset voltage. The offset voltage is a measurement of the noise voltage that is output from the instrumentation amplifier when no signal is being passed through. It is the difference between the two ground inputs that the AD620 amplified. Ideally, the input offset voltage should be 0 V. It is necessary to test the input offset voltage to ensure that a huge offset is not being amplified and corrupting the signal. Since this value is extremely small, we implemented a very high gain in the instrumentation amplifier, so we could measure the output accurately with a voltmeter. The input offset voltage is then determined by dividing the noise output voltage by the gain, which is equivalent to the large gain we implemented (Analog

Devices, 2019). It was important we tested the offset voltage of our implementation amplifier in order to ensure our output voltage was not skewed by too large of an offset.

After connecting the inputs to ground and setting the gain of the instrumentation amplifier, we measured the DC output voltage of our AD620 to be 2.7 μV. Due to the fact that the voltage is very small, we implemented a gain of 495 by setting the value of R_G equal to 100 Ω by using Table 1. We found the input offset voltage to be 5.45 nV after dividing the 2.7 μV output voltage by the different gain of 495. We were pleased to find the input offset voltage of our instrumentation amplifier was a small negligible value because it meant it was unlikely to have an impact on our output signal.

4.1.4 Input Bias Current

The input bias current on an operational amplifier is the DC current required by the inputs of the amplifiers in order to operate the first stage. The input offset current is the difference between the two input bias currents. Ideally, it is best not to have current flowing into the input terminals when using an operational amplifier (Analog Devices). To measure the current, we would use an ammeter to read the current values flowing into the input terminals. For instance, we would read I_{B+} and I_{B-} shown in Figure 35. While doing so, we would ensure the values were within the specified range of 0.3 - 1 nA.

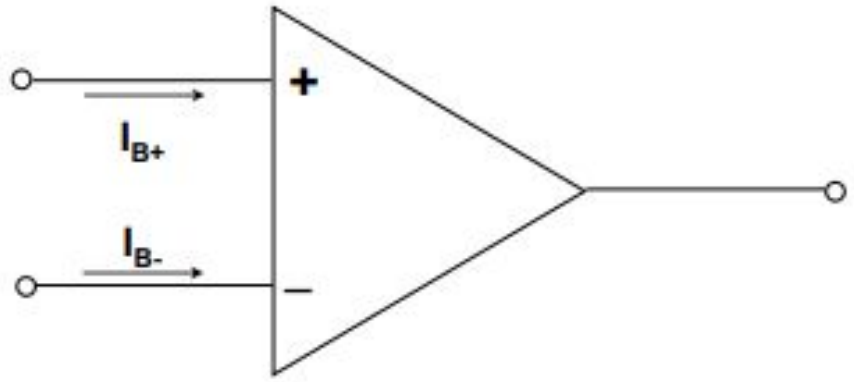

Figure 71 Definition of Operational Amplifier Input Bias Current (Analog Devices)

In order to find the input offset current, annotated as I_{OS}, we would need to subtract the differential currents I_{B+} and I_{B-} to find I_{OS}:

$$(I_{OS} = I_{B+} - I_{B-})$$

However, the value of I_{OS} is only meaningful if the two input bias currents are fundamentally reasonably well-matched to begin with (Analog Devices). An example where the value of I_{OS} would not be meaningful is for a current feedback operational amplifier because in such a scenario, the currents are radically unmatched. Unfortunately, the equipment we had available to us at Worcester Polytechnic Institute was not sensitive enough to measure these small currents, so we were not able to conduct these tests.

4.2 High-pass Filter Stage

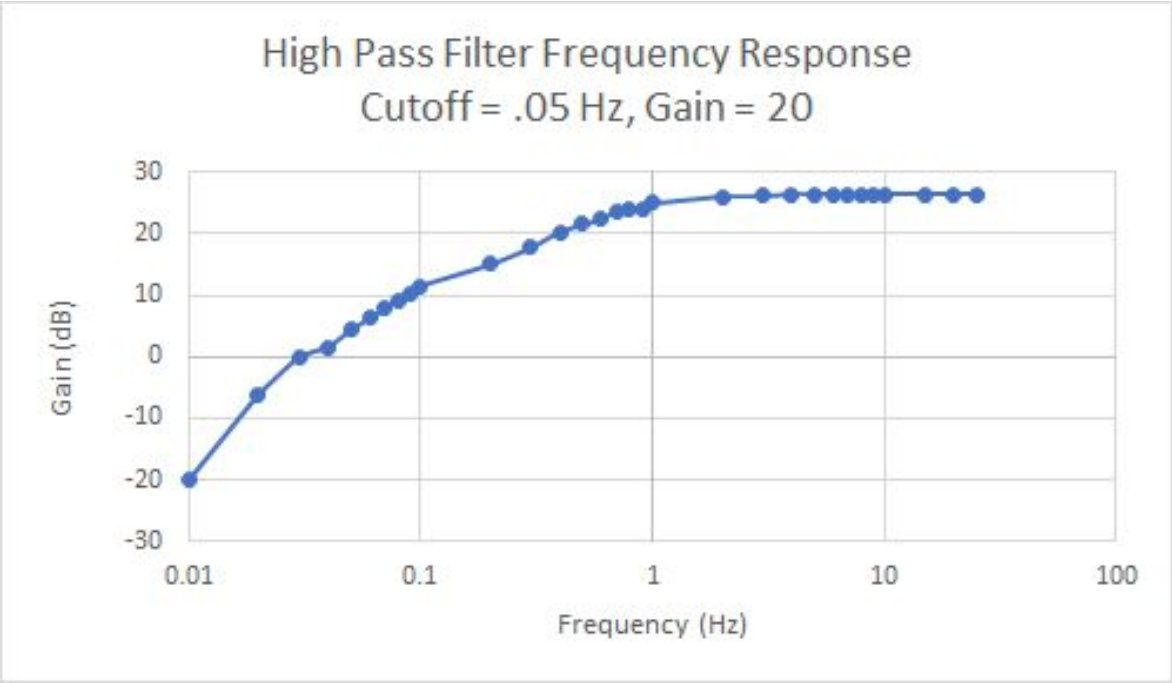

Figure 72 Magnitude Response of the High-pass Filter

Figure 72 depicts the magnitude response of a second order high-pass filter with a cutoff frequency of 0.05 Hz. This test was run by inputting a 0.1 V pk-pk sine wave into the high-pass filter and measuring the magnitude of the signal at frequencies from 0.01 Hz to 30 Hz. The measured results show that high-pass filter is performing closely to the idealized results that are discussed in the Methods section 3.2.3. The measured gain in the high-pass stage was 20.8 V/V, which is within the tolerance range of the designed filter gain, 20 V/V. The filter is rejecting frequencies under 0.05 Hz and amplifying signals that are above that threshold. As the frequency of the signal increased, the gain approached 20.8 V/V. Table 2 shows the results from the gain testing of the high-pass stage.

	High-Pass Filter
Theoretical	20 V/V
Measured	20.8 V/V
Vin	0.1 V pk-pk
Vout	2.08 V pk-pk
Error	4%

Table 2 Comparison of Theoretical to Measured Gain Values for High-pass Filter Stage

4.3 Low-pass Filter Stage

For the next test, we created magnitude responses for the three low-pass filters that were designed for the snap circuits. The filters designed were all second order Butterworth filters. The Sallen-Key topology also remained the same for all iterations. The only difference between the circuits are the resistor and capacitor values. All three filters worked as expected. The theoretical results of the filters are shown in the methods section 3.2.3 above. Since all three of the filters worked as they were expected to, it is hard to see any advantages to either of the filters by looking at just the magnitude response. The differences between the filter outputs are more visible by comparing the recorded ECG signal outputs. These results are shown in the Recorded ECG section below.

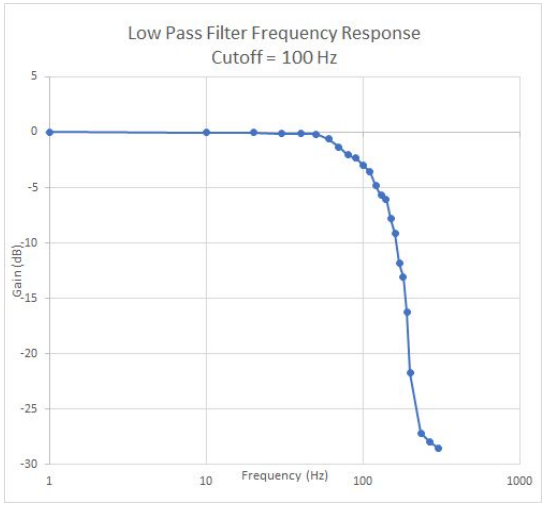

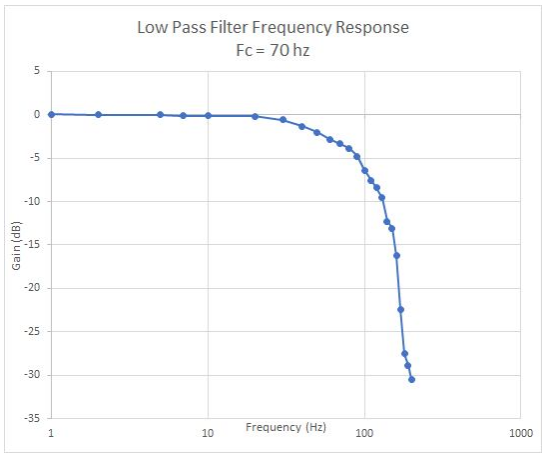

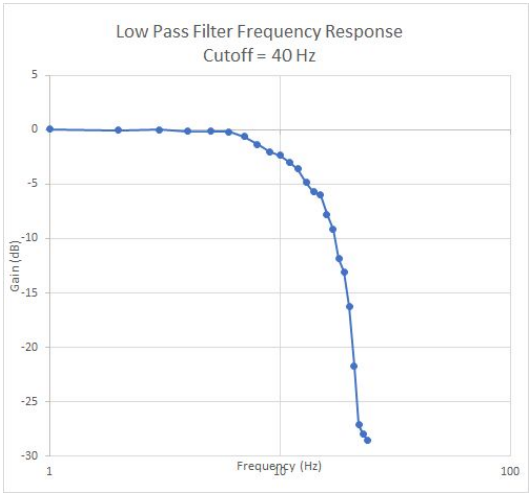

Figure 73 Magnitude Response of the Low-Pass Filter with 100 Hz (top), 70 Hz (middle), and 40 Hz Cut-off Frequency (bottom)

4.4 Variable Gain Stages

The next test was to measure the gain of the variable gain snap circuit pieces that were created for the display. The gain values were chosen as discussed in the methods sections. The purpose of this test was to measure the accuracy of the gain pieces and also to ensure that no saturation occurs when measuring an ECG signal. Table 3 shows the results from measuring the gains of the snap circuits. The pieces worked as they were expected to and no issues were found with the circuits.

	Gain of 2	**Gain of 3**
Theoretical	2 V/V	3 V/V
Measured	2.3 V/V	3.1 V/V
Vin	0.1 V pk-pk	0.1 V pk-pk
Vout	0.23 V pk-pk	0.31 V pk-pk
Error	15%	3.3%

Table 3 Comparison of Theoretical to Measured Variable Gain Values of Snap Circuits

4.5 Notch Filter Stage

The next magnitude response that we created was for the Twin "T" notch filter that was designed in the method section 3.2.4 of this paper. This filter was designed to eliminate 60 Hz noise from the signal. The filter did not work as effectively as it theoretically could have, as discussed in the methods section. Despite the noise present in the magnitude response, the addition of this circuit piece to the circuit seemed to significantly reduce the 60 Hz noise in the signal. An example of the output signal with and without the notch filter is shown in the recorded ECG section below.

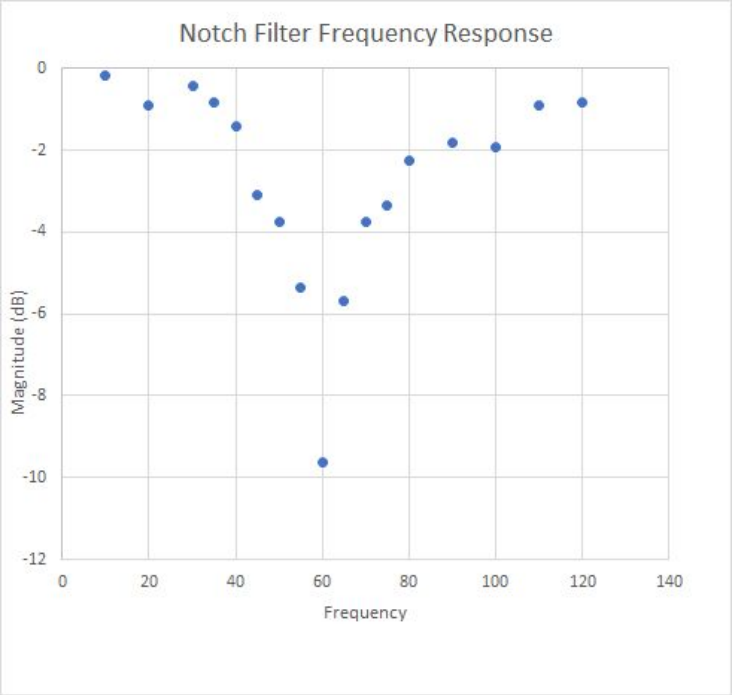

Figure 74 Magnitude Response of the 60 Hz Notch Filter

4.1.9 Recorded ECG

The screenshot shown in Figure 75 is the oscilloscope display of a filter output when using the low-pass filter with a cut-off frequency of 100 Hz, gain stage of 2 V/V, and an overall gain of 1028 V/V. This output has a visible ECG signal with clear QRS waveforms at each heartbeat. Due to the noise, the P and T waves are not visible. We then tested the circuit by changing the gain to 3. This output is shown in Figure XX below. When the gain was increased to an overall gain of 1542 V/V, more features of the waveform became visible. Then, the notch filter was added to the snap circuit and the 60 Hz was reduced. The signal could still be clearer, but it was a big improvement over the original output.

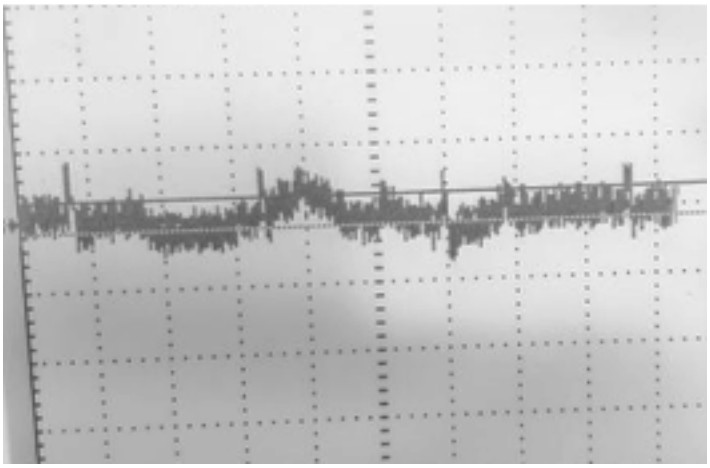

Figure 75 Recorded ECG with 100 Hz LPF, Overall gain of 1028 V/V, and No 60 Hz Notch Filter (Time division of 20 ms and 200 mV per division)

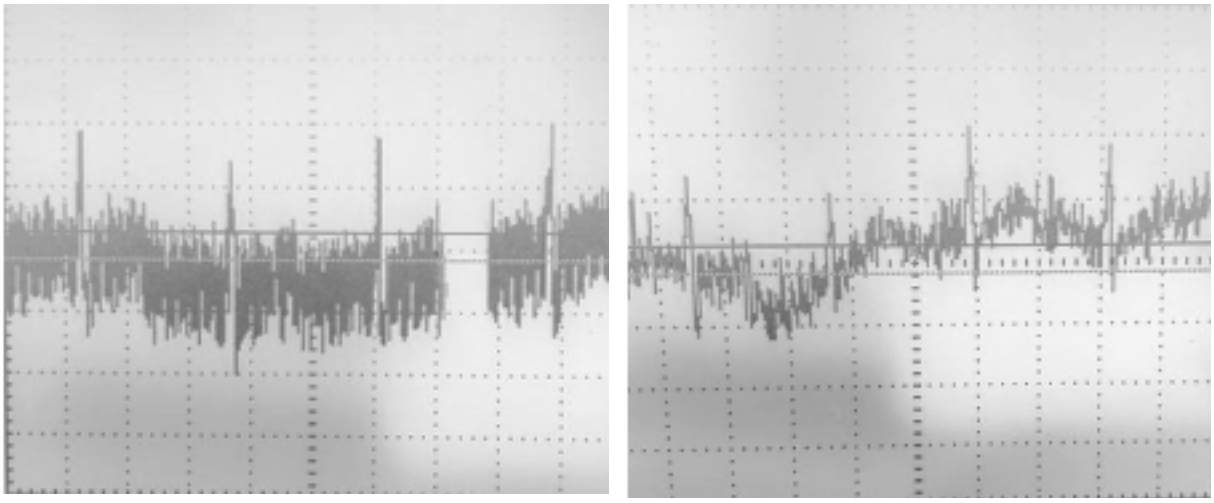

Figure 76 Recorded ECG with 100 Hz LPF, Overall gain of 1542 V/V, before (left) and after (right) 60 Hz notch filter is added (Time division of 20 ms and 200 mV per division)

The last configuration that we tested used the 40 Hz LPF, a Gain of 2, and the 60 Hz notch filter. This set-up produced a clean signal with clear QRS waves, as well as visible P and T waveforms. The downside to this set-up is that the amplitude of the peak is reduced. The resulting output is shown in the figure below.

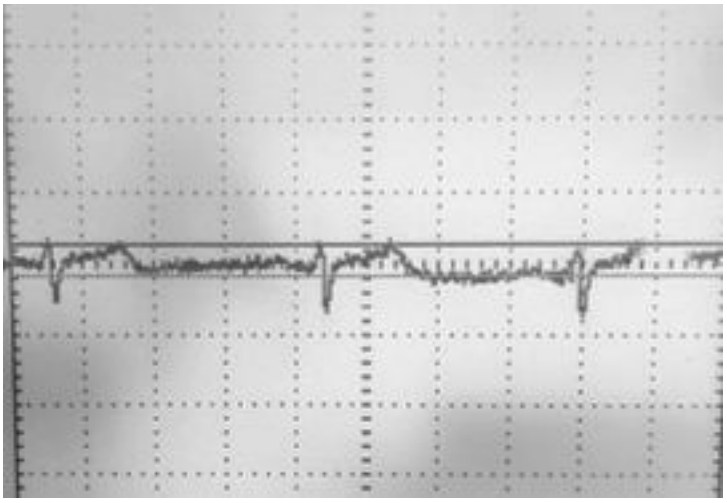

Figure 77 Recorded ECG with 40Hz LPF, a Gain of 2, and 60 Hz notch filter (Time division of 20 ms and 200 mV per division)

5. Discussion

We worked closely to determine what the criteria of our final design should be: an interactive educational display that represented the biomedical instrumentation concentration of ECE at WPI. The constraints we considered included time, cost and size while the objectives consisted of sustainability, reliability, safety and user friendliness. The final display was required to be capable of generating a clean ECG signal and had to be fully prepared to be on display for the "Touch Tomorrow" event in the Spring of 2020. To better describe our design process with respect to our constraints and objectives, we have divided this discussion by each portion of the ECG circuit, following the layout of Section 3.0.

In order to produce a successful display we had to create a display that worked with - not against our constraints and took into consideration our objectives. In designing our display we ensured to ask ourselves whether the ideas we pictured would be feasible within our constraints: time, cost and size. When we produced the electrode handles we took into consideration whether the handles we chose to implement would be feasible enough to build within our allotted time of fourteen weeks. This was a strict deadline for our group being that two out of the three members would not be able to extend the project into a third term. In addition, we wanted to ensure the handles we created were aesthetically pleasing, and within our budget, being that the display was meant to attract students from K-12 grade. This meant, we had to find a balance between one of our objectives, user-friendliness, and our second constraint: cost. For instance, in Section 3.2.1 we discuss that our first design iteration of the handles utilized adhesive electrodes (featured in Figure 31) because of how convenient the electrodes were for testing purposes. Although, we were aware that for the display the electrodes were an inefficient method. This is because adhesive electrodes are not reusable which means that WPI would need to purchase the electrodes in bulk to accomodate all visitors of the event, and even then it is possible for the event to run out of them. Adhesive electrodes can also be uncomfortable to remove and this could be a possible issue when working with young children. With these factors in mind, we knew in order to achieve the objectives of user-friendliness and sustainability we would have to

find another option for the electrode handles. After reviewing our options, we were pleased with our final decision to utilize exercise handles from an elliptical exercise machine (depicted in Figure 32). This is because the electrodes met each of our constraints and objectives. We received the electrodes from our Advisor, meaning we did not have to allocate our budget to purchasing them, or any additional time to finding them online. In addition, the electrodes are considered a standard size for hands - meaning the electrodes would be fine for all individuals visiting our display. As for our objectives, we were happy to provide stationary handles for the users to rest their hands on because it created a more kid-friendly and efficient method of measuring ECG signals. The stationary handles would limit possible inconveniences with measuring the ECG signals compared to the adhesive electrodes.

In order to design the fixed stage of the circuit, consisting of the instrumentation amplifier, high-pass filter, and isolation amplifier, we mainly took into consideration our objectives: sustainability, reliability, safety and user friendliness. Each of these stages were essential to the overall performance of the circuit, so we wanted to ensure the components we decided to utilize would be capable of performing to our expectations. In short, we were fine with spending more of our budget and time on these stages in order to perfect them. The only constraint we wanted to ensure we followed was keeping the perforated breadboards within their specified size of 44x28mm.

The fixed stage of the circuit was created to be non-interactive to ensure the reliability of the circuit, due to how sensitive this part of the circuit was and to ensure the safety of the users. This is because, the isolation amplifier galvanically isolated the fixed stage of the circuit from the interactive portion of the circuit as described in detail in Section 3.2.4. In addition, we wanted to ensure the display was sustainable and we knew if we kept the most difficult portion of the circuit secluded from the users it would only add to the longevity of the project. We were proud of our final design for the fixed portion of the circuit because we believe it balanced each objective well. Initially, we were worried that secluding a portion of the circuit would make the overall display less interactive. We were able to avoid this dilemma by adding variable cut-off frequencies for the low-pass filter and by producing a gain stage. By adding these additional

components to the circuit we believe we made the overall circuit more interactive while still protecting the fixed stage.

When creating the interactive portion of the circuit (the variable low-pass filter, gain stage, and the notch filter) we took into consideration the objectives and constraints of our project. We wanted to make certain that this portion of the circuit was user-friendly, sustainable and reliable. Users would interact with this portion of the circuit the most, and we wanted to make sure the users left feeling as though they learned something. When we designed this portion, we took into consideration our budget as well as the limited amount of time we had to produce something both creative and useful. We had to ensure the variable frequencies and gains we chose produced a large enough difference in the signal that users could visualize the differences on the oscilloscope.

References

Ai, Q., Liu, Q., Meng, W., Xie, S.Q. (2018). *Advanced Rehabilitative Technology: Neural Interfaces and Devices.* (1st ed., Vol. 1, pp. 33-66). Philadelphia, PA: Elsevier. doi: 10.1016/B978-0-12-814597-5.00003-5.

Albano, A.J., Badilini, F., Downey, J., Kakuhire, B., Koplan, B., Kraemer, J., Magadoro, I.M., Muthalaly, R., North, C.M., Siedner, M.J., Tsai, A.C., Vaglio, M., & Vořechovská, D. (2019). *Global Heart: Population Prevalence and Correlates of Prolonged QT Interval: Cross-Sectional, Population-Based Study From Rural Uganda.* (1st ed., Vol. 14, p. 17-25). Philadelphia, PA: Elsevier. doi: 10.1016/j.gheart.2018.11.002.

Analog Devices. (2009). *Analog Isolation Amplifiers.* Norwood: Analog Devices, Inc.

Anderson, P. G., Anderson, S.I., Lowe, J.S., & Stevens, A. (2015). *Stevens & Lowe's Human Histology*. (4th ed., Vol. 1, pp. 143-165). Philadelphia, PA: Elsevier. doi: 10.1016/B978-0-7234-3502-0.00009-7.

Ay, A. N., Güler, M., Türker, A.Y., Yildiz, M.Z. (2017). Design Of A Microcomputer Based Real-time ECG Holter Device. Retrieved from: https://www.researchgate.net/figure/ECG-Circuit-Block-Diagram_fig3_318913145.

Bag, S., Banerjee, I., Khasnobish, A., Kraatz, H.B., Kuruganti, U., & Pal, K. (2019). *Bioelectronics and Medical Devices: From Materials to Devices - Fabrication, Applications, and Reliability*. (1st ed., Vol. 1, pp. 591-614). Cambridge, MA: Woodhead Publishing. doi: 10.1016/B978-0-08-102420-1.00030-3.

Beckerle, P., Bowers, M.P., Liarokapis, M., Popovic, M.B., Willwacher, S. (2019). *Biomechatronics: Prosthetic Limbs*. (1st ed., Vol. 1, pp. 235-278). Philadelphia, PA: Elsevier. doi: 10.1016/B978-0-12-812939-5.00009-4.

Bitar, S.J., Ludwig, R., Makarov, S.N. (2016). *Practical Electrical Engineering.* (1st ed., Vol. 1, pp. 59-64). Berlin, Germany: Springer Science & Business Media.

Brayner, A.R.A., Cortez, P.C., Filho, J.M.S.M., Madeiro, J.P.V.M. (2019). *Developments and Applications for ECG Signal Processing: Modeling, Segmentation, and Pattern Recognition.* (1st ed., Vol. 1, pp. 53-87). Philadelphia, PA: Elsevier. doi: 10.1016/B978-0-12-814035-2.00009-8.

Carter, B., Mancini, R. (2018). *Op Amps for Everyone.* (5th ed., Vol. 1, pp. 199-258). Philadelphia, PA: Elsevier. doi: 10.1016/B978-0-12-811648-7.00016-9.

Crowley, V., Huang, S., Rajotte, K., Wartman, W. (2019). *Wireless ECG and Pulse Oximeter: Creating a Multi-Modal Device for Clinical and Monitoring Applications.* Worcester: Worcester Polytechnic Institute.

Davey, P., & Sharman, D. (2018). *Medicine*. (8th ed., Vol. 46, pp. 443-452). Philadelphia, PA: Elsevier. doi: 10.1016/j.mpmed.2018.05.004.

ELPROCUS. (2019). *Isolation Amplifier: Working and Its Applications.* Retrieved from https://www.elprocus.com/isolation-amplifier-working-and-its-applications/.

Emery, W.J., Thomson, R.E. (2014). *Data Analysis Methods in Physical Oceanography*. (3rd ed., Vol 1, pp. 593-637). Philadelphia, PA: Elsevier. doi:10.1016/B978-0-12-387782-6.00006-5.

Francis, J. (2016). *ECG Monitoring Leads and Special Leads.* (16th ed., Vol 3, pp. 92-95). Indian Pacing Journal and Electrophysiology. doi: 10.1016/j.ipej.2016.07.003.

Gerstenhaber, M., Hunt, S., Johnson, R. (2015). *No Pain, High Gain: Building a Low-Noise Instrumentation Amplifier with Nanovolt Sensitivity.* Norwood: Analog Devices, Inc.

Goldberger, A.L., Goldberger, Z.D., & Shvilkin, A. (2018). *Goldberger's Clinical Electrocardiography.* (9th ed., Vol 1, pp. 21-31). Philadelphia, PA: Elsevier. doi: 10.1016/B978-0-323-40169-2.00004-4.

Hirsch, E.D., Kett, F.D., Trefil, J. (2002). *The New Dictionary of Cultural Literacy*: *What Every American Needs to Know* (3rd ed., Vol 1, pp. 546-586). Boston, MA: Houghton Mifflin.

Farnsworth, B. (2019). *What is an ECG and How Does it Work?* IMOTIONS.

Issa, Z.F., Miller, J.M., & Zipes, D.P. (2019). *Clinical Clinical Arrhythmology and Electrophysiology: A Companion to Braunwald's Heart Disease.* (3rd ed., Vol. 1, pp. 1-14). Philadelphia, PA: Elsevier. doi: 10.1016/B978-0-323-52356-1.00001-3.

Kester, W. (2012). *Grounding and Decoupling: Learn Basics Now and Save Yourself Much Grief*

Later! Part2: Decoupling. Norwood: Analog Devices, Inc.

Kutz, M. (2009). *Biomedical Engineering and Design Handbook: Bioelectricity and its Measurement.* (2nd ed., Vol 1, pp. 327-346).New York City, NY: McGraw-Hill.

Meek, S., & Morris, F. (2002). ABC of Clinical Electrocardiography. Introduction: I-Leads, Rate,

Rhythm, and Cardiac Axis. London, UK: BMJ Publishing.
doi: 10.1136/bmj.324.7334.415.

Okawa Electric Design. (2019). Sallen-Key High-pass Filter Design Tool. Retrieved from: http://sim.okawa-denshi.jp/en/TwinTCRkeisan.html.

Okawa Electric Design. (2019). Sallen-Key Low-pass Filter Design Tool. Retrieved from: http://sim.okawa-denshi.jp/en/TwinTCRkeisan.html.

Okawa Electric Design. (2019). Twin-T Notch Filter Design Tool. Retrieved from: http://sim.okawa-denshi.jp/en/TwinTCRkeisan.html.

Pashtoon, N.A. (1987). *Handbook of Digital Signal Processing: Engineering Applications.* (1st ed., Vol. 1, pp. 137-168). Philadelphia, PA: Elsevier. doi: 10.1016/C2009-0-21739-9.

Pieter, P. (2018). *Butterworth Filters.* Retrieved from: https://tttapa.github.io/Pages/Mathematics/Systems-and-Control-Theory/Analog-Filters/

Butterworth-Filters.html.

Rempfer, W.C. (2011). *Analog Circuit Design: A Tutorial Guide to Applications and Solutions.* (1st ed., Vol. 1, pp. 406-413). doi: 10.1016/B978-0-12-385185-7.00021-4.

Salinet, J.L., Silva, O.L. (2019). *Development and Applications for ECG Signal Processing: Modeling, Segmentation, and Pattern Recognition.* (1st ed., Vol. 1, pp. 29-51). Philadelphia, PA: Elsevier. doi: 10.1016/B978-0-12-814035-2.00008-6.

Terrell, D.L. (1996). *Op Amps: Design, Application, and Troubleshooting*. (2nd ed., Vol. 1, pp. 404-423). Philadelphia, PA: Elsevier. doi: 10.1016/B978-0-7506-9702-6.X5000-8.

Texas Instruments. (2015). LMC6484 CMOS Quad Rail-to-Rail Input and Output Operational Amplifier. Dallas, TX: Texas Instruments Incorporated.

Texas Instruments. (2018). SimpleLink™ MSP432P401R high-precision ADC LaunchPad™ Development Kit. Dallas, TX: Texas Instruments Incorporated.

Thompson, M.T. (2006). *Intuitive Analog Circuit Design*. (1st ed., Vol. 1, pp. 385-416). Philadelphia, PA: Elsevier. doi: 10.1016/B978-075067786-8/50014-8.

University of Iowa Department of Physics and Astronomy. (2017). *Percent Error Formula.* Retrieved from: http://astro.physics.uiowa.edu/ITU/glossary/percent-error-formula/.

Winder, S. (2008). *Analog Circuits: World Class Designs.* (1st ed., Vol. 1, pp. 347-267). Philadelphia, PA: Elsevier. doi: 10.1016/B978-0-7506-8627-3.00011-X.

Worcester Polytechnic Institute. (2019). Touch Tomorrow: A Festival of Science, Technology, &

Robots.

Zumbahlen, H. (2008). *Linear Circuit Design Handbook.* Norwood: Analog Devices, Inc.

Appendix A: Bill of Materials

	Product	Quantity	Price Per Item	Personal Funds	Part Number
ECG Display					
	Cutting Board (Base of Display)	1	$0.00		
	Elenco Electronics Snap-Circuits	1		$80.00	756619002187
	ECG Electrodes: Excersize Machine Handles	2		$0.00	
	ECG Electrodes: Surface Electrodes	1 Packet	$0.00		
	Oscilloscope	1	$0.00		
	Monitor	1	$0.00		
	Exercise Handles	1		$0.00	
	Fitness Maniac Home Gym Handle	1	$19.69		
	EDGELEC 120pcs Dupont Wire	1	$19.98		
	Breadboard General Purpose PTH	24	$2.09		SBBTH1510-1
	Elenco Snap Circuits: Recording Integrated Circuit IC U6	6	$6.96		
	Ceramic Capacitor 0.1uF 50V Z5U Radial	20	$0.24		C315C104M5U5TA7303
	Ceramic Capacitor 1uF 50V X7R AXIAL	20	$0.43		C420C105K5R5TA91707200
	IC Instrumentation Amplifier 1 Circuit 8DIP	12	$16.91		AD620BNZ
	Metal Film Resistors: Through Hole 1/2W 250Kohms 0.25%	20	$0.58		71-CMF55250K.25%T2
	Resistor 200k Ohm 1/4W 1% AXIAL	20	$0.10		RNF14FTD200K
	Ceramic Capacitor .47uF 50V Z5U AXIAL	20	$0.30		C430C474M5U5TA7200
	Resistor 7.5k Ohm 0.4W 1% AXIAL	20	$0.44		MBA02040C7501FC100
	Ceramic Capacitor .33uF 50V Z5U AXIAL	20	$0.33		C412C334M5U5TA7200
	IC Operational Amplifier GP 4 Circuit 14DIP	10	$3.16		LMC6484AIN/NOPB
	IC Instrumentation Amplifier 1 Circuit 8DIP	6	$11.26		AD620ANZ
	IC Operation Amplifier Isolation 1 CIRC 8DIPGW	5	$6.80		ACPL-790A-500E
	IC Operational Amplifier GP 4 Circuit 14DIP	5	$1.04		MCP604-I/P
	Ceramic Capacitor, 0.1UF, 50V, Y5V, +80,-20%, 0805	6	$0.10		C0805C104Z5VACTU
	Ceramic Capacitor 1uF 25V Y5V 0805	2	$0.15		CC0805ZRY5V8BB105
	Resistor 200k Ohm 0.1% 1/8W 0805	2	$0.36		ERA-6AEB204V
	Resistor 250k Ohm 1% 2W 2512	2	$6.29		HVCB2512FDC250K
	Resistor 15k Ohm 1% 1/4W 0805	1	$0.10		RNCP0805FTD1K50
	Resistor SMD 1k Ohm 5% 1/8W 0805	1	$0.10		RC0805JR-071KL
	IC Operational Amplifier GP 4 Circuit 14SOIC	2	$0.46		LM348DR
	Resistor SMD 2k Ohm 1% 1/8W 0805	1	$0.10		CRCW08052K00FKEAC
	IC Instrumentation Amplifier 1 Circuit 8SCOIC	1	$6.20		AD620ARZ-REEL7
	Ceramic Capacitor, 0.33UF 25V Y5V 0805	2	$0.21		CC0805ZRY5V8BB334
	Resistor 7.5k Ohm 1% 0805	2	$0.10		RNCP0805FTD7K50
	High Pass Filter PCB Order	10		$0.97	
	Low Pass Filter PCB Order	10		$0.97	
	Instrumentation PCB Order	10		$0.97	
	Sharpie: Extra Bold Poster Paint Markers, Black	1		$9.99	
	Liquitex: Basics Acrylic Paint 4oz.	3		$4.99	
	Black Belmont Shadow Box by Studio Decor	1		$11.49	
	Necessities Bristle Round Brushes by Artist's Loft	1		$7.99	
Total			**$534.91**	**$156.48**	

Appendix B: Directions for Touch Tomorrow Event

Step 1: Plug in the 9 V batteries

Step 2: Turn on the oscilloscope. Set to AC coupling. Set the time scale to 250 ms and set the volts per division to 100 mV.

Step 3: When you are handed the board, connect the wires as connected in the photo below. [Both the right and left side of the photo have wires connected. Right side is oscilloscope and left side are the wires from the fixed portion of the circuit] If a signal does not appear, press the autoscale (or auto set) button and adjust the time scale back to 250 ms.

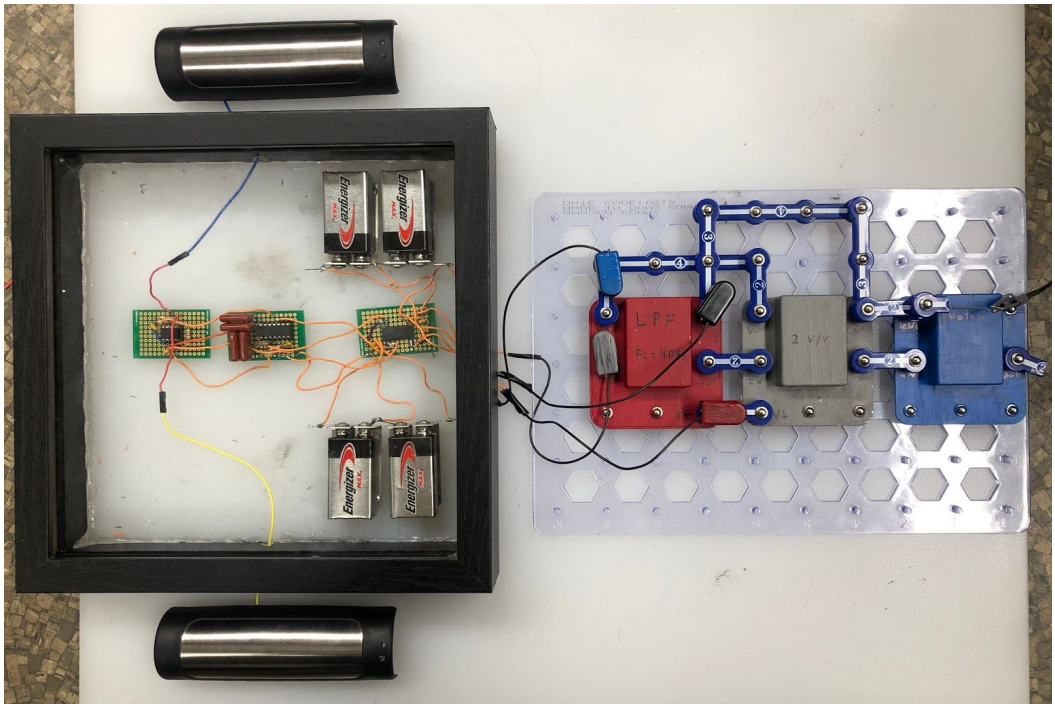

On the left side of the photo:

- Grey wire head is connected to the input pin of the low-pass filter
- Red wire head is connected to V+ of the low-pass filter
- Blue wire head is connected to V- of the low-pass filter
- Black wire head is connected to ground

On the right side of the photo:

- Oscilloscope alligator clip (common) is connected to ground
- Oscilloscope head (positive reference) is connected to output

Step 4: Tell the participant to place their hands lightly on the handles. After they see their ECG signal, clean the handles

Step 5: Repeat the process for all participants

Step 6: When packing the display make sure to unplug the batteries

Appendix C: Posters for Touch Tomorrow Event

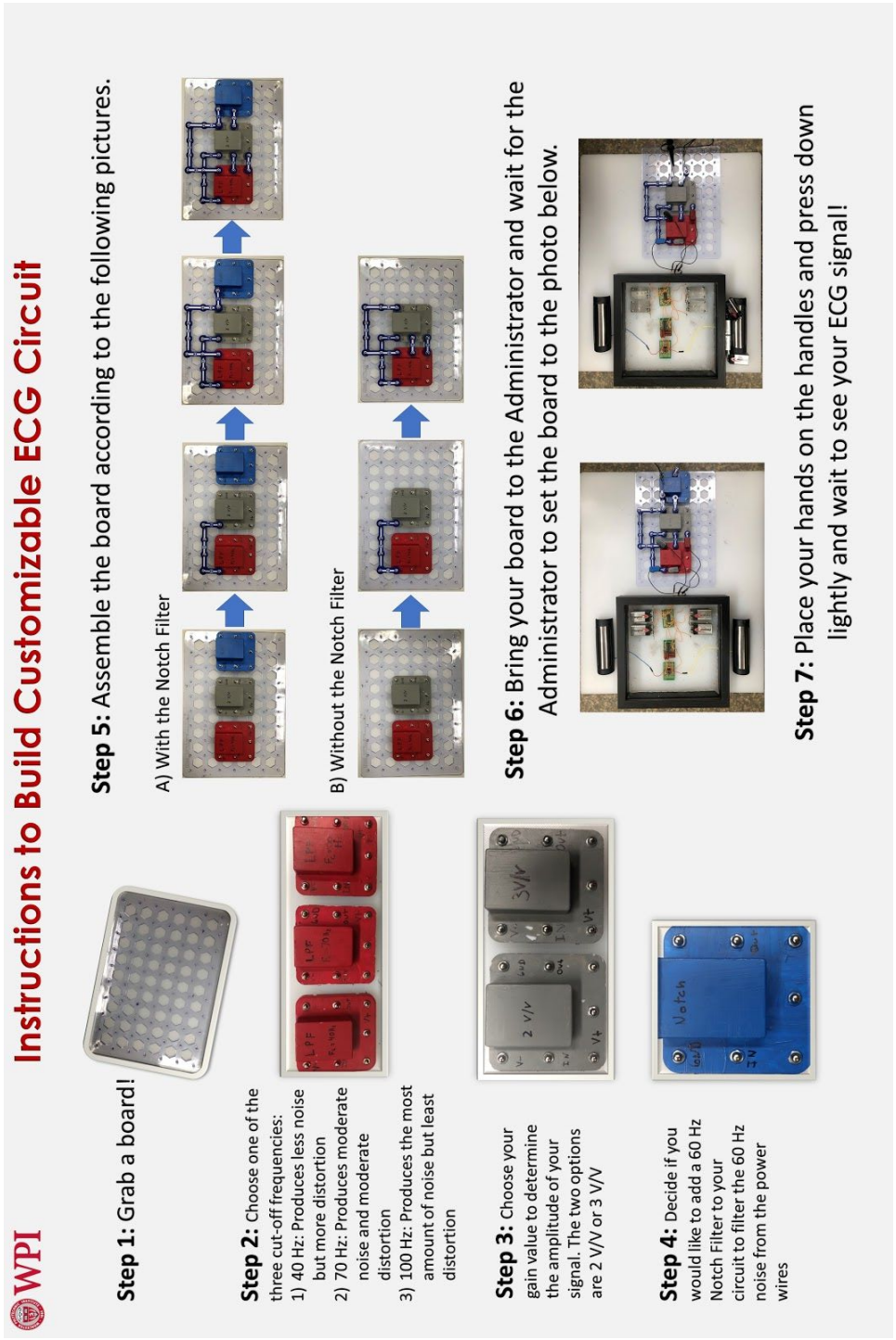

Interactive Electrocardiograph Display

Created By: Jody Carregal, William Crafa and Morgan Shubert

Q: What is an electrocardiogram (ECG)?

A: An ECG is a method used to measure and record the electrical activity of the heart. With every beat our heart contracts and relaxes producing electrical impulses monitored by the ECG.

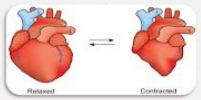

Q: Why is an ECG important?

A: ECG can tell us the condition of the heart. ECG can also detect areas of the heart that may be deprived of oxygen or contain dead tissue.

Q: How is ECG measured?

A: ECG is measured through electrodes that are placed on the human body at significant points to detect the electrical changes occurring when your heart beats.

Q: What does the ECG look like?

A: ECG depicts your heart rhythm, and like the example shown in the diagram below.

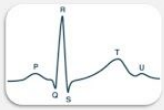

Q: Does an ECG hurt?

A: Not at all! The electrodes placed on your body are harmless and can be compared to a sticker. They simply stick on your skin and peel right off! You may sometimes see electrodes that clip onto the skin as well.

Q: What is the useful bandwidth of an ECG signal?

A: To understand the useful bandwidth of an ECG you should first understand what a wave represents. From this, you can gain an understanding of what frequency means and how frequency is measured.

Q: What does a wave represent?

A: Examples of waves include sound, light, water and earthquakes. Each of these waves are signals summed up. Sine waves have a length called wavelength, a frequency which is the number of oscillations (or cycles) in a period of time and an amplitude (height).

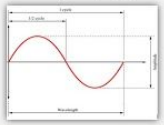

Q: What is frequency and how is it measured?

A: The frequency of a wave is the number of times per second the wave cycles and is measured in Hertz (Hz). Frequency is often represented by a lower case "f".

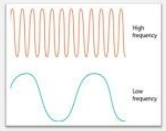

Q: What is the bandwidth of a signal?

A: For our purposes, the bandwidth of a signal is a range of frequencies that are used for transmitting a signal.

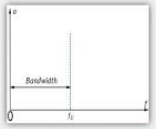

Q: So, what is the useful bandwidth of an ECG signal?

A: The useful bandwidth of an ECG signal ranges from 0.05 Hz to 100 Hz dependent on the application.

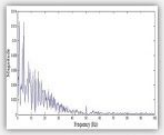

Q: What is a high-pass filter?

A: A high-pass filter passes signals with frequencies higher than the cut-off frequency and rejects signals with frequencies lower than the cut-off frequency. The cut-off frequency is a chosen value depicted by Fc.

Q: What is a low-pass filter?

A: A low-pass filter passes signals with frequencies lower than the cut-off frequency and rejects signals with frequencies higher than the cut-off frequency.

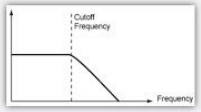

Q: What is a bandpass filter?

A: A bandpass filter is made by combining a low-pass and high-pass filter. Bandpass filters allow signals between two frequencies to pass, any signals outside of that range cannot pass.

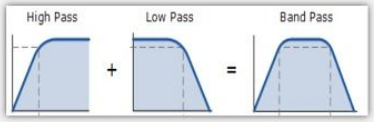

Q: What is a Notch Filter?

A: A notch filter only allows frequencies outside of a certain range (known as the stopband) to pass. This passband range is small in size.

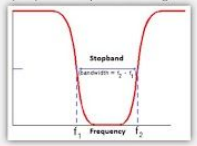

Q: What is an instrumentation amplifier?

A: An instrumentation amplifier allows amplifies the difference between the two inputs. Essentially, the amplitude of the signal being measured is increased. Increasing the amplitude helps to reduce the amount of noise effecting the signal. The amplifier also rejects additional noise effecting the signal from the inputs of the amplifier.

Q: What is noise?

A: Noise is unwanted disturbances that are captured when measuring and/or recording a signal. The first plot depicts a standard ECG while the bottom plot depicts a noisy ECG.

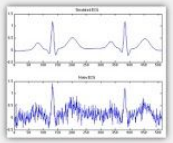

Q: What is an isolation amplifier?

A: The isolation amplifier can be found in the protection stage of our circuit. This amplifier limits the input range, rejects high frequencies and provides a barrier for high voltages. The isolation amplifier was added for precautionary measures to isolate the human body from the circuit.

Q: Why WPI?

A: WPI provides students with the ability to design their own path within their majors. At WPI students are immersed in a project-based curriculum where their work has an impact, and they gain hands-on experience within their major.

Q: Why study Electrical and Computer Engineering (ECE)?

A: WPI provides ECE students with the opportunity to learn more about a wide range of fields within ECE. Including, but not limited to: Machine Learning, Cryptography, Information Security, Signal Processing, Autonomous Vehicles, Prosthetic Controls and much more. In addition, ECE is now a growing field in the working world.

Appendix D: Final Presentation Poster

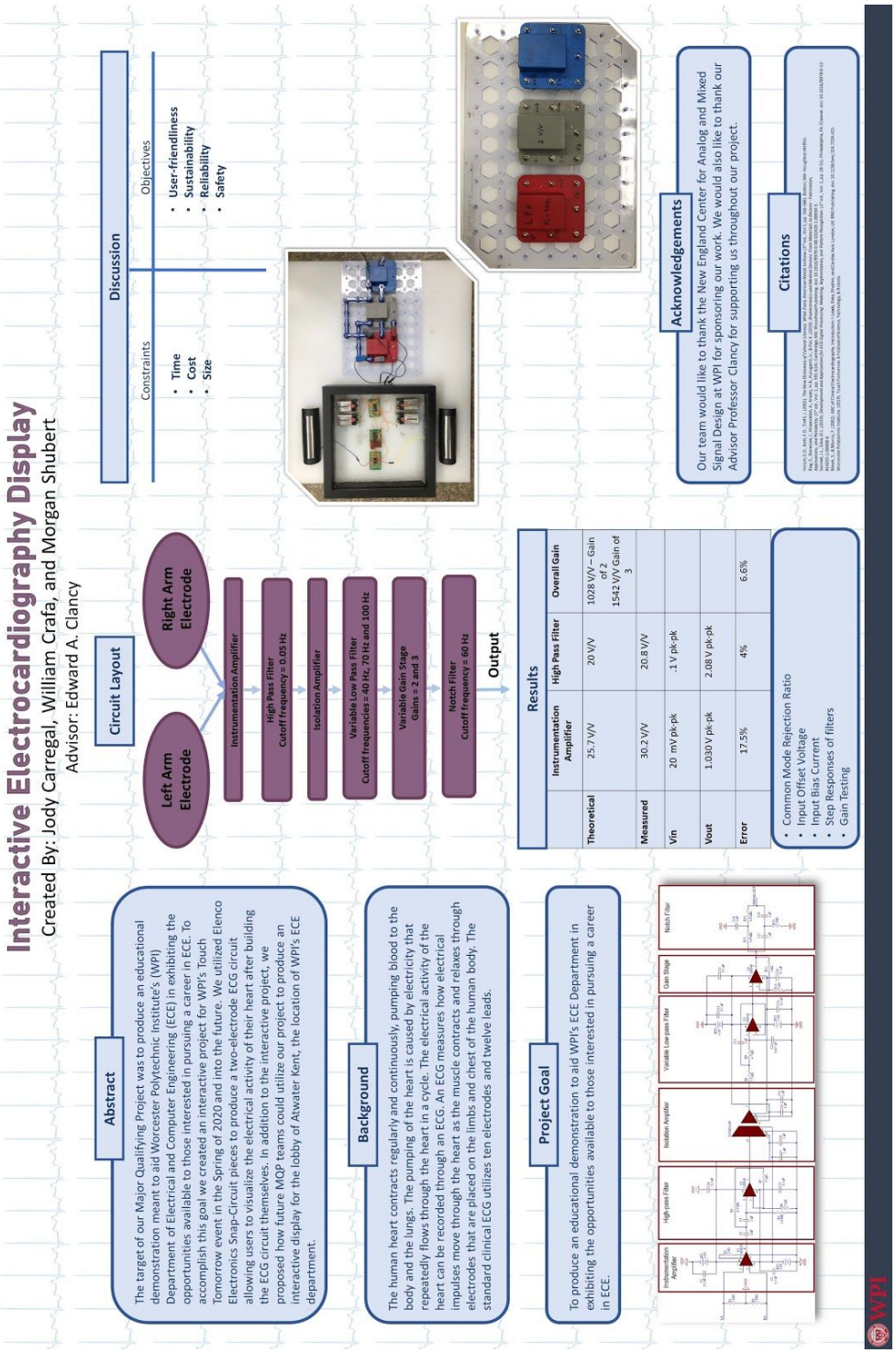

Appendix E: EMG Recommendations

The ECG Circuit can be Redesigned to Produce an Interactive EMG Display

The EMG circuit needs to be redesigned to produce a high quality experience for the interactive EMG display. This display would incorporate a microcontroller, an interactive game using two robotic arms, and a cuff to record the user's physiological signal. Currently, the EMG circuit design we created is based off of the parameters of the instrumentation amplifier, isolation amplifier, and filters we chose based on our design constraints. Such constraints included our two term MQP deadline, $600 budget, and unexpected inconveniences. To ensure the longevity of the EMG display and clarity of the signal, future MQP teams should create the display over a time period of at least three terms.

The EMG display was designed to feature an interactive game where the user's goal is to mirror the movements of a "target" prosthetic arm located behind the user-controlled prosthetic arm. The user will be able to mirror the movements of the target arm by wearing a cuff that contains electrodes placed within the lining. Once the cuff is on and the game begins, the user-controlled prosthetic arm will try to mimic the target's movements within the designated parameters. The game would include three levels: easy, medium, and hard. Dependent on how well the user follows the movements of the standard arm, they will receive a score on the LCD screen. In addition to the user-controlled and target prosthetic arms, the display would showcase the circuitry of the EMG, directions depicting how to play the game, an explanation of the project, and a detailed explanation of the analog front end circuitry.

The MQP team adopting this project should contact the Robotic Engineering Department in hopes of utilizing their robotic arms within the first week of their MQP. This is to ensure a repore is made with the department and to avoid a time delay in receiving the robotic arms. In addition, the team should dissect each datasheet of every component they choose to utilize in their EMG circuit. After doing so, the team should choose which tests they would like to implement to ensure each phase works individually and as a whole. Prior to building their

display the team should have a reliable circuit design that can clearly display the EMG signal of any user. For the benefit of the future MQP team, we have attached the material we have produced on creating such a display in Appendix D.

Appendix F: EMG Background

1.0 Background

1.1 Electromyogram (EMG)

Electromyography (EMG) can be utilized in both diagnostic procedures as well as for prosthetics. For diagnostic purposes, an EMG is a procedure that assesses the health of the muscle by measuring the electrical activity within the muscle to detect neuromuscular abnormalities. In all uses, an EMG captures the electrical signal from the muscle through tiny electrodes. After the signal is captured it is sent to an oscilloscope to display the signal for interpretation. When performing an EMG for diagnostic purposes, the muscle signals are recorded during rest, slight contraction, and forceful contraction. It is important to keep in mind that at rest, electrical signals would not be produced. The muscle is measured at each of these positions in order to capture multiple action potentials of the muscle. By capturing the action potentials of the muscle, the individual administering the EMG is able to assess the muscles' ability to respond when the nerves are stimulated (Ai et al., 2018).

An EMG can also be used to produce myoelectric prosthesis. The term “myoelectric” refers to the electrical properties of human muscles. A myoelectric-controlled prosthesis is an externally powered artificial limb that can be controlled with the electrical signals generated by an individual's active muscles after amputation (Beckerle et al., 2019). To record these signals, similar steps are followed as when a diagnostic procedure is being performed.

In order to understand how a nerve is stimulated, one must first have a basic understanding of how the human body carries electricity. The human body has the same number of positive and negative charges, making the body electrically neutral. When the human body is in a resting state, nerve cell membranes are polarized due to differences in concentrations and iconic compositions across the plasma membranes. Within this cell, a potential difference exists between the intracellular and extracellular fluids. In response to stimuli from neurons, muscle fiber depolarizes as the signal propagates along its surface causing the fiber to twitch. When the

depolarization and movement of ions occurs, an electric field is produced near each muscle fiber. An EMG records the response of the muscle to the stimulus, typically referred to as the motor unit action potential. The EMG must be able to detect extremely weak signals ranging from 0.5 mV to 10 mV. The appropriate bandwidth of an EMG signal ranges from 0.5 to 500 Hz (Beckerle et al., 2019). As shown in Figure 1, an EMG signal appears random in nature due to the sum of many MUAPs which fire at random times (Hussain et al., 2006).

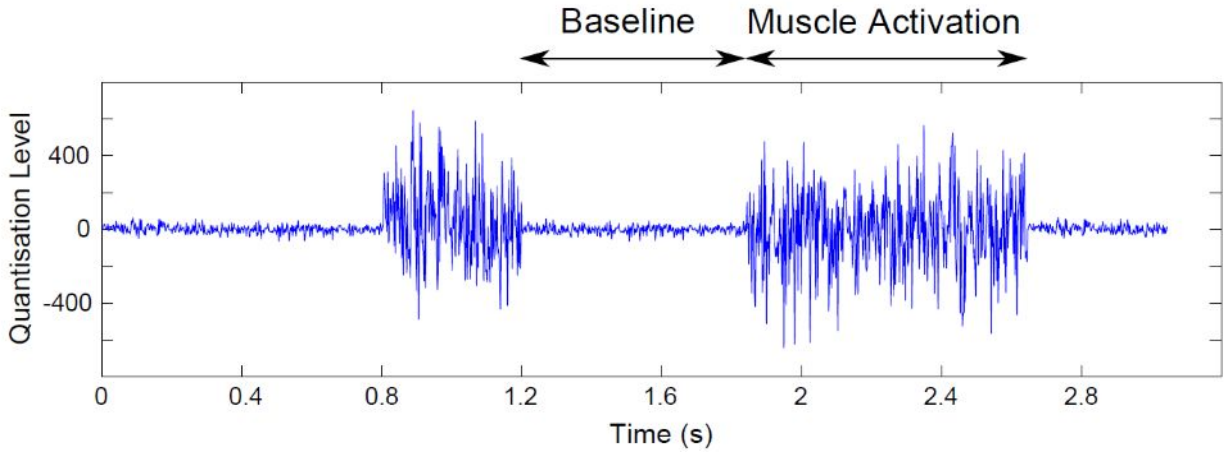

Figure 1 Typical EMG Signal (Beckerle et al., 2019)

To record the electrical signal, two forms of EMG electrodes can be implemented: skin (surface) electrodes and inserted electrodes. Inserted electrodes have two configurations: concentric (needle) or monopolar (fine wire) electrodes. Inserted electrodes are typically used in clinical procedures in neuromuscular evaluations. Concentric electrodes are comprised of a cannula (the reference electrode) and a core (active electrode) generally made of different materials (Mazzaro, 2007). The outer diameter of the cannula ranges from 0.45 mm to 0.7 mm and the core is approximately 0.1 mm in diameter. The core is embedded in an insulating material making the two electrode parts electrically insulated. As depicted in Figure 2 below, the tip of the needle has a flat elliptical shape and is ground to an angle of approximately 15 degrees (Mazzaro, 2007). Concentric needles are typically produced from stainless steel, silver and platinum.

To measure using the concentric needle, the needle is inserted as close as possible to the potential of interest and a ground electrode is placed relatively away from the needle. Concentric

needles have an excellent common mode rejection ratio (CMRR) due to the proximity of the active and reference electrodes. The excellent CMRR produces a more stable signal, allowing for more specific measurements. In addition, the recording process using concentric needles is much simpler as only one needle and one ground electrode are used. (Mazzaro, 2007).

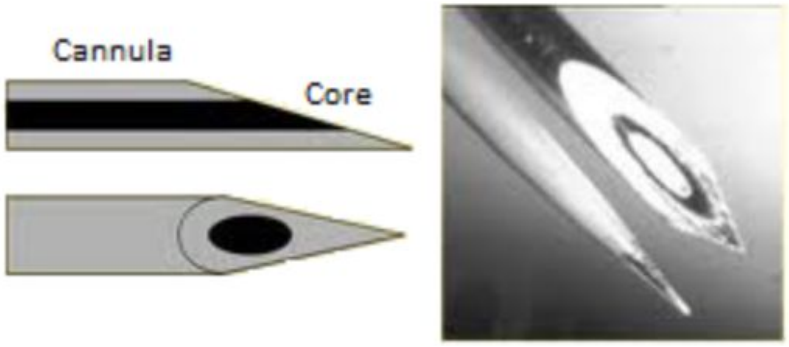

Figure 2 Concentric Needle Electrode (Jamal, 2012)

Monopolar needles, shown in Figure 3 below, are made of stainless steel with a gauge ranging from 26 to 31 in size. A monopolar needle is covered with an insulating material layer that covers the whole needle except for the tip. The tip of a monopolar needle is the portion of the needle that measures the signal and is traditionally sharpened to a conical shape (Mazzaro, 2007). The area of the tip is vital in the recording process, as it is related to the pick up field and amplitude of the recorded activity. To perform an EMG measurement with the monopolar needle, the needle must be inserted as close to the potential of interest as possible. Simultaneously, a reference electrode must be placed close to the active electrode but not on the active tissue and a ground electrode must be placed relatively away from the two previous electrodes.

Monopolar needles are well-liked for their large measuring area averaging 0.10 mm to 0.50 mm, which is approximately three times larger than the total area of exposure of the concentric needle (Mazzaro, 2007). Additionally, the impedance of a monopolar needle is lower by a factor of several times. The lower impedance of monopolar needles allows for a larger pickup field than concentric needles. As a result, the amplitude of potentials recorded with monopolar needles is larger (Mazzaro, 2007).

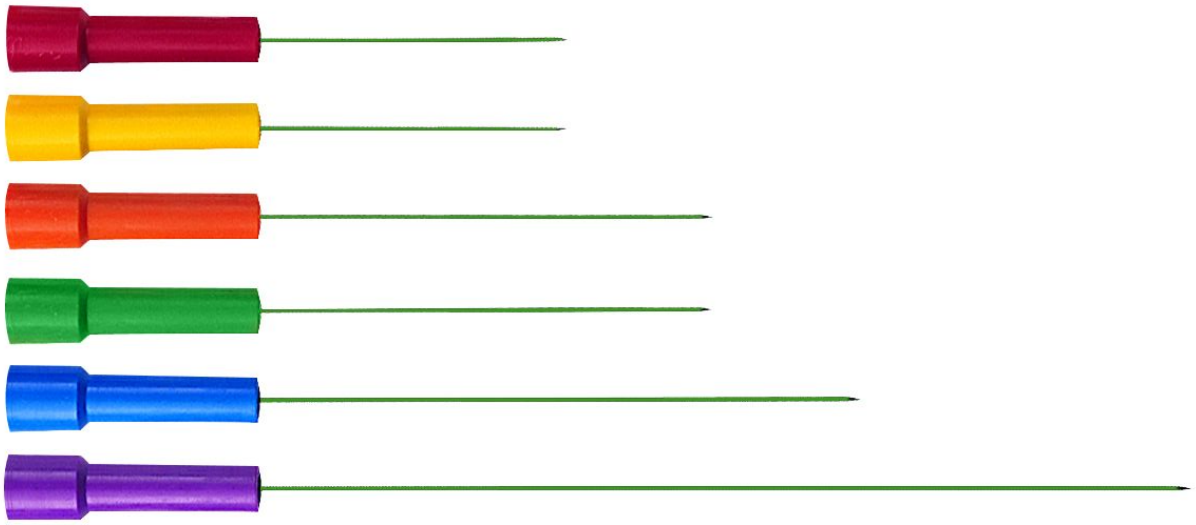

Figure 3 Monopolar Needle Electrode (Jamal, 2012)

Skin electrodes, commonly referred to as surface electrodes, provide a non-invasive technique for measurement and detection of EMG signal. Unlike needle electrodes, skin electrodes do not require strict medical supervision and certification. Surface electrodes have been used in many applications ranging from neuromuscular recordings to sports medical evaluations, in addition to prosthesis applications. Skin electrodes are typically used for superficial muscles only, which allows for more noise affecting the signal (Jamal, 2012).

Figure 4 Dry Electrode (Right) and Gel Electrode (Left) (Jamal, 2012)

Skin electrodes come in two forms: gelled and dry. Gelled EMG electrodes contain a gelled electrolytic substance as an interface between skin and electrodes. The gel allows current from the muscle to pass more freely across the junction between the electrolyte and the electrode.

This is because oxidation and reduction reactions take place at the metal electrode junction. This reaction introduces less electrical noise into the measurement (Jamal, 2012). Dry EMG electrodes do not require a gel interface. Dry electrodes can have more than one detecting surface, and at times these electrodes include an in-house pre-amplification circuit. Dry electrodes are typically heavier than gel electrodes, which can cause issues for electrode fixation; a material for stability of the electrode is then required (Jamal, 2012).

1.2 EMG Analog Front End

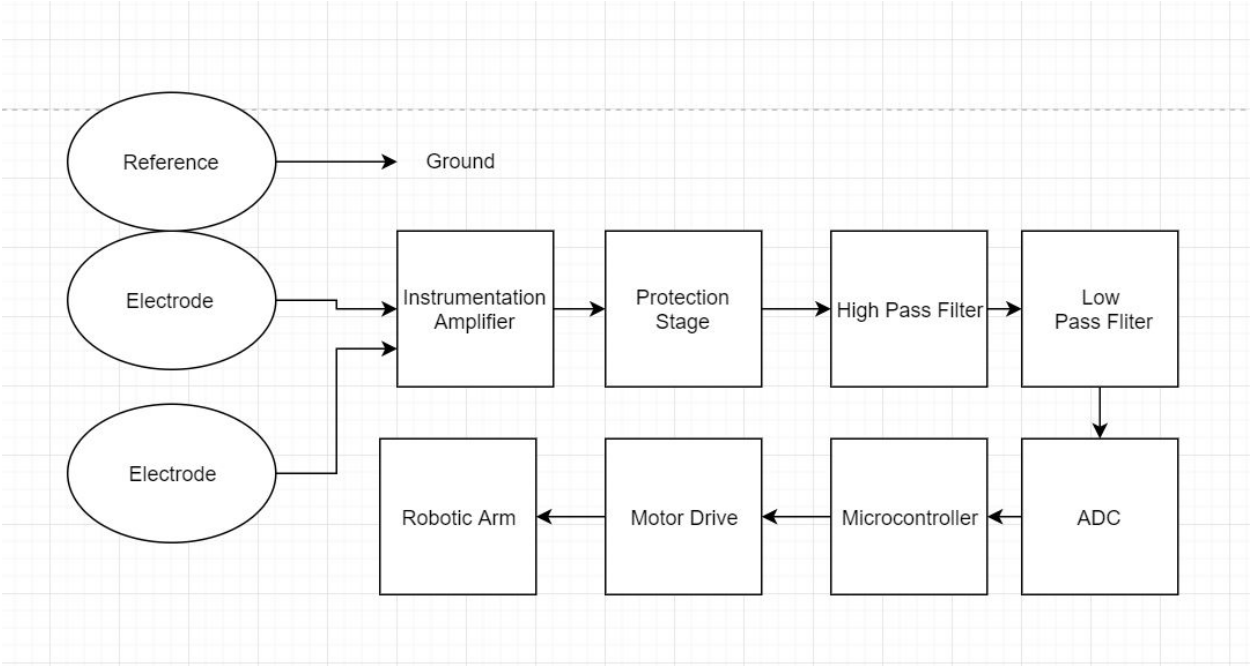

Figure 5 Block Diagram of Three Lead EMG Circuit

1.2.1 Instrumentation Amplifier

The EMG signal will first pass through an instrumentation amplifier. An instrumentation amplifier has a high input impedance, common-mode noise rejection, differential output, and a high gain set by an external resistor. An instrumentation amplifier is comprised of non-inverting amplifying stages whose outputs act as the inputs to the differential amplifier. A differential amplifier is an inverting amplifier with negative feedback that amplifies the difference between

the two input voltages. The differential amplifier will amplify the difference between the two signals being recorded and reject the common-mode voltage. The two input buffers provide a key function in the instrumentation amplifier. The ideal non-inverting amplifiers have an infinite input resistance. Therefore, the input buffers will not sink or source any current. In this stage, the differential amplifier will reject the common-mode voltage and will amplify the differential signal (Bitar et al., 2016).

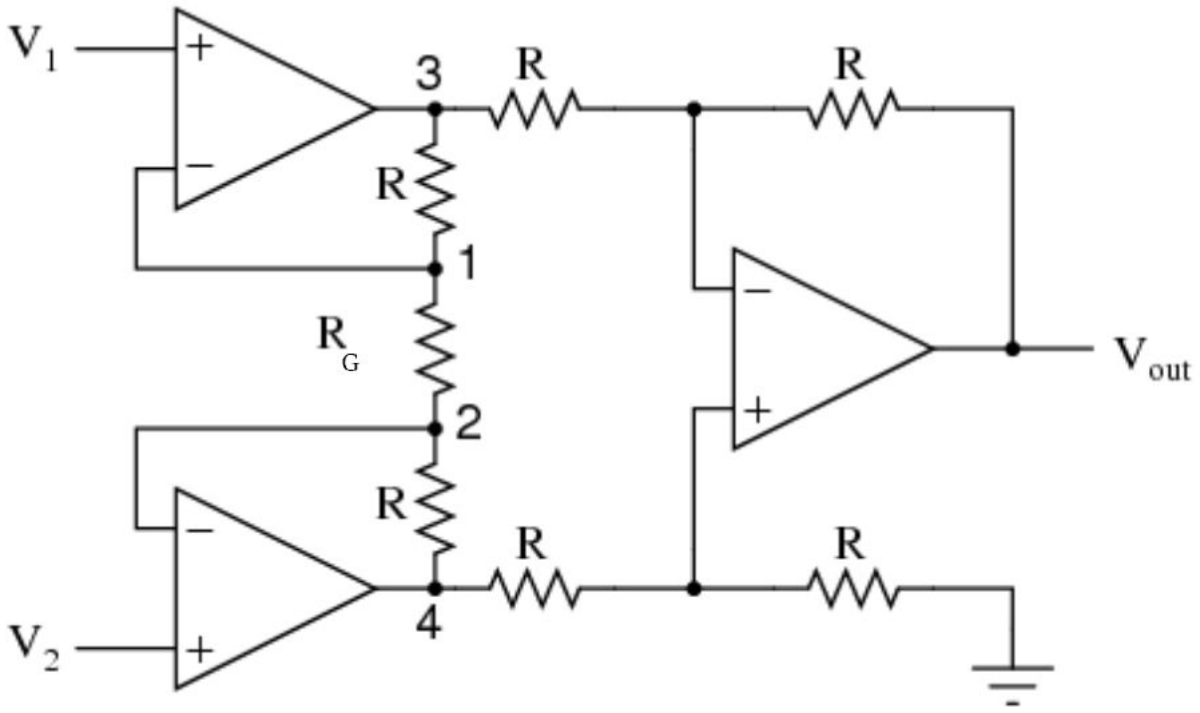

Figure 11 Model of a Basic Instrumentation Amplifier (EETech Media LLC, 2018)

We utilized an instrumentation amplifier because it allowed us to adjust the gain of the circuit by adjusting a single external resistor. Another option would have been to utilize a differential amplifier. However, we would not have had a high impedance input and we would have had to adjust multiple resistors in order to reach our desired gain. Referring to the basic

instrumentation amplifier depicted in Figure 11, an instrumentation amplifier can be modeled as two buffer differential amplifiers linked by three resistors with an additional differential amplifier stage. In order to explain this circuit, we will assume all of the resistor values to be equal except for R_G. The voltage at point 1 (found above R_G) is equal to the voltage at V_1 due to the negative feedback loop of amplifier A1. In the same way, the voltage at point 2 (found below R_G) is equal to the voltage at V_2. This then causes a voltage drop across R_G thus creating a current through R_G. Due to the fact that the amplifier inputs draw no current, the only current that can travel through the resistors labeled as "R" must be the current through R_G. This current then produces a voltage drop between points 3 and 4 (found at the top and bottom of the circuit). The equation to solve for the voltage drop between points 3 and 4 is:

$$V_{3-4} = (V_2 - V_1) * (1 + \frac{2R}{R_G})$$

The differential amplifier furthest to the right then takes this voltage drop and amplifies it by a gain of 1 (due to the fact that all of the "R" resistors in this circuit are of equal value). Therefore, the output voltage is simply the voltage drop between points 3 and 4:

$$V_{OUT} = V_{3-4}$$

To solve for the gain of a typical amplifier the following equation would be utilized:

$$A_V = (1 + \frac{2R}{R_G})$$

Equation 1 Gain Equation to solve for Gain (A_V) (EETech Media LLC, 2018)

1.2.2 Isolation Amplifier

Once the electrical signal is amplified from the instrumentation amplifier the signal will travel through the isolation amplifier, which acts as the protection stage. An isolation amplifier is an operational amplifier circuit which provides electrical isolation of one portion of a circuit from another. The protection stage is responsible for limiting the input range, rejecting high frequencies, and providing a barrier for dangerous voltages. Since the electrodes will be connected to a human body, precautions will have to be made to ensure the safety of the

individuals utilizing our product. Isolation amplifiers enhance safety by preventing fault currents from flowing through the human body through a ground-referenced biopotential electrode (Kutz, 2009). We utilized an isolation amplifier in order to ensure that the human body had no direct electrical path to the earth-grounded portion of the circuit. An isolation amplifier requires two different power sources in order to pass the signal through successfully. The portion of the circuit preceding the isolation amplifier, which will be connected to the human body, needs to be powered by an isolated power supply or by batteries. The portion of the circuit following the isolation amplifier, which is earth-grounded, is powered by a non-isolated power supply. This ensures that the only phenomenon being transferred through the isolation amplifier is the signal itself, not power (Analog Devices, 2009).

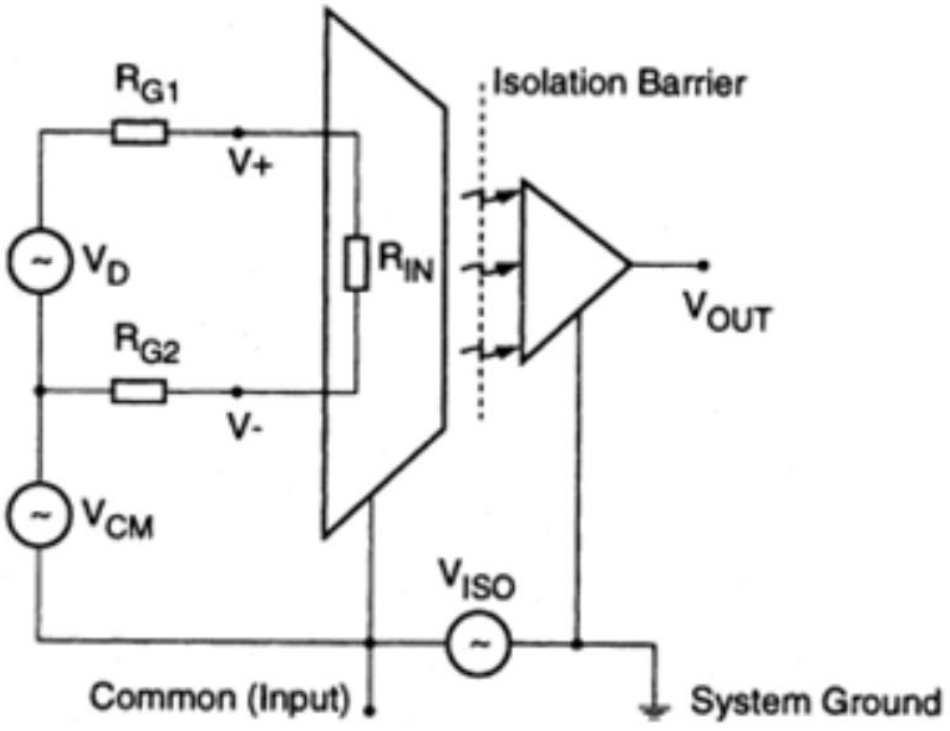

Figure 12 Isolation Amplifier Circuit Diagram (Kester, 2012)

An isolation amplifier serves as a buffer between two portions of a circuit to ensure the rightmost portion of the circuit does not influence the currents and voltages in the leftmost portion of the circuit. There are many different methods of achieving electrical isolation, but one

common technique is to modulate the input signal and then demodulate to obtain the output signal. The input signal is duty-cycle modulated and then transmitted digitally across the isolation barrier. The output section of the isolation amplifier receives the duty-cycle modulated signal, converts the signal back to an analog voltage, and removes the ripple component that generated in the demodulation produced (Analog Devices, 2019). The basic concept of an isolation amplifier is visually depicted in Figure 12.

1.2.3 Bandpass Filter

To ensure the signal is smooth and contains minimal noise we needed to filter the signal by utilizing a bandpass filter. The physiological signal will contain multiple forms of noise. Noise can be produced from other muscles throughout the body, from heat in the electronics, and from the 60 Hz input power interference. A popular method used to filter out the many forms of noise is through high-pass and low-pass filtering. High-pass filters are employed to remove low-frequency components such as motion artifacts, respiratory variations, and baseline wander. Low-pass filters are employed to remove high frequency muscle artifacts and external interferences. As previously stated in Section 2.1, the frequency range of a typical EMG circuit is 0.05 Hz to 100 Hz. The EMG circuit must be able to function properly for signals ranging from 0.5 mV to 5 mV in amplitude (Beckerle et al., 2019). The bandpass filter will be comprised of a high-pass filter cascaded with a low-pass filter. A high-pass filter passes signals with frequencies higher than the cut-off frequency and rejects any signals with frequencies lower than the cut-off frequency. A low-pass filter has the exact opposite effect compared to the high-pass filter. A low-pass filter passes any signal with frequencies smaller than the cut-off frequency and rejects signals with frequencies higher than the cut-off frequency.

If a high-pass filter is cascaded with a low-pass filter, the result will be a bandpass filter (see Figure 13). Bandpass filters allow signals between two specific frequencies to pass through and rejects any signal with frequencies outside of the operating range, or passband.

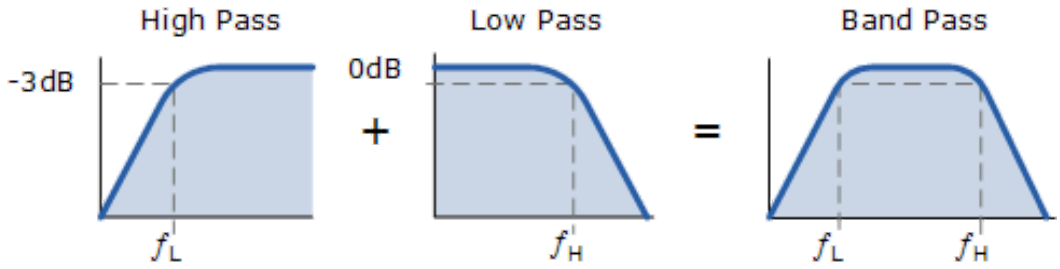

Figure 13 Bandpass Filter Comprised of High-pass and Low-pass Filters (Thompson, 2006)

Out of the many filter topologies that exist, there are two main categories: Sallen-Key and multiple feedback. The Sallen-Key topology is typically utilized in circuits which require high-gain accuracy and low Q factors, typically less than 3. A common characteristic of the Sallen-Key topology is to design the filter with equal resistances and equal capacitances. For example, a second-order Sallen-Key filter would have $R = R_1 = R_2$ and $C = C_1 = C_2$ (Carter & Mancini, 2018). However, the resistances and capacitances do not need to be equal for Sallen-Key topology. See Figure 14 for topologies of unity-gain (gain of 1) Sallen-Key second-order high-pass and low-pass filters.

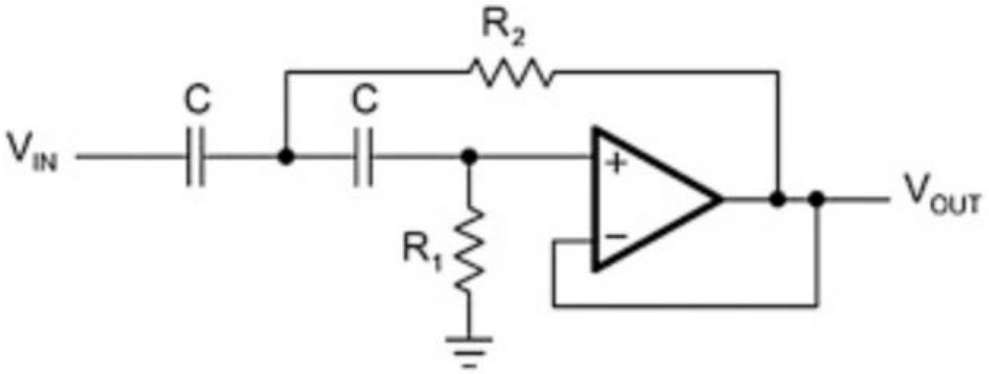

High-Pass

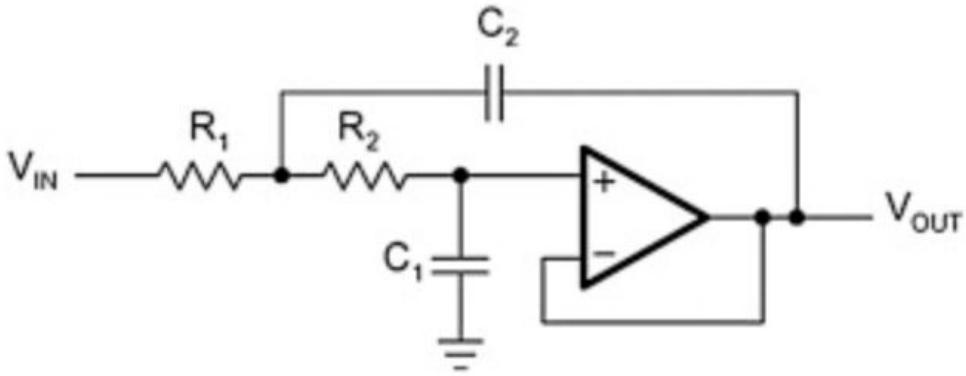

Low-Pass

Figure 14 Unity-gain Topologies for Second-order Sallen-Key filters: High-pass (Top) & Low-pass (Bottom) (Carter & Mancini, 2018)

The multiple feedback topology is generally utilized in circuits which require high gain and high Q factors. Unlike the Sallen-key topology, multiple feedback filters have unequal resistances and capacitances. For a second-order multiple feedback high-pass filter $C_1 = C_2 \neq C_3$ and $R_1 \neq R_2$. For a second-order multiple feedback low-pass filter $R_1 \neq R_2 \neq R_3$ and $C_1 \neq C_2$ (Carter & Mancini, 2018). See Figure 15 for unity-gain multiple feedback high-pass and low-pass filters.

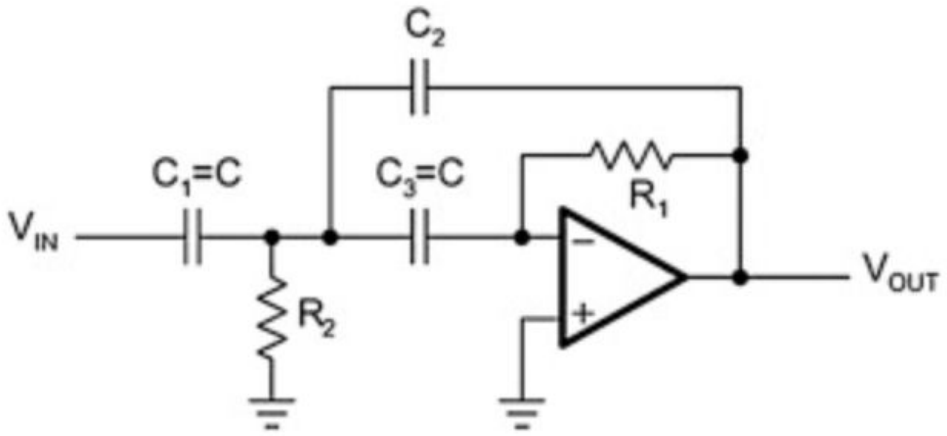

High-Pass

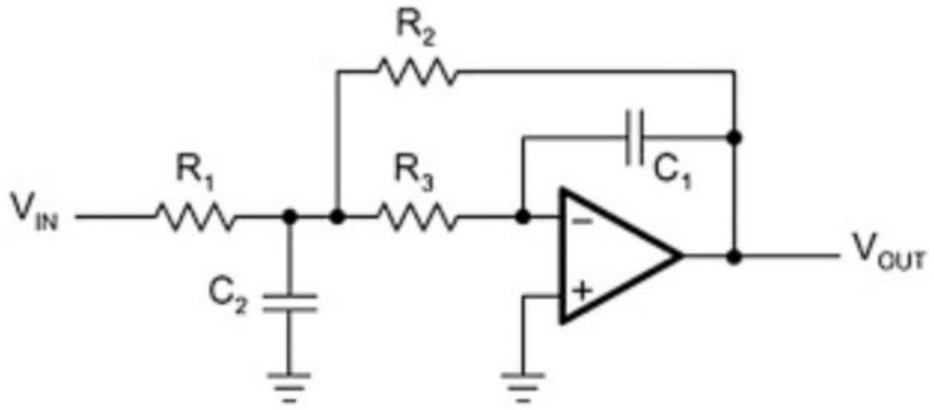

Low-Pass

Figure 15 Unity-gain Topologies for Second-order Multiple Feedback filters: High-pass (Top) & Low-pass (Bottom) (Carter & Mancini, 2018)

In a typical EMG circuit, active high-pass and low-pass filters are utilized. Out of the many forms of active filters, there are four common types: Bessel, Butterworth, Chebyshev (Type I), and Elliptic filters. Bessel filters are all-pole filters, which means that their transfer functions have no zeros. Bessel filters have no ripples in the passband and stopband in their frequency responses. The Bessel filter is optimized to obtain better transient responses due to a

linear phase, or constant delay, in the passband. As a consequence, Bessel filters will have relatively poorer frequency responses, or less amplitude discrimination (Thompson, 2014). The poles of the Bessel filter can be found by locating all of the poles on a circle and separating their imaginary parts by $\frac{2}{n}$, where n is the number of poles. The distance between the top and bottom poles are determined by where the circle crosses the jω axis by $\frac{1}{n}$, or half the distance between the other poles (Zumbahlen, 2008).

Butterworth filters are also all-pole filters and their frequency responses are monotonically flat within the passbands and stopbands. The Butterworth filter is the best compromise between attenuation and phase response. To attain the Butterworth filter's ideal flatness, the filter has a relatively wide transition region from passband to stopband, with average transient characteristics (Zumbahlen, 2008). The sharpness of the roll-off from the passband to the stopband is determined by the order of the Butterworth filter. Due the square response of a Butterworth filter, there is no phase shift and the amplitude is attenuated by a factor of two at the cutoff frequency (Emery & Thomson, 2014). The poles of the Butterworth filter can be found by:

$$-\sin\frac{(2K-1)\pi}{2n} + j\cos\frac{(2K-1)\pi}{2n} \quad K = 1, 2 \ldots n$$

Equation 2 Pole Positions for Butterworth Filter (Thompson, 2014)

where K is the pole pair number and n is the number of poles. The poles are equidistant from one another, which means that the angles between the poles are equal (Thompson, 2014).

Chebyshev (Type I) filters, similar to Bessel and Butterworth filters, are also all-pole filters. However, a Chebyshev (Type I) filter's frequency response has ripples in its passband or stopband which is a trade-off for the Chebyshev (Type I) filter's smaller transition region compared to Butterworth filters. The Chebyshev (Type I) filter minimizes the height of the maximum ripple, which is the Chebyshev (Type I) criterion. The poles of the Chebyshev (Type I) filter can be found by moving the poles of the Butterworth filter to form an ellipse. The real part of the pole is multiplied by K_r and the imaginary part of the pole is multiplied by K_I. K_r and K_I are found by utilizing the following equations:

$$K_r = \sinh A$$

Equation 3 (Zumbahlen, 2008)

$$K_I = \cosh A$$

Equation 4 (Zumbahlen, 2008)

where:

$$A = \frac{1}{n} \sinh^{-1} \frac{1}{\varepsilon}$$

Equation 5 (Zumbahlen, 2008)

where n is the filter order and:

$$\varepsilon = \sqrt{10^R - 1}$$

Equation 6 (Zumbahlen, 2008)

where:

$$R = \frac{R_{dB}}{10}$$

Equation 7 (Zumbahlen, 2008)

where R_{dB} is the passband ripple in dB. Typically, Chebyshev filters are normalized so that the edge of the ripple band is at normalized angular cut-off frequency of $\omega_o = 1$.

The 3dB bandwidth is given by:

$$A_{3dB} = \frac{1}{n} \cosh^{-1} \frac{1}{\varepsilon}$$

Equation 8 (Zumbahlen, 2008)

Now, the amplitude, step, and impulse responses of the three all-pole filters (Bessel, Butterworth, and Chebyshev (Type I)) will be compared. Figure 16 portrays the amplitude response of an eight pole 0.5dB ripple filter comparison of the Bessel, Butterworth, and Chebyshev (Type I) filters. Figure 17 portrays the step and impulse responses of the same filter. The responses have been normalized for a cut-off frequency (f_c) of 1 Hz. It is easy to see in Figure 16 that amplitude discrimination (the ability to distinguish between the desired signal from noise and other signals) increases in quality with Bessel as the poorest and Chebychev (Type I) as the best (Zumbahlen, 2008). The Bessel signal starts to attenuate at frequencies much lower than the cut-off frequency of 1 Hz, while the Chebyshev (Type I) signal seems to attenuate almost immediately at 1 Hz. The Butterworth signal attenuates only slightly before the Chebyshev (Type I) signal, which is why it is a close second.

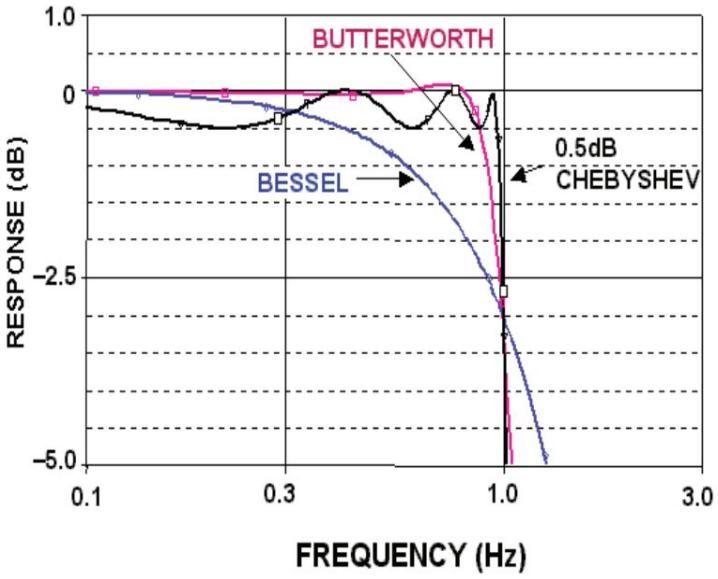

Figure 16 Comparison of Amplitude Response of Bessel, Butterworth, and Chebyshev (Type I) Filters (Zumbahlen, 2008)

Filters with better amplitude responses have poorer time responses. This trade-off phenomenon is evident in Figure 17. The transient behavior increases in quality with Chebychev (Type I) as the poorest and Bessel as the best. The left graph in Figure 17 portrays a step response comparison of all three filters. The Chebyshev (Type I) signal does not even remotely emulate a step response due to its gradual transition and multiple ripples. The Bessel signal has a very sharp transition which closely reproduces a step response. The Butterworth signal looks

very similar to the Chebyshev (Type I) signal; it is only slightly better due to its decrease in ripples at a faster rate. The right graph in Figure 17 portrays an impulse response comparison of all three filters. The Bessel signal has a large, narrow initial impulse and immediately transitions into a very steady signal. The Chebyshev (Type I) signal has a smaller, wider initial impulse and has many ripples. The Butterworth signal has a slightly larger, more narrow initial impulse with fewer ripples compared to the Chebyshev (Type I) signal.

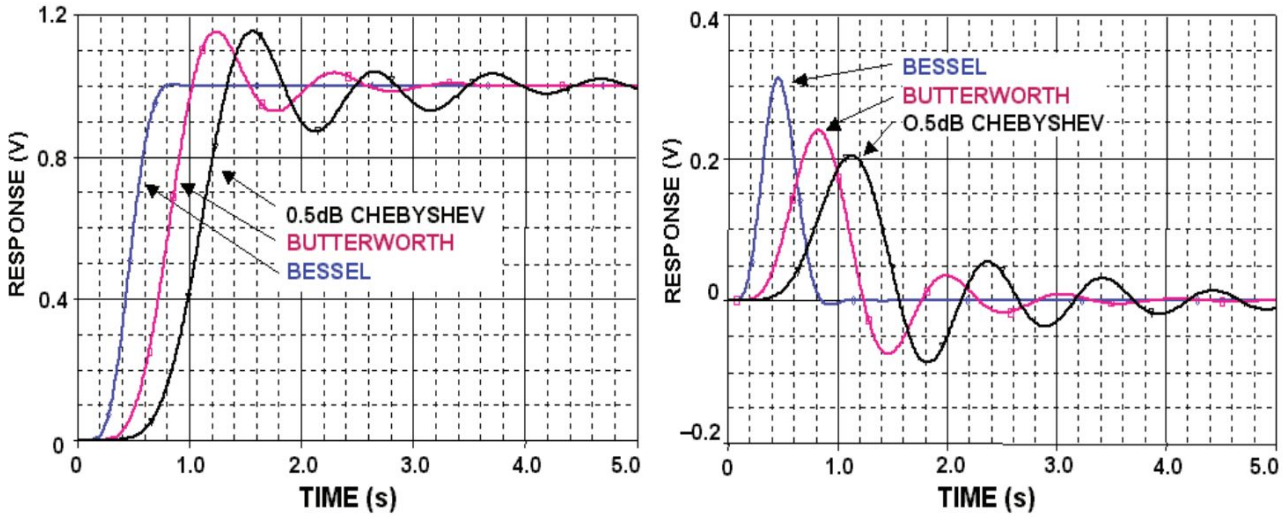

Figure 17 Comparison of Step (Left) and Impulse (Right) Responses of Bessel, Butterworth, and Chebyshev (Type I) Filters (Zumbahlen, 2008)

Elliptic filters are not all-pole filters, meaning their transfer functions contain zeros. Elliptic filters have shorter transition regions than the previously mentioned filters because there are ripples in both the passbands and stopbands. The zeros also mean that the attenuation will be very high in the stopband and "there will be some 'bounceback' of the stopband response between the zeros" (Zumbahlen, 2008). This "bounceback" is the stopband ripple. The poles of an Elliptic filter lie on an ellipse, which means that the time domain responses are degraded, similar to Chebyshev filters. The mathematical operations behind an Elliptic filter are much more complicated than Bessel, Butterworth, and Chebyshev filters. It is not simple to solve for poles and zeros. Alternatively, the modulation angle, θ, which determines the rate of attenuation is also an alternative method to defining the filter order, n:

$$\theta = \sin^{-1} \frac{1}{F_s}$$

Equation 9 (Zumbahlen, 2008)

Another important parameter to solve for is ρ, which determines the passband ripple:

$$\rho = \sqrt{\frac{\varepsilon^2}{1 + \varepsilon^2}}$$

Equation 10 (Zumbahlen, 2008)

where ε is the ripple factor and the passband ripple is defined by:

$$R_{dB} = -10 \log(1 - \rho^2)$$

Equation 11 (Zumbahlen, 2008)

As the ripples of the Elliptic filter response increase, the value of A_{min}, the minimum attenuation in the stopband, increases as well. Also, as θ approaches 90°, the stopband frequency (F_s) approaches the cut-off frequency (F_c). When this occurs, the result is an extremely short transition region, which results in sharp rolloff. The trade-off is a lower value of A_{min}. Lastly, ρ determines the input resistance for a passive Elliptic filter, which then relates to the VSWR, or Voltage Standing Wave Ratio (Zumbahlen, 2008).

1.2.4 Notch Filter

A notch filter, also known as a bandstop filter or band-reject filter, is utilized to attenuate signals within a specific band of frequencies (stopband). All frequencies greater than or fewer than the stopband will not attenuate. Figure 18 depicts the role of a notch filter, where frequencies between f_1 and f_2 are attenuated and all frequencies less than f_1 and greater than f_2 are passed.

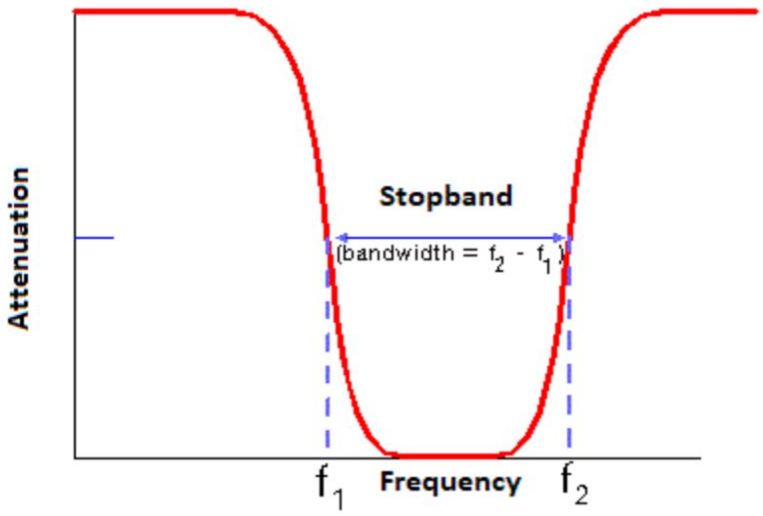

Figure 18 Example of the Role of a Notch Filter (Winder, 2008)

There are three different cases of notch filter characteristics: standard notch, high-pass notch, and low-pass notch. These cases are determined based on the relationship between the pole frequency (ω_0) and the zero frequency (ω_z). A standard notch occurs if the pole frequency is equal to the zero frequency ($\omega_0 = \omega_z$). A high-pass notch occurs if the pole frequency is greater than the zero frequency ($\omega_0 > \omega_z$). A low-pass notch occurs if the zero frequency is greater than the pole frequency ($\omega_z > \omega_0$) (Zumbahlen, 2008). Figure 19 depicts the frequency responses of the three different cases of notch filter characteristics.

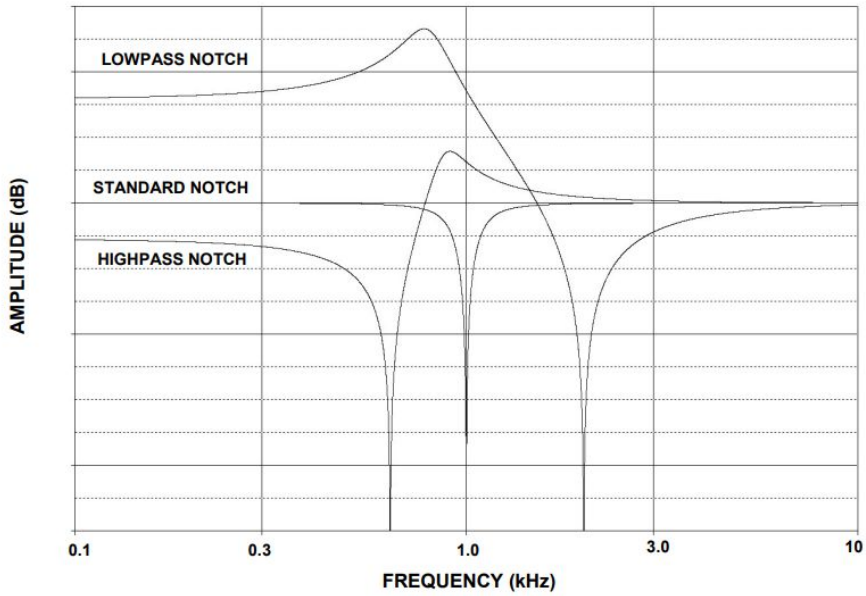

Figure 19 Comparison of Standard, High-pass, and Low-pass Notches (Zumbahlen, 2008)

Out of the many different configurations of notch filters, there are four common designs: 1 - Bandpass (1 - BP), Bainter, Boctor, and twin T. The 1 - BP notch filter is built as a bandpass filter whose output is subtracted from the input of the filter. There are two different configurations of the bandpass filter. The bandpass filter can either be inverting, similar to multiple-feedback topology (see Figure 20) or non-inverting, similar to Sallen-Key topology (see Figure 21). These configurations are important depending on which topology is being utilized to ensure that the output of the bandpass filter is being subtracted from, not added to, the input (Zumbahlen, 2008).

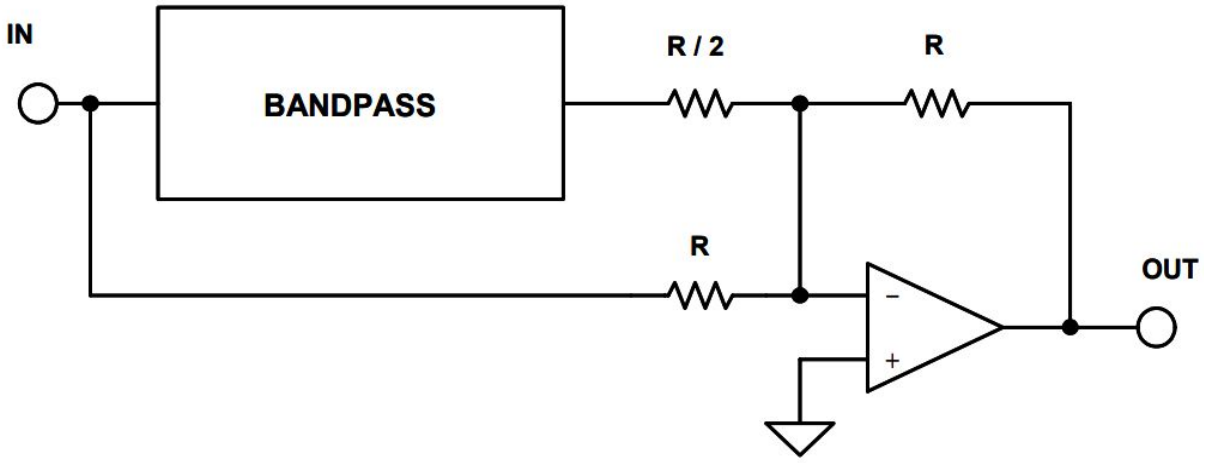

Figure 20 General Configuration for Inverting 1 - Bandpass Filter (Zumbahlen, 2008)

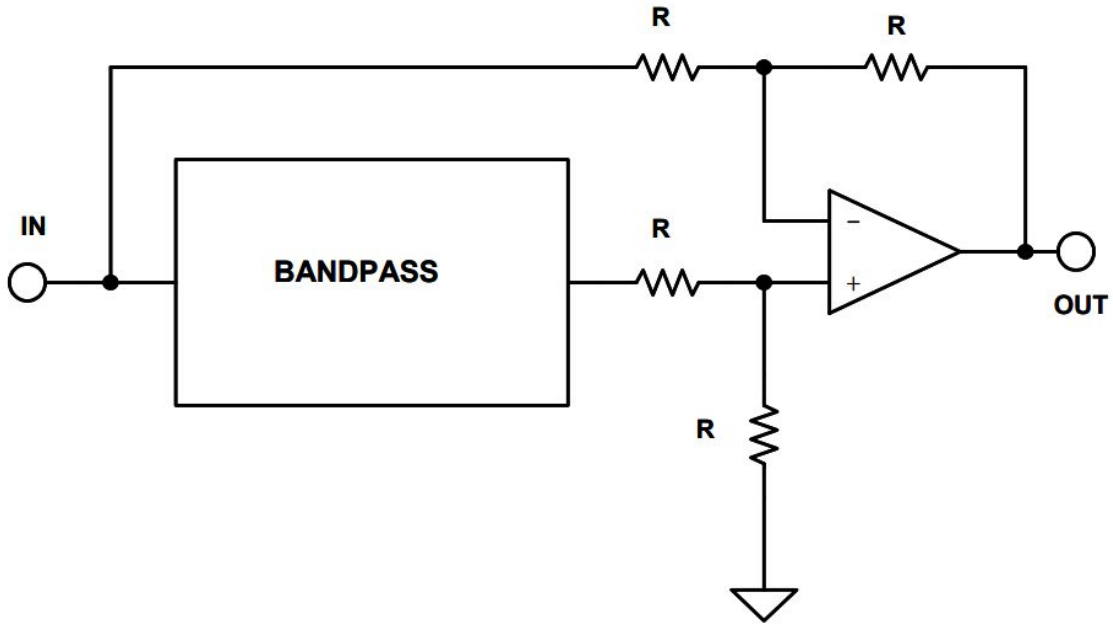

Figure 21 General Configuration for Non-inverting 1 - Bandpass Filter (Zumbahlen, 2008)

The Bainter filter is a simple notch filter which is composed of circuit blocks with two feedback loops. The Q factor of the Bainter filter is not determined by the resistance and capacitance values in the circuit, unlike other notch filters, and therefore the Bainter filter has low component sensitivity. The Q factor is dependent solely on the gains of the amplifiers in the circuit, which means that the notch depth, or amplitude of the notch, will not drift with

temperature, aging, and other environmental factors. However, the notch frequency may shift (Zumbahlen, 2008). See Figure 22 for the general configuration of a Bainer notch filter. R6 tunes the Q factor and R1 tunes the zero frequency (ω_z). Changing the value of R3 determines the ratio of pole frequency to zero frequency (ω_0 / ω_z). If R3 = R4, then the notch filter produces a standard notch. If R3 > R4, then the notch filter produces a high-pass notch, and if R3 < R4, then the notch filter produces a low-pass notch (Zumbahlen, 2008).

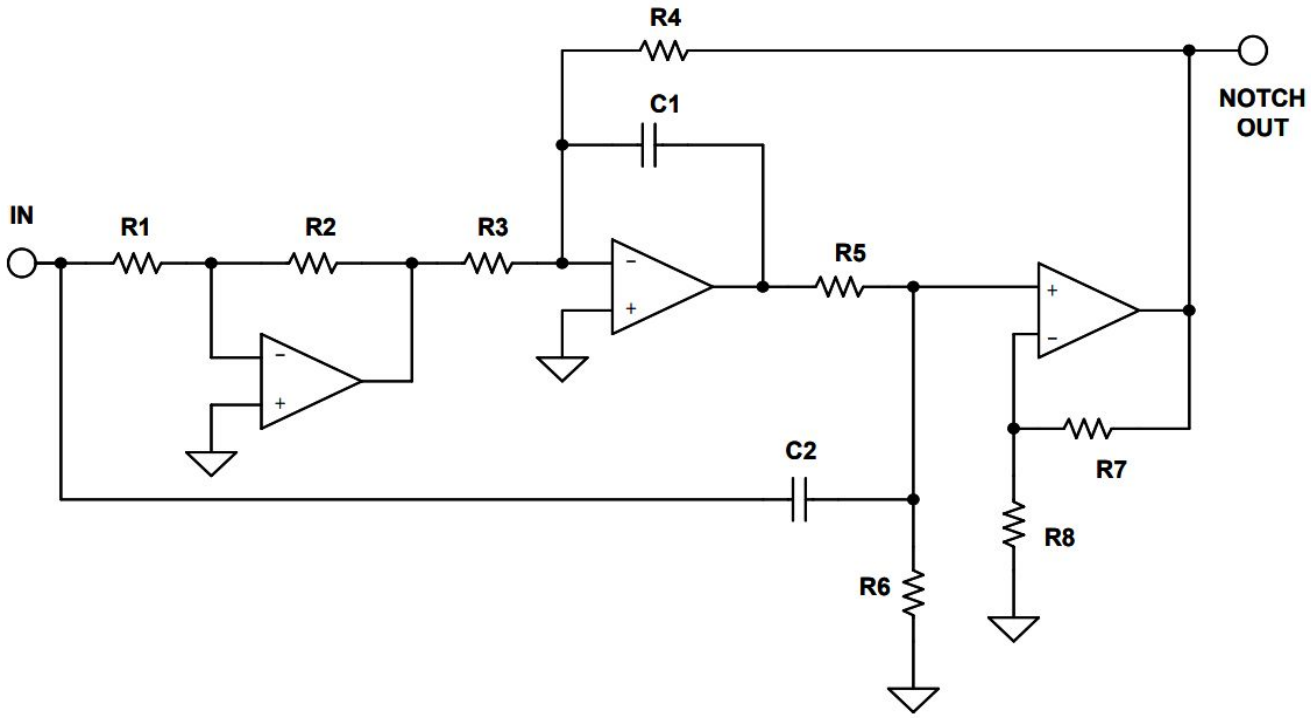

Figure 22 General Configuration of Bainter Notch Filter (Zumbahlen, 2008)

The Boctor notch filter only utilizes one operational amplifier, but has a relatively large amount of components in a moderately intricate configuration. The number of components utilized in the Boctor filter allows flexibility when it comes to component value selection. Boctor filers have low sensitivity and also possess the ability to tune the parameters of the filter independently to an extent. There are two different configurations of a Boctor filter: a high-pass notch (see Figure 23) and a low-pass notch (see Figure 24).

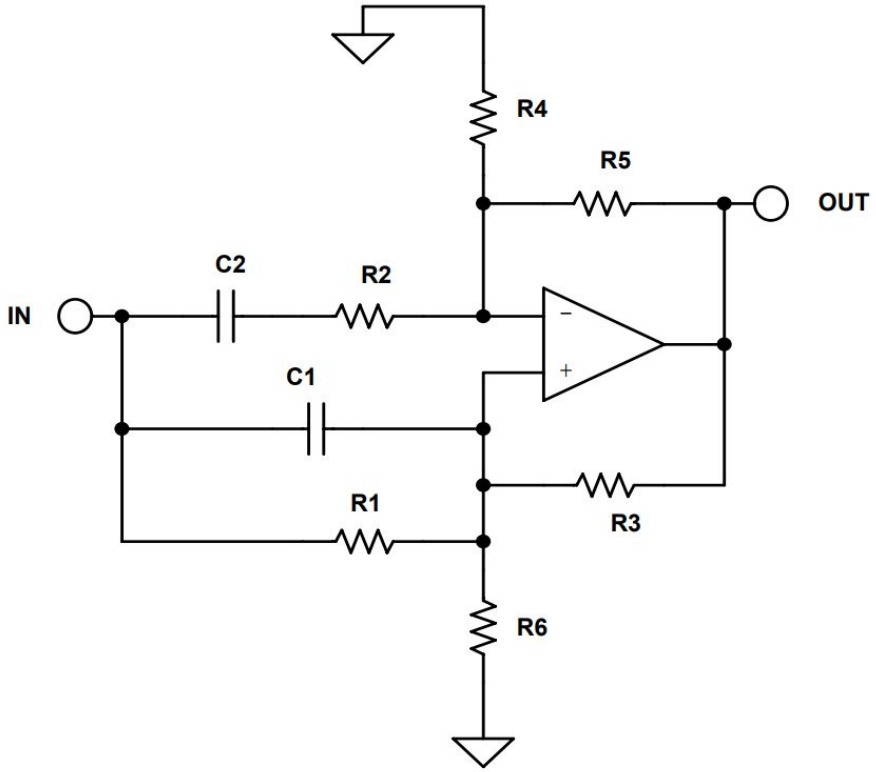

Figure 23 General Configuration of Boctor High-pass Notch Filter (Zumbahlen, 2008)

A circuit gain is required for a high-pass Boctor notch filter. The following must be true for the circuit to be considered a high-pass Boctor notch filter:

$$Q < \frac{1}{1 - \frac{\omega_z^2}{\omega_0^2}}$$

Equation 12 (Zumbahlen, 2008)

A high-pass Boctor notch filter can be comprised of only one amplifier and two capacitors, which can be the same value. The pole and zero frequencies (ω_0 and ω_z) are completely independent of the gain of the amplifier (Zumbahlen, 2008).

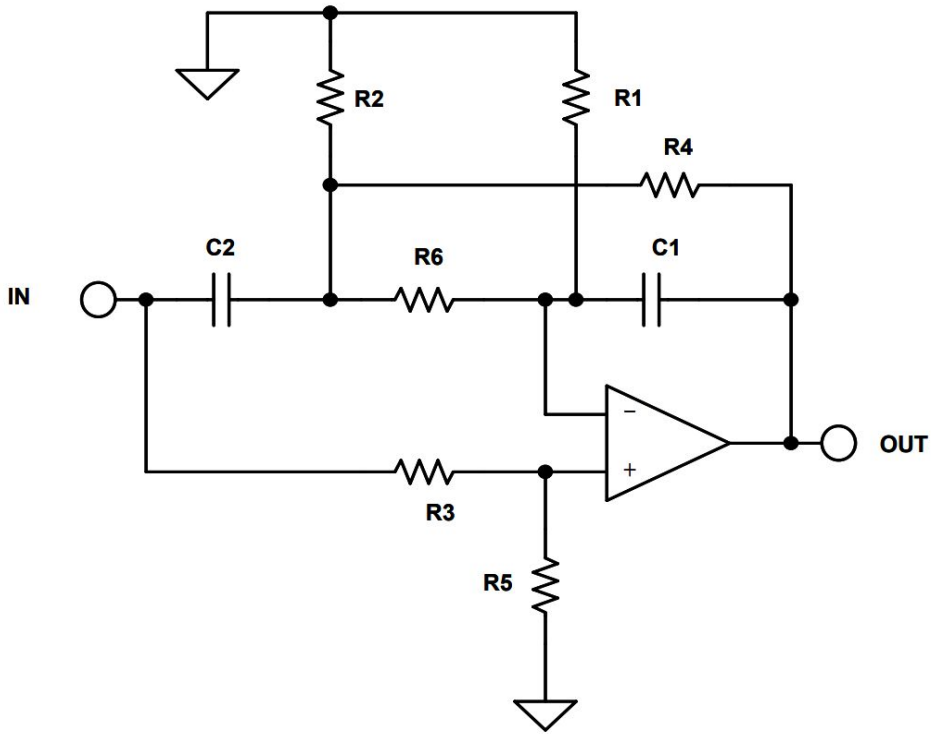

Figure 24 General Configuration of Boctor Low-pass Notch Filter (Zumbahlen, 2008)

For a low-pass Boctor notch filter, R4 tunes the pole frequency (ω_0), R2 tunes the Q factor of the poles (Q_0), R3 tunes the Q factor of the zeros (Q_z), and R1 tunes the zero frequency (ω_z) (Zumbahlen, 2008). In order for the filter to work properly with the desired components, the following must be true about parameter k1, the gain factor:

$$\frac{\omega_0^2}{\omega_z^2} < k1 < 1$$

Equation 13 (Zumbahlen, 2008)

The twin T notch filter is the most commonly utilized notch filter. A passive twin T notch filter does not have any amplifiers in its configuration, meaning there is no feedback. Passive twin T notch filters (see Figure 25) have a fixed Q factor of 0.25 (Zumbahlen, 2008).

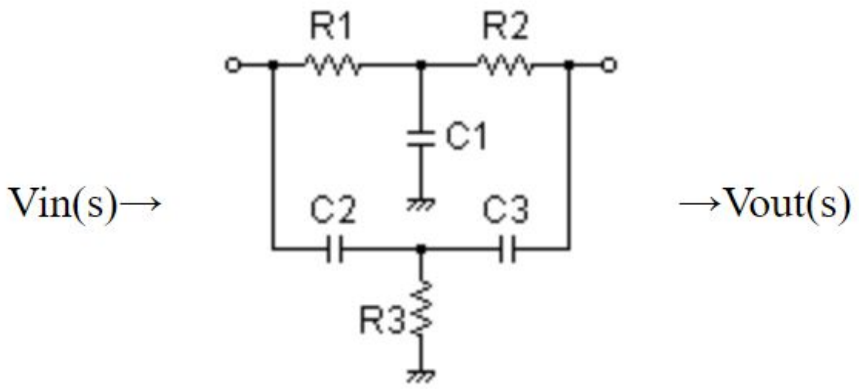

Figure 25 General Configuration of a Passive Twin T Notch Filter (Okawa Electric Design, 2019)

An active twin T notch filter contains positive feedback to the reference node. Unlike the passive twin T notch filter, the active configuration has a variable Q factor, which is determined by the ratio R4/R5. This ratio also determines the notch depth of the filter signal. To reach a maximum notch depth, resistors R4, R5, and the associated operational amplifier can be eliminated. If this were to happen, then the node connecting R3 and C3 would be directly connected to the output. See Figure 26 for a general configuration of an active twin T notch filter.

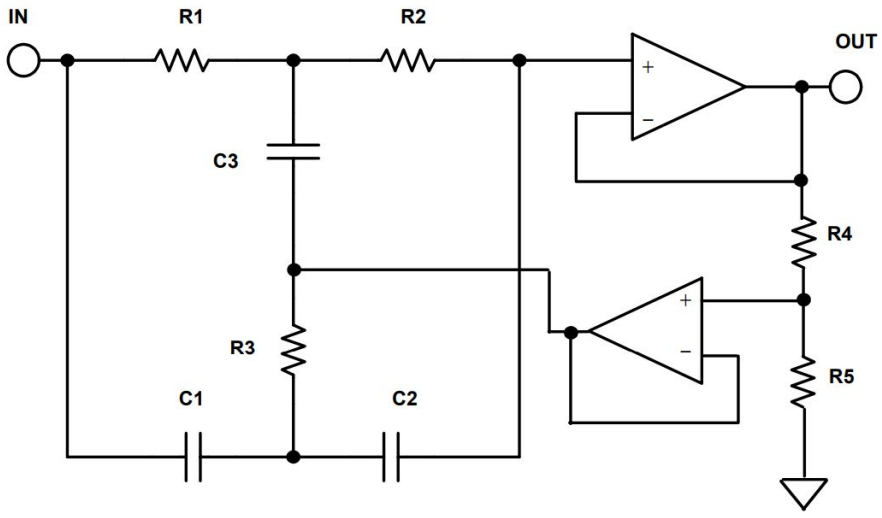

Figure 26 General Configuration of an Active Twin T Notch Filter (Zumbahlen, 2008)